Theses and Dissertations

Summer 2015

Hydrologic response of land use and land cover changes

Nicholas Persak Leach

University of Iowa

HYDROLOGIC RESPONSE OF LAND USE AND LAND COVER CHANGES

by

Nicholas Persak Leach

A thesis submitted in partial fulfillment of the
requirements for the Master of Science degree in Civil and Environmental
Engineering
in the Graduate College of
The University of Iowa

August 2015

Thesis Supervisor: Professor A. Allen Bradley

Graduate College
The University of Iowa
Iowa City, Iowa

CERTIFICATE OF APPROVAL

_____

MASTER'S THESIS

_____

This is to certify that the Master's thesis of

Nicholas Persak Leach

has been approved by the Examining Committee for the
thesis requirement for the Mster of Science degree in Civil
and Environmental Engineering at the August 2015 grad-
uation.

Thesis committee: _____
                  A. Allen Bradley, Thesis Supervisor

                  _____
                  Larry J. Weber

                  _____
                  Gabriele Villarini

"Failure is not a reason for you to stop trying. It is actually a reminder that you should keep going." - Unknown

"Success is to be measured not so much by the position that one has reached in life as by the obstacles which he has overcome." - Booker T. Washington

ACKNOWLEDGEMENTS

ABSTRACT

Throughout the years, land use and land cover (LULC) changes have directly impacted the water cycle in Iowa. To better understand the hydrological response to LULC change, the Hydrological Simulation Program - FORTRAN (HSPF) model will be used to qualitatively evaluate the effects of different LULCs and quantify the associated adjustments to model parameters. Anecdotal and observational evidence of the hydrologic response will be employed to define how model parameters should be adjusted to represent certain LULC changes. The hydrologic assessment will be of the Turkey River Watershed located in northeast Iowa, which covers approximately 1,693 square miles.

PUBLIC ABSTRACT

Throughout the years, land use and land cover (LULC) changes have directly impacted the water cycle in Iowa. To better understand the hydrological response to LULC change, the Hydrological Simulation Program - FORTRAN (HSPF) model will be used to qualitatively evaluate the effects of different LULCs and quantify the associated adjustments to model parameters. Anecdotal and observational evidence of the hydrologic response will be employed to define how model parameters should be adjusted to represent certain LULC changes. The hydrologic assessment will be of the Turkey River Watershed located in northeast Iowa, which covers approximately 1,693 square miles.

TABLE OF CONTENTS

LIST OF TABLES

LIST OF FIGURES

Figure

CHAPTER 1
INTRODUCTION

1.1   Background and Motivation

The Midwestern United States produced approximately 35 percent of the world's total annual corn yield in 2014 (*USDA*, 2014). This massive production occurred because the Corn Belt of the Midwest experienced one of the most dramatic and complete landscape conversions from native perennial ecosystems to microculture annual cropping systems during the mid 1800's. The land use and land cover (LULC) change occurred at an astonishing rate over the first three decades of European settlement in Iowa. This was due to the fact that prairies, which were prevalent in Iowa, were much easier to convert to agricultural lands (*Hernandez-Santana et al.*, 2013; *Wehmeyer and Weirich*, 2010). Over the years, these LULC changes have directly impacted the hydrological cycle and streamflow quality, particularly in Iowa. The increase in agricultural lands (mostly corn and soybean) has directly led to the increase in annual runoff and streamflow in Iowa. In order to understand these hydrological changes to LULC, a mathematical model will be developed to simulate the changing hydrology. Understanding these hydrological processes will qualitatively assess the effects of different types of land use and land covers and quantify the associated adjustments to model parameters.

1.2   Study Objectives

There are two different types of hydrologic models, lumped (low resolution) and distributed (high resolution) based models. The lumped model represents hydrologic processes with equations based hydrologic laws or empirical relations. As where the distributed (differential or physical) model incorporates conservation of mass, energy, and momentum, the lumped models are unable to properly account for natural phenomena at a localized scale (*Arnold et al.*, 1998). The lumped model is a practical way to substitute for more complex, distributed processes while preserving the main feature of the system at larger scales. This is portrayed in this study of the Turkey River Watershed. Lumped models preserve the average features of the natural phenomena but do not specifically describe the spatial and temporal variability (*Ponce and Hawkins*, 1996). Hydrological Simulation Program — FORTRAN (HSPF), a lumped parameter model, will be used to study the Turkey River Watershed located in the northeast part of Iowa. The Environmental Protection Agency (EPA) was responsible for the development of the mathematical model HSPF to simulate hydrologic and water quality processes in natural and man-made water ways. The objectives of this study will be to evaluate how well the continuous simulation model HSPF can predict the water cycle and flood hydrology using LULC as driving factors; assess trends in streamflow and determine whether land use or climate change play a role; and lastly, use HSPF to run two hypothetical flood mitigation strategies, comparing the continuous HSPF model results with a event based simulation model HEC-HMS used in the Hydrologic Assessment of the Turkey River Watershed report.

1.3   Overview

This analysis of the Turkey River Watershed is one of four watersheds studies part of Iowa Watershed Projects (IWP). The report, Hydrologic Assessment of the Turkey River Watershed (HATRW), was previously completed using event based HEC-HMS model. Some of the same information used for the HATRW report is used for this study. The four study watersheds for the IWP can be seen in Figure 1.1. IWP is created in part due to the devastating flood of 2008, which brought catastrophic social and economic damages to 85 of Iowa's 99 counties. After the flood, the federal government declared the 85 counties as federal disaster areas. This lead to federal funding from the United States Department of Housing and Urban Development (HUD) to the state of Iowa for watershed flood mitigation projects. The IWP was created and its purpose is to plan, implement, and evaluate watersheds to lessen the severity and frequency of flooding in Iowa (*IFC*, 2014). The Iowa Flood Center (IFC) at the IIHR - Hydroscience & Engineering at the University of Iowa is responsible for the study. Funding for this study came from the HUD federal funding.
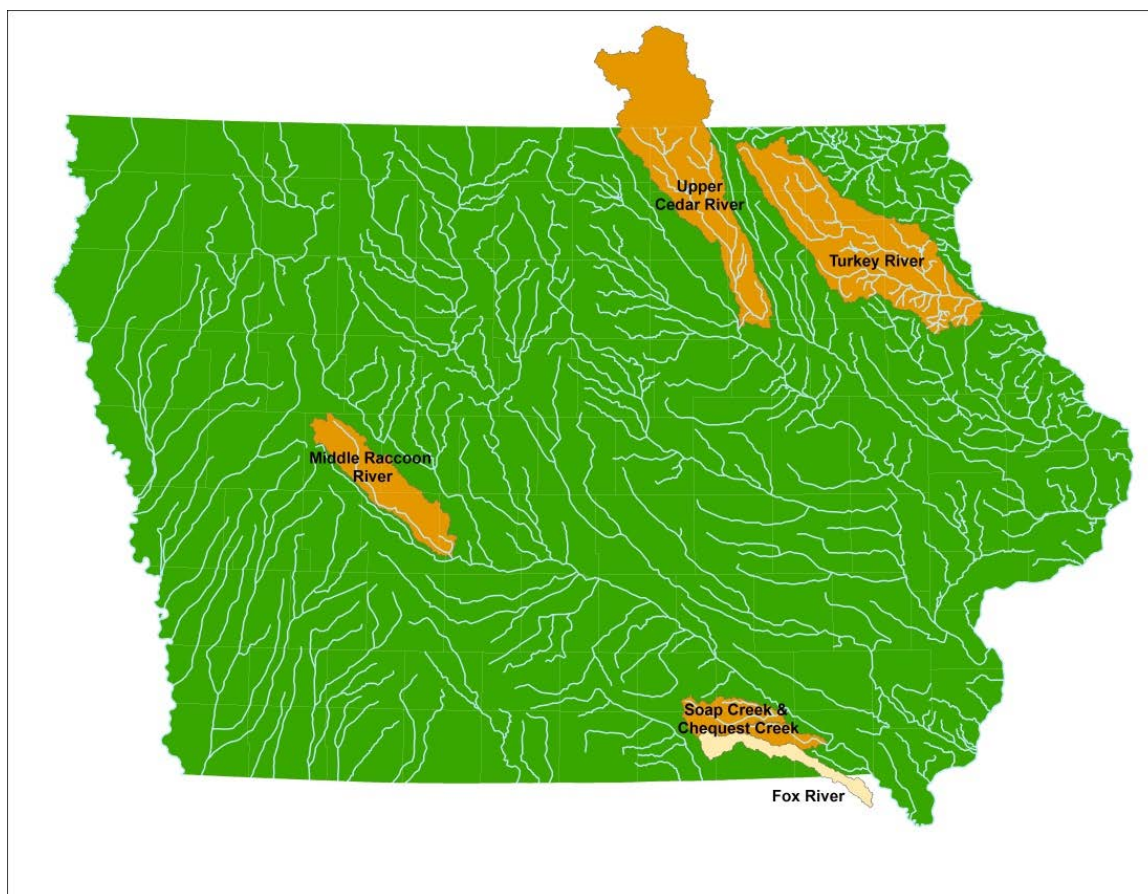
Figure 1.1: Iowa Watershed Project study areas. The Turkey River Watershed is located in the northeast corner of Iowa just east of the Upper Cedar River (*IFC*, 2014).

CHAPTER 2
LITERATURE REVIEW

2.1   Introduction

For centuries, humans have been altering the natural landscape for reasons such as agriculture (food) and shelter (urban development). Agricultural development has expanded to a point where it has become a growing concern, particularly in relation to rainwater runoff. Increased runoff leads to greater amounts of water in rivers and streams, producing high peak flows and flooding. The Midwest, especially Iowa, has seen catastrophic flooding, which brings major economic losses, as seen in 1993, 2008, and most recently in 2013.

Both social and economic factors are affected when discussing the consequences of flooding. The social aspect is affected when urban development becomes inundated. For example, in 2008, the city of Cedar Rapids had to be evacuated due to record setting water levels in the Iowa River. The economic aspect is important when the flood water damages residences, agriculture, businesses, and transportation. The 2008 flood cost upwards of 2 billion dollars in damages (*Linhart and Eash*, 2010). A report from the KCRG-Television Station reported that both, Spillville and Elkadar, which are within the Turkey River Watershed, saw significant flood waters. Spillville lost a 1 year old bridge on Iowa Highway 24 and Elkadar saw damages exceeding 8 million dollars.

Due to the Midwest's continuously changing hydrology, determining whether

increased streamflow/flooding is due to increased precipitation or increased agriculture is an important aspect to understand. In Chapter 7, a hydrologic analysis is presented for the Turkey River Watershed to determine whether increased streamflow/flooding is due to increased precipitation, increased agriculture, or both. This chapter will review previous hydrologic watershed model studies on the issue of land use and land cover changes.

2.2 Hydrologic Watershed Studies

The potential for agricultural land use change to reduce flood risk in a large watershed

The Raccoon River has seen its fair share of flooding. In 1993, flood waters overtopped a water treatment facility levee in Des Moines, leaving the region without water for 19 days. The economic losses totaled an estimated 152 million dollars in flood damages. Then again in 2008, the Raccoon flood waters inundated the facility and caused significant damage. A hydrologic study was performed for the Raccoon River Watershed, which determined the effects of different land uses for the intensely farmed watershed to assess the downstream flood risk using Soil and Water Assessment Tool (SWAT). Agricultural lands comprise 76% of the Raccoon River Watershed and a baseline was developed to model current land uses (*Schilling et al.*, 2008). Simulations were then conducted at varying levels of perennial vegetation to reduce flood risk. Results from the 19 year SWAT simulation showed converting 100% of the cultivated lands to switchgrass decreased flood events by 50%. Even converting

half of the landscape to switchgrass or extending crop rotations reduced flood events by 25-35%. In addition, it was found that frequency of severe floods decreased with the conversion of landscape to perennial grasslands and alfalfa. This study showed that converting all or even some of the cropland to perennial vegetation had major effects on reducing flooding potential (*Schilling et al.*, 2014).

Relative importance of climate and land surface changes on hydrologic changes in the US Midwest since the 1930s: Implications for biofuel production

Another study by *Xu et al.* (2013) evaluated 55 watersheds in the Midwest. They were evaluated based on sensitivity of changes to annual streamflow and baseflow with climate and land surface changes using an elasticity (sensitivity) evaluation method. This study used conceptual and empirical methods (e.g Trend Analysis and Climate Elasticity) to separate the contributions of changes in land surface and climate from hydrologic changes at large scales. In contrast, the physically based hydrologic models (e.g SWAT and HSPF) are difficult to apply to a large number of watersheds simultaneously because they rely on parameters and are structurally dependent. The study quantified the relative contribution of changes in land surface and climate (anthropogenic climate change) to hydrological changes, particularly to different components of the hydrologic cycle like streamflow and baseflow. The term, climate, describes precipitation and potential evapotranspiration changes. It was found that streamflow significantly increased in 35% of the watersheds and baseflow increased in 58% of the watersheds. Overall, climate change rather than LULC

changes was the major driver for increased streamflow when climate variability occurred. However, baseflow was found to be affected by LULC changes more than climate change even when there was a significant variability in climate. Interestingly enough, 45% of the watersheds that showed no significant trend in climate but a significant increase in streamflow showed that LULC changes significantly impacted the flow processes within these watersheds. In summary, watersheds with no significant trends in climate variability but with significant flow trends provided enough evidence that the Midwest LULC changes significantly impacted flow processes (*Xu et al.*, 2013).

2.3   Chapter Summary

Agriculture is a necessity, however, it brings with it an increased water yield and nutrient runoff. That is why flooding will always be a problem when soils become less permeable and natural landscapes become altered. Hydrologic modeling provides insight on what causes the flooding and whether its associated with increases in precipitation or increases in agriculture or both. It is able to capture high flood risk areas and incorporate theoretical flood prevention tactics like BMP's (Best Management Practices) or altering the annual cropping systems back to their native perennials. Continued research should and will continue on flood mitigation practices throughout the world, specifically here in the United States, which has a major task in providing the world with over a third of its corn market. Hydrologic modeling is a very inexpensive method of studying potential flood mitigation strategies. Within this study,

a hydrologic model using HSPF will be performed on the Turkey River Watershed.

CHAPTER 3
TURKEY RIVER WATERSHED HYDROLOGY

3.1   Introduction

This chapter illustrates the facts about the water cycle and flood hydrology of the Turkey River watershed based on historical observations. The historical records for precipitation and streamflow are examined to describe how much precipitation falls, how that water moves through the landscape, and when storms typically produce river flooding.

3.2   Hydrology of the Turkey River Watershed

The Turkey River Watershed drains 1,693 square miles (mi^2) of the northeast corner of Iowa in the Iowan Surface and Paleozoic Plateau region. Precipitation measurements are either available from stations within the watershed or in close proximity just outside the watershed. Streamflow measurements are available at the long record from the U.S. Geological Survey (USGS) stream-gage at Garber (USGS 05412500 Turkey River at Garber, IA).

3.2.1   Statewide Precipitation

Iowas climate is marked by a smooth transition of annual precipitation from the southeast to the northwest. The average annual precipitation reaches 40 inches in the southeast corner, and decreases to 26 inches in the northwest corner. Over the Turkey River Watershed, using the rain gauge data from eleven meteorological

stations, the mean annual precipitation is 33.5 inches.

3.2.2   The Water Cycle of the English River

Of the precipitation that falls across the Turkey River Watershed, the water either evaporates into the atmosphere or drains into rivers and streams. Table 3.1 shows the partitioning of precipitation among these components.

1948-2012	Depth (inch)	Percentage %
Precipitation	33.5	100.0%
Evaporation	23.7	70.8%
Baseflow	6.7	20.0%
Surface Flow	3.1	9.2%

Table 3.1: Annual water cycle for the Turkey River Watershed. The components are shown as a depth (in inches) and as a percentage of average annual precipitation (100% of the water).

Evaporation: In the Turkey River Watershed, the majority of water leaves by evaporation, as in other Iowa watersheds. The water evaporates either directly from lakes and streams, or by transpiration from crops and vegetation. Evaporation accounts for about 70.8% of precipitation.

Surface Flow: The precipitation that drains into streams and rivers can take two different paths. During the wet periods, some water quickly drains across the land surface and causes streams and rivers to rise in the hours or days following the storm. This portion of the flow is often called surface flow, even though some of the

water may soak into the ground and discharge later, like in tile drainage systems. In the Turkey River Watershed, surface flow accounts for about 9.2% of precipitation.

Baseflow: The water that is left over after evaporation and surface flow is baseflow which drains into streams and rivers. Baseflow takes a slower path because it first infiltrates into the ground, then percolates down to the groundwater, and then the groundwater slowly moves towards a stream or river. The groundwater eventually reaches the stream or river maintaining the flows in a river during extended dry periods. This portion of the flow is often called baseflow. In the Turkey River, baseflow accounts for about 20.0% of precipitation.

Additionally, the soil type and the watershed's geology helps determine the partitioning of precipitation runoff, whether into surface flow or baseflow. Within the Turkey River Watershed more water is able to reach the river and streams through baseflow rather than surface flow. The ratio of baseflow to surface flow is 2.16.

3.2.3   Monthly Water Cycle

The Turkey River Watershed cycle for average monthly precipitation and streamflow is typical of Iowa watersheds as seen in Figure 3.1. Precipitation is always at its lowest in the winter months in the form of snow, which can accumulate within the watershed until it melts. Spring is marked by an increase in precipitation plus the melting of accumulated snow during the winter months. The spring months also have some of the lowest evaporation periods before growing season begins. These factors combined produce the high springtime streamflows.
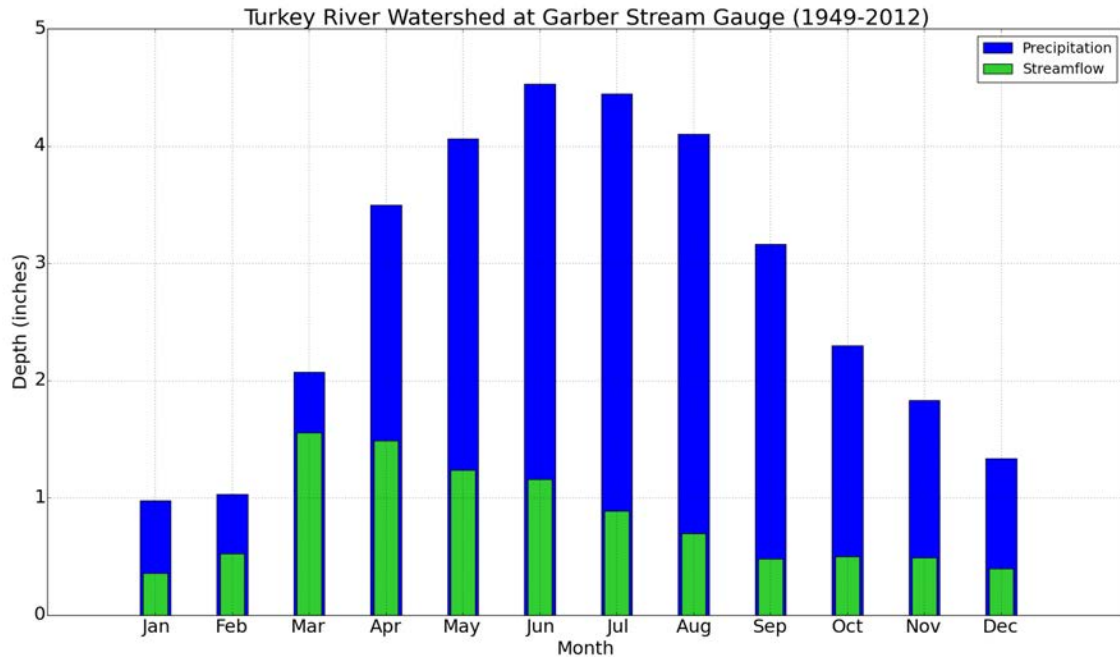
Figure 3.1: Monthly water cycle for the Turkey River Watershed. The plots show the average monthly precipitation (in inches) and the average monthly streamflow (in inches). The average monthly estimates for precipitation and streamflow are based on a 64-year period (1948-2012).

Within Figure 3.1, the watershed has different peaks for streamflow and precipitation. The peak for monthly streamflows happen in early spring (March), as snow accumulation melts rapidly. The peak for monthly precipitation occurs in late spring/early summer (June), for precipitation as crops and vegetation evaporate more and more water as the summer months approach. Moisture within the soil becomes depleted and the average monthly streamflow decreases even though average monthly precipitation amounts remain relatively high.

3.3 Flood Climatology

Figure 3.2 shows the annual maximum peak discharges, for the largest stream-flow observed each year, and the calendar day of occurrence for the Turkey River Watershed. Only those peaks greater than the average annual maximum are shown. The average annual maximum, also known as the mean annual flood, is a common threshold for "flooding". The size of a river's channel is often closely related to the mean annual flood. The results shown in Figure 3.2 are a proxy for the flood events that have occurred over the historical record. Note that in the 95 years of record, flood events occurred in 36 years or roughly 38% of the years.

The flood flow on the Turkey River Watershed have a distinct seasonal pattern. The majority of floods occur between February and late August. This period defines the "flood-season" for most Iowa streams. Only three, out of 36 floods occurred outside this season in the Turkey River Watershed at Garber. Some events occur in late-winter and early-spring where these maximums may be associated with snow melt, rain on top of snow events, or heavy spring rains when soils are often near saturation. Still, the largest annual maximums tend to occur in the summer season, when the heaviest rainstorms occur. Also note that 14 out of 36 floods occurred in the 3-month period between May and July.
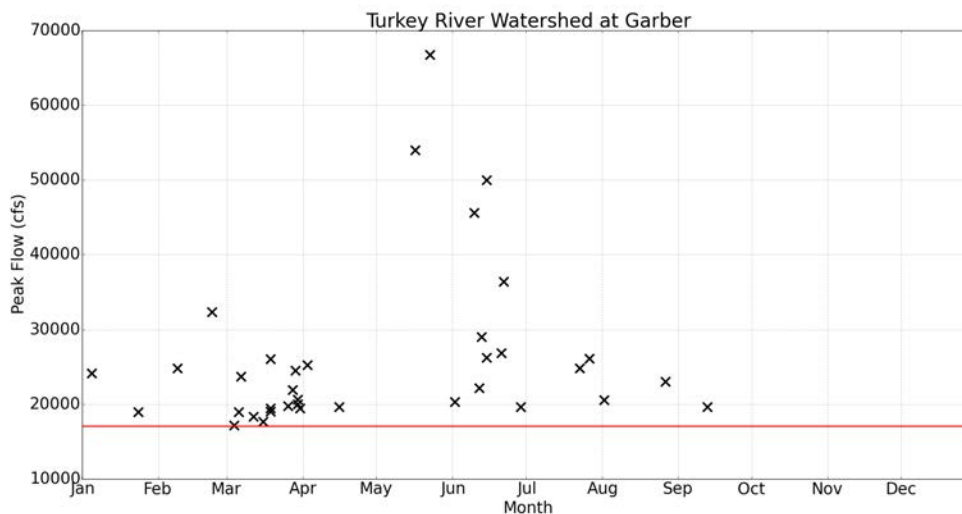
Figure 3.2: Annual maximum peak discharges and the calendar day of occurrence for the Turkey River at Garber (USGS 05412500). The plots show all annual maximums greater than the mean annual flood (horizontal line). The annual peaks are for the period of record from 1914 to 2014.

3.4 Chapter Summary

Within this chapter, the Turkey River Watershed's hydrology is reviewed. The annual mean precipitation for the Turkey River Watershed is approximately 33.5 inches. Of that precipitation, approximately 70.8% leaves through evaporation, 20.0% becomes baseflow, and 9.2% travels as surface flow (runoff). The highest amount of precipitation occurs during the May, June, and July months even though March is the time when the Turkey River receives the highest streamflows. This is partially due to precipitation but the majority is due to snow melt. After March, streamflow slowly decreases in April through August. It then remains fairly constant throughout September into February. Flood season occurs between February and late August

with May, June, and July producing the largest flood events.

CHAPTER 4
CONDITION WITHIN THE TURKEY RIVER WATERSHED

4.1   Introduction

This chapter gives a brief background on the current geology, soil classes, topography, land uses, and how they will be represented in the HSPF model of the Turkey River Watershed. The Turkey River Watershed is a HUC8 (HUC8 07060004) watershed located in the northeast corner of Iowa. HUC8 is an eight-digit Hydrologic Unit Code (HUC) from the U.S. Geological Survey (USGS) Watershed Boundary Dataset (WBD). WBD is a nationally consistent data set for watersheds at local, regional, and national levels. It establishes a base-line drainage boundary accounting for all land and surface areas. Depending on the size of the watershed, it is classified into 6 levels (2-, 4-, 6-, 8-, 10-, 12-digit HUCs) (*FGDC*, 2002). The smaller the hydrologic unit code the larger the watershed. The drainage area of the Turkey River Watershed is roughly 1,693 square miles (mi^2). The watershed falls across eight counties and encompasses two rivers, the Turkey and the Volga Rivers. Figure 4.1 displays where the Turkey and Volga rivers are in relation to each other. The flows patterns of both rivers flow south/southeast into the Mississippi River.

4.2   Geology & Soils

The Turkey River Watershed is split into two geologic regions, Iowan Surface and Paleozoic Plateau. Iowan Surface is located in the northeast part of the Turkey River Watershed and is dominated by flat terrain created by the last glacial period.
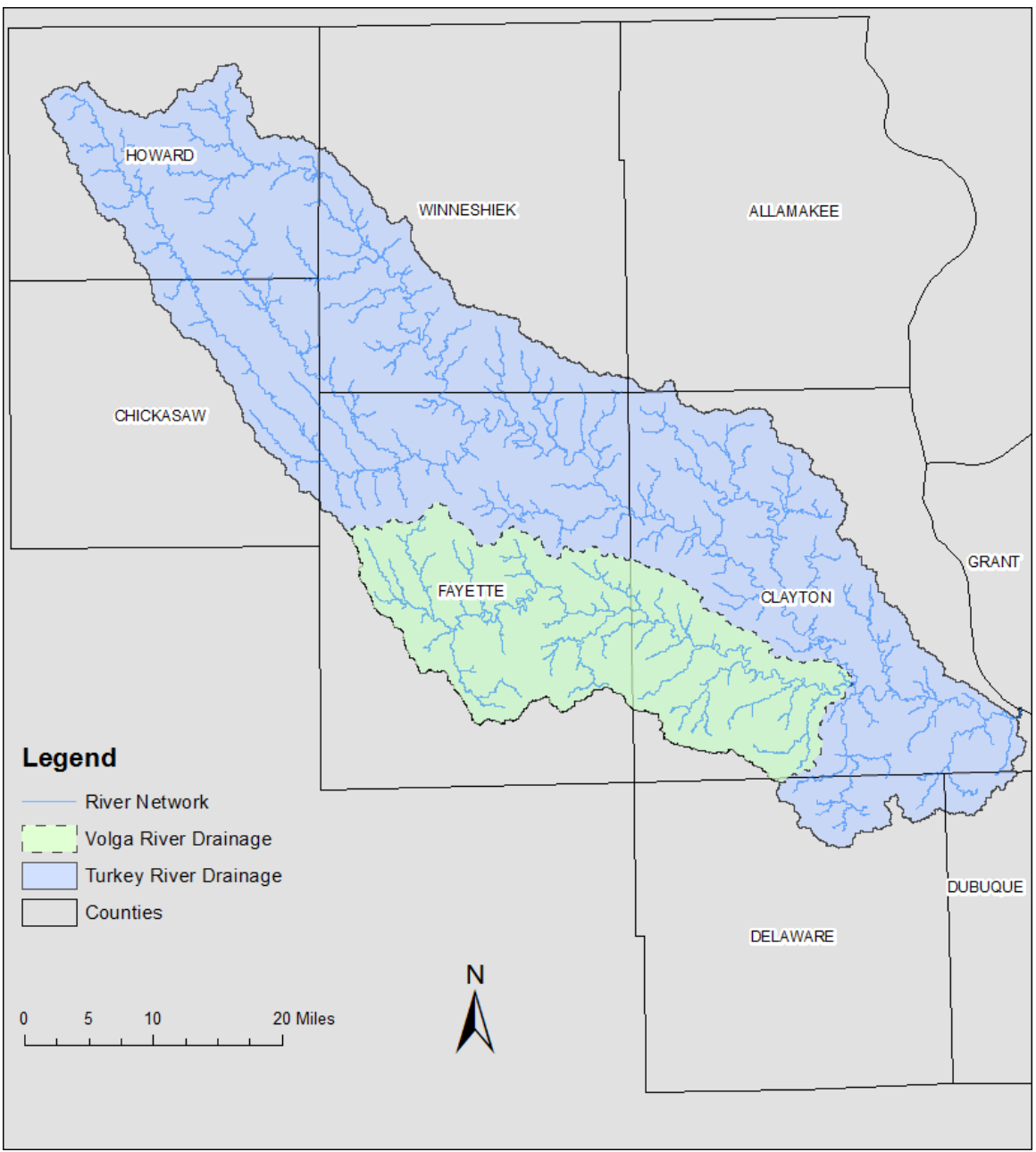
Figure 4.1: The Turkey River Watershed (HUC8 07060004), drains 1,693 mi^2. The Volga River is a major tributary within the Turkey located in teal.

The Paleozoic Plateau region, also called the drift-less area, is very hilly with deeply carved river valleys creating bluffs, waterfalls, and rapids. Figure 4.2 displays both the Iowan Surface and Paleozoic Plateau regions. The Iowan Surfaces occupies about 43% of the entire watershed as where the Paleozoic occupies roughly 57%.

Soils are classified into four Hydrologic Soil Groups (HSGs) by the Natural Resources Conversation Service (NRCS). They are based on the soil runoff potential. The four classes are A, B, C, and D, where A soil class has the lowest runoff potential and D soil class has the highest runoff potential. There are also dual soil classes like A/D, B/D, and C/D which are assigned to certain wet soils or shallow groundwater tables. For example, A/D soil group would have A soil runoff potential if the shallow water table were to be drained but D soils if was not. USDA-NRCS National Engineering Handbook, Part 630-Hydrology, Chapter 7 provides more on the HGS (*NRCS*, 2004). The Iowan Surface primarily B, C, B/D, and C/D soils groups; the Paleozoic region is primarily C type soils. Table 4.1 breaks down the soil distribution for the entire Turkey River Watershed and Figure 4.3 shows the soil distribution of the Turkey River Watershed. The data came from USDA-NRCS 2012 Web Soil Survey (WSS) the digital soils data SSURGO (*IFC*, 2014). For modeling the watershed with HSPF, the soil type of the Iowan Surface is assumed to be B soils and for the Paleozoic region the soil type assumed to be C soils. The classes are chosen based off majority within each region.
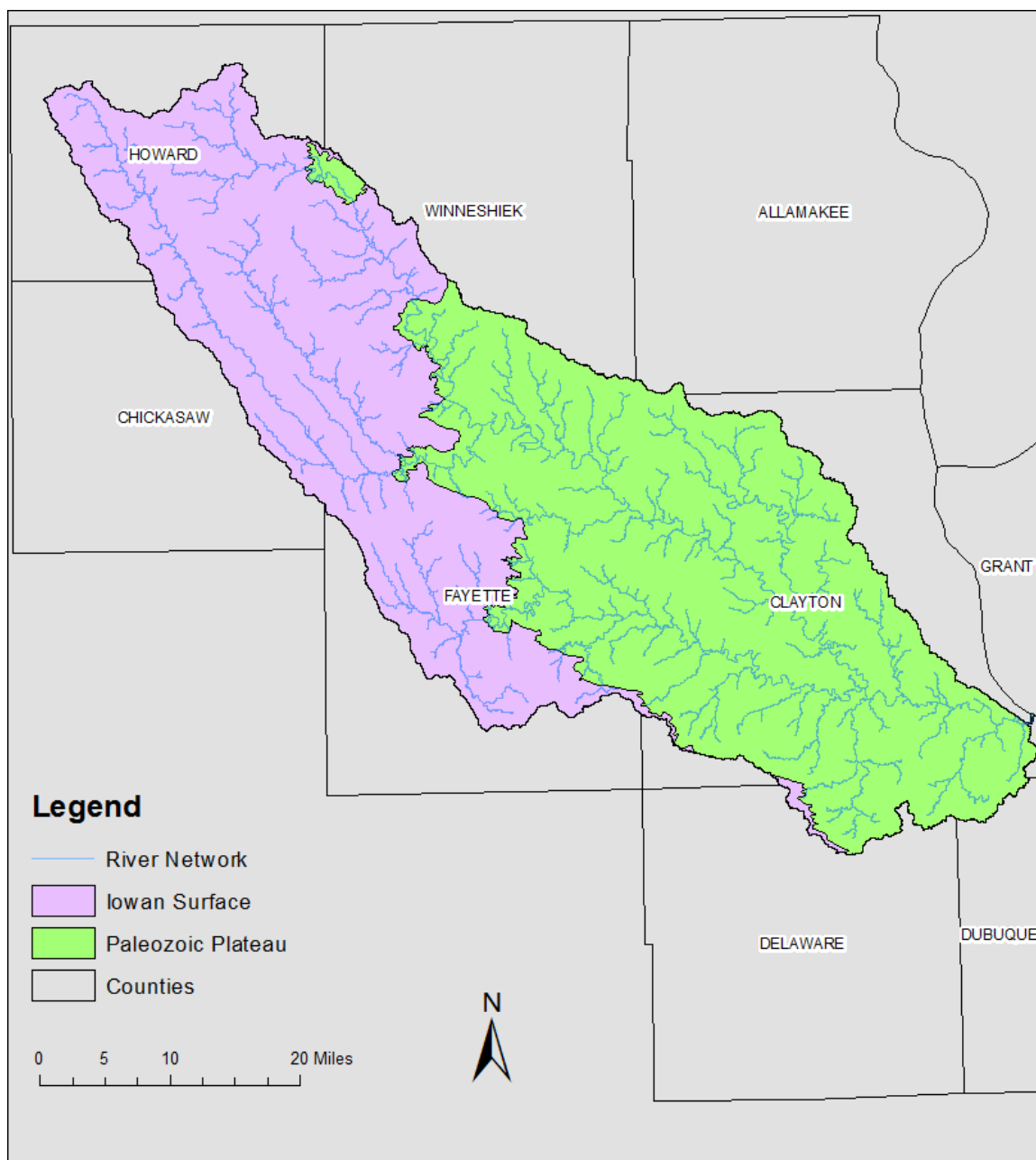
Figure 4.2: Landform Regions of the Turkey River Watershed. Purple region is the Iowan Surface and the green regions is the Paleozoic Plateau.
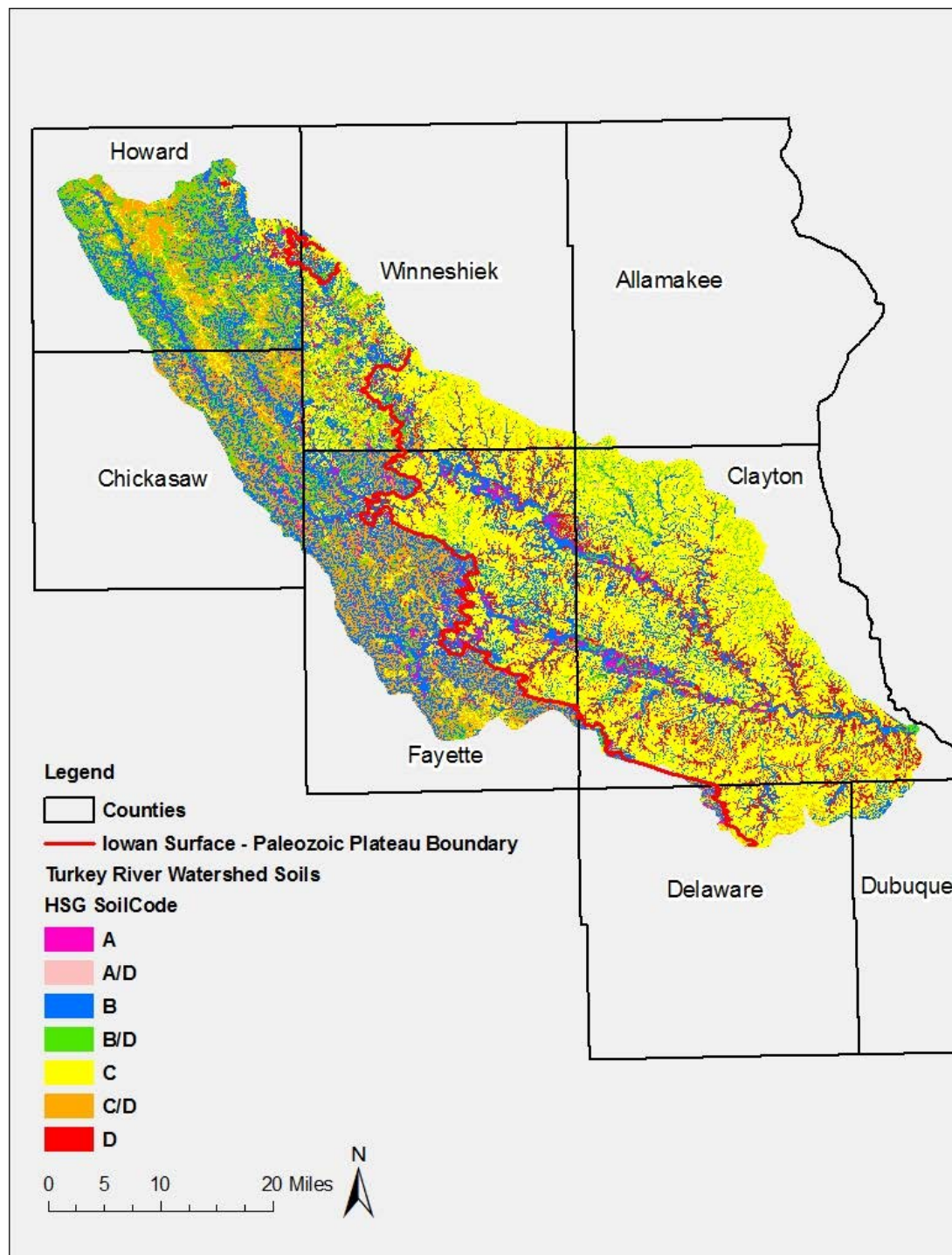
Figure 4.3: Turkey River Watershed soil groups (2012) (*IFC*, 2014). Red line is the Iowan Surface and Paleozoic Plateau divide.

Iowan Surface		Paleozoic Plateau	
HSG	%	HSG	%
A	3.9	A	2
A/D	0.1	A/D	0
B	33.1	B	17.6
B/D	16.4	B/D	4.4
C	14.3	C	62.9
C/D	30.6	C/D	2
D	1.6	D	11.1

Table 4.1: Soil class breakdown of the Turkey River Watershed. Table is from the Hydrologic Assessment of the Turkey River Watershed (*IFC*, 2014).

4.3 Turkey River Watershed Topography

Howard, Chickasaw, and parts of Winneshiek and Fayette counties all have moderately low slopes with flat terrain within the Iowan Surface. Streams all flow south/southeast within in this region. When streams cross into the Paleozoic Plateau region, Clayton, Delaware, Dubuque and parts of Winneshiek and Fayette countines, the slopes becomes greater with carved valleys. From upstream to downstream the elevation ranges from approximately 1400 ft to 600 ft above sea level. The topography map can be seen in Figure 4.4

4.4 Turkey River Land Use

Land use in the Turkey River Watershed is dominated by cultivated crops (corn and soybeans) at approximately 56% of the total area, followed by grasslands (9%) and pastures (15%). The remaining area in the watershed is about 14% forest, 5% developed land, and 1% open water and/or wetlands (Seen Figure 4.5). Approx-
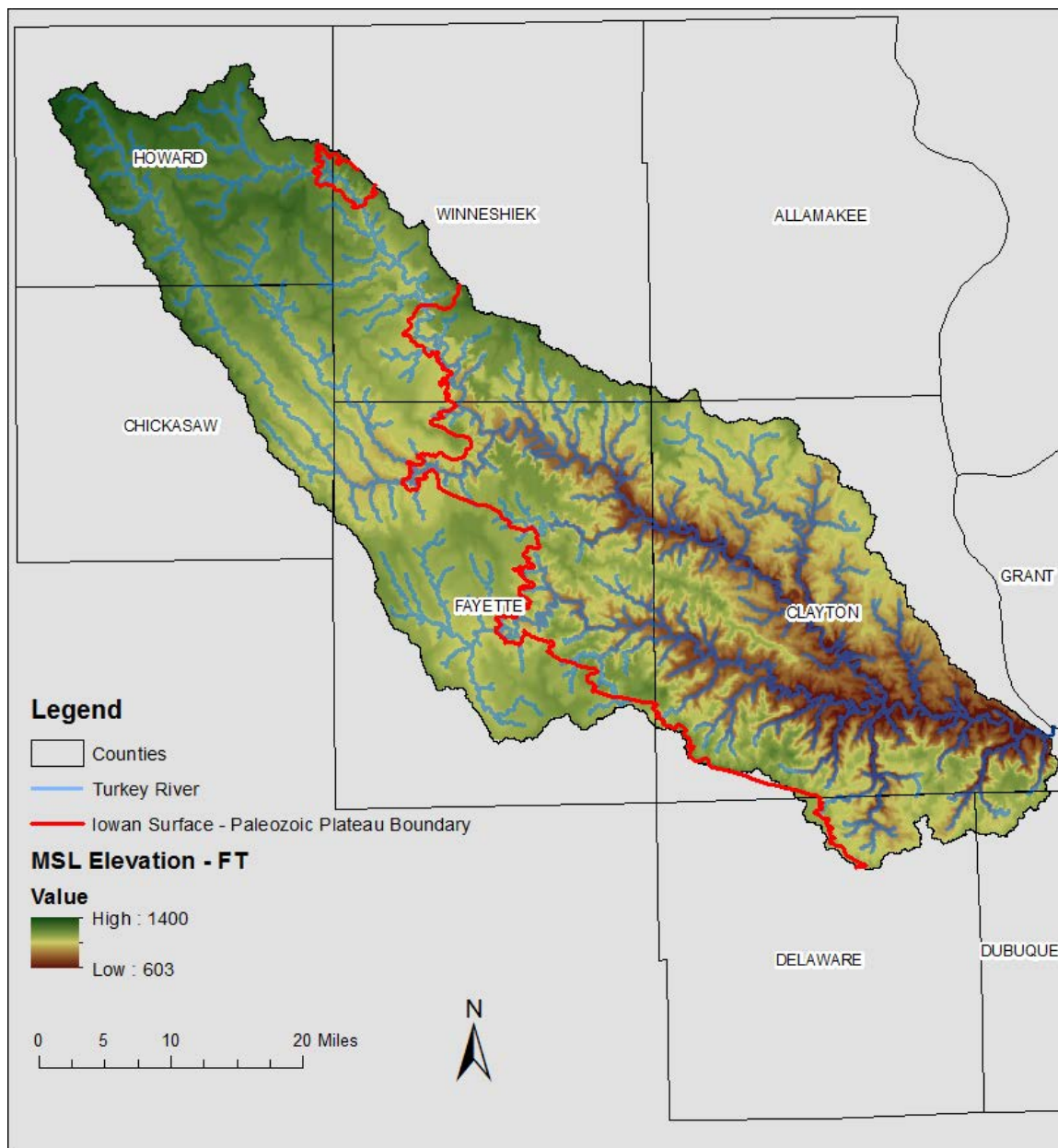
Figure 4.4: Turkey River Watershed elevation map with Iowan Surface and Paleozoic Plateau Boundary in red.

	Crops	Forests	Grasslands	Pastures	Wetlands	Urban
Iowan Surface (B soils)	59%	10%	28%	18%	33%	52%
Paleozoic Plateau (C soils)	41%	90%	72%	82%	67%	48%

Table 4.2: This table shows the breakdown between the two geologic regions within the Turkey River Watershed. Each column represents a distribution (out of 100%) of each land type within the Turkey River Watershed two regions.

imately 91% of the land within the watershed is privately owned (*IFC*, 2014). The 2006 National Land Cover Data (NLCD) Set, which can be seen in Appendix D, is used and is modified to simplify the model conditions. All developed lands where summed into urban development. Deciduous forest, evergreen forest, and mixed forest is summed into Forest. Cultivated lands combined corn and soybean (About a 80-20 spilt between corn and soybean respectively according to the Iowa State Extension and Outreach Ag Decision Maker for Iowa Corn and Soybean County Yields (*Extension and Outreach*, 2015)). Grassland and Pastures have their own classes. Table 4.2 shows how each geologic region differs. The Iowan Surface has a higher percentage of agricultural lands (row crops) of corn and soybean in contrast Paleozoic Plateau has more forests, grasslands, and pastures.

4.5 Chapter Summary

From a hydrologic model perspective with HSPF, the Turkey River Watershed is summarized into 6 different land uses (cultivated lands, forest, pastures, grasslands, wetlands, and urban development) and 2 different soil types (B soils-Iowan Surface
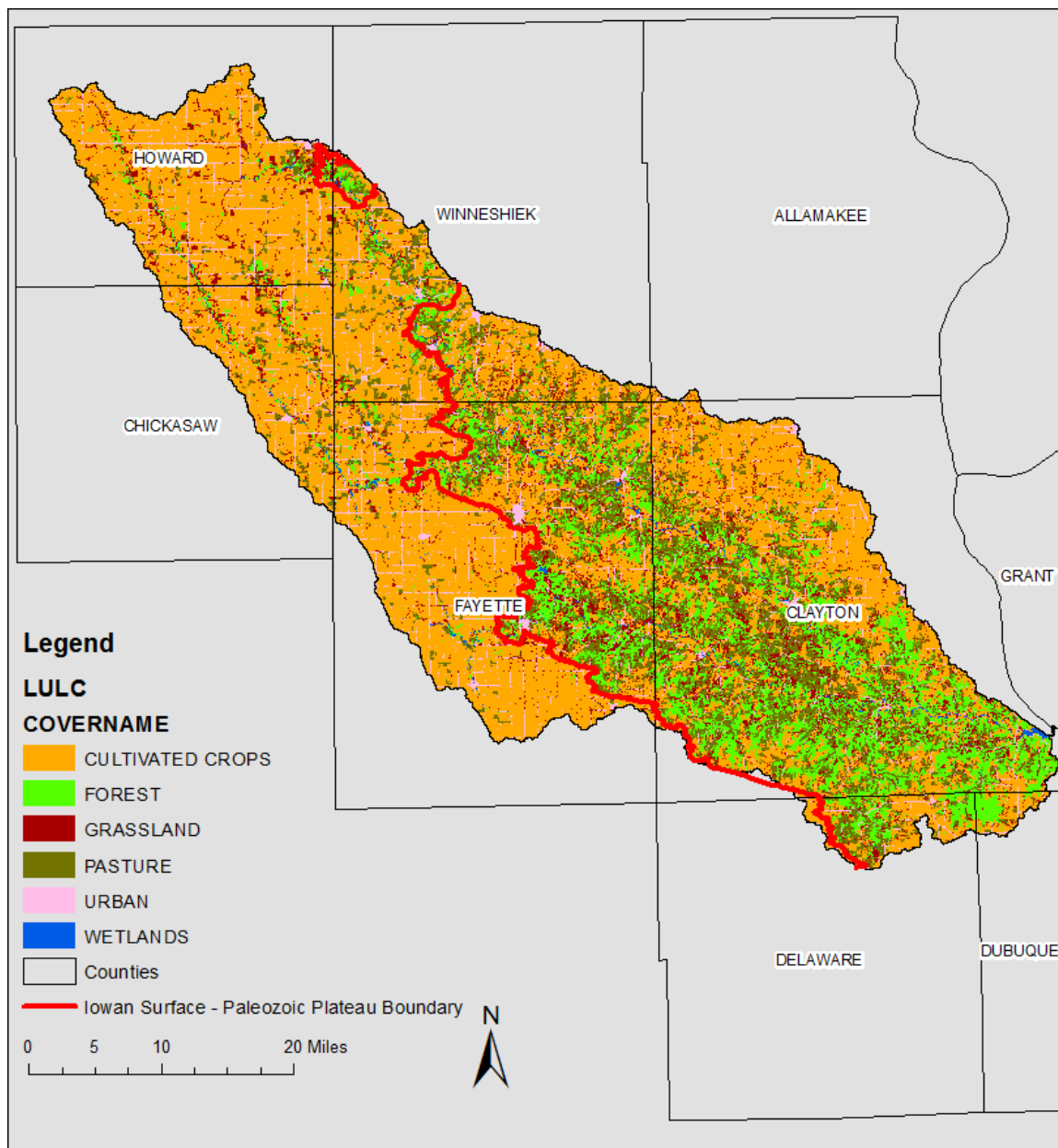
Figure 4.5: Turkey River Watershed LULC map with Iowan Surface and Paleozoic Plateau Boundary in red.

and C soils-Paleozoic Plateau soils). Even though the land uses are summarized they still kept their percent impervious and pervious surfaces (Figure D.3 has all the recommended percentages for impervious and pervious surfaces.). The model would be too complex if all land uses and soil types were used.

CHAPTER 5
TURKEY RIVER HYDROLOGIC MODEL DEVELOPMENT

5.1 Introduction

This chapter provides information on the historical data used for the HSPF model, data processing methods, watershed delineation, details on HSPF model sections, and the simulation process.

5.2 Historical Weather Observation

Historical weather information and historical streamflow observations are required to simulate river flows and and verify the models parameters for the HSPF model of the Turkey River Watershed. Weather information such as precipitation, air temperature, dewpoint temperature, cloud cover, and wind speed are needed inputs to accomplish the simulation of the Turkey River Watershed. Streamflow observations are used for calibrating model parameters and validating the predictability of the model. The weather data sets are downloaded from NOAA's National Climate Data Center (NCDC), the world's largest climate data archive in the United States (*NOAA*, 1995). The streamflow observations are downloaded from the United States Geological Survey (USGS).

To run a simulation in HSPF for Turkey River Watershed precipitation and air temperature are used as weather inputs. NCDC, which supplies the weather inputs, uses the Global Historical Climatology Network (GHCN) for its daily data. The daily data sets are available for all the stations and provide a long and relatively complete

record. The GHCN database addresses the critical need for historical daily records over global land areas (*Menne et al.*, 2012). The GHCN data sets for precipitation and air temperature are from a water year period of 64 years, from October 1, 1948 to September 30, 2012. Precipitation and air temperature data sets come from the eleven meteorological stations (met stations) listed in Table 5.1. The eleven met stations provide a better representation of the watershed because the weather inputs vary spatially. Recorded length, data availability, and location play a role in choosing the met stations.

In Table 5.1 Spillville, McGregor, and Strawberry Point met stations provide hourly precipitation time series data and the other eight provide daily precipitation time series. When hourly or daily time series data sets are incomplete, the Inverse Distance Weighting (IDW) method is used to fill in the missing data points. IDW equates similarity to proximity. In other words, stations that are closer to each other will be more similar than stations farther apart. Stations that are closer to the predicted station have more influence/weights on the predicted value than stations farther away. If missing data are present, three or more of the closest met stations are selected to complete the data from the met station of interest. Once all the hourly and daily data sets are complete, the daily time series are disaggregated to hourly time steps using the three hourly time step (Spillvillle, McGregor, and Strawberry Point) met station precipitation patterns. All stations provide daily maximum and minimum air temperatures. For any missing data the same IDW process is used. The daily air temperature is disaggregated into hourly time steps using a fix daily cycles.

WDMUtil is used to compute the disaggregation from daily to hourly time steps for both precipitation and air temperature data sets . WDMUtil is a tool which allows users to import available weather data into Watershed Data Management (WDM) files and perform a variety of operations such as disaggregation of precipitation and air temperature.(met stations other than the ones listed in Table 5.1 are used and can be seen in Appendix B in Tables B.1, B.2, & B.3 with the same time step.)

Station	Station ID	Latitude (N)	Longitude (W)	Area(%)
Saratoga	IA137410	43.366	-92.366	9.8
Guttenberg	IA133517	42.785	-91.095	9.3
New Hampton	IA135952	43.045	-92.312	2.4
Waucoma	IA138742	43.094	-92.032	13.9
Elkader	IA132603	42.775	-91.453	15.5
Fayette	IA132864	42.850	-91.815	18.2
Postville	IA136766	43.090	-91.558	11.4
Spillville	IA137855	43.205	-91.953	8.2
McGregor	IA135315	43.017	-91.183	2.3
Strawberry Point	IA138009	42.684	-91.535	4.7
Cresco	IA131954	43.389	-92.093	5.1

Table 5.1: Meteorological Station for the Turkey River Watershed

The Thiessen Polygon Method (TPM) is used to segment the met stations in Table 5.1 within Turkey River Watershed. The stations are chosen based on length of data, completeness of data, and the location respected to the Turkey River Watershed. The TPM is a common approach in determining average precipitation over an area and gives a good spatial representation of rainfall. The TPM is a set of polygons

whose boundaries define the area that are closest to each point relative to all other points. The points in this case are the met stations representing a segment of land. The polygon are mathematically defined by the perpendicular bisectors of the lines between all points (*Techniques*, 2012). A station's meteorological data represents the geographical area within the polygon, giving the best meteorological representation of what events actually occur within that area. HSPF uses this information for its simulation by grouping each different kind of land type by it meteorological station. For example the Saratoga station will have different weather inputs for cropland than the crop land for New Hampton Station because the respected areas are associated with different meteorological rainfall events. To generate the Thieseen Polygons, ArcGIS-ArcMap is used. Figure 5.1 shows the outputted Thiessen Polygons for the Turkey River Watershed.

Figure 5.1: The Thissen Polygon Method for the Turkey River Watershed.

HSPF also uses input time series for wind speed, dewpoint temperature, and cloud cover. These data sets are primarily for the winter and into spring months to predict snowfall, snow accumulation and snow melt. The data sets acquired are

at an hourly time step and are measured from the Waterloo Municipal Airport met station, the public station with the longest record closest to Turkey River Watershed. Although the Waterloo station lies outside the Turkey River Watershed, wind speed, dewpoint, and cloud cover vary relatively smoothly in space and remain relativity constant across large areas, so the distance from the watershed is not a major factor.

Wind travel, solar radiation, and potential evapotranspiration are the last three hourly time series inputs HSPF uses for simulation. These data sets, difficult to measured directly, are computed using the previously mentioned WDMUtil. Each of the data sets for this stage of HSPF data collection is calculated differently. Wind travel is calculated using wind speed input. Solar radiation is calculated using cloud cover input. Potential evapotranspiration is calculated based on the Penman Approach (*Penman*, 1948; *Shuttleworth*, 1993a) using weather inputs such as air temperature (Min. and Max. Temperature), dewpoint temperature, wind movement, and solar radiation. Of all the data sets mentioned previously potential evapotranspiration and precipitation are two very important data sets, predicting the overall water balance and storage of water in subsurface terrain for HSPF simulations (*Hummel et al.*, 2001).

5.3 Basin & River Reach Delineation

The Turkey River Watershed is approximately 1,693 square miles and is delineated into 710 subbasins. The subbasins ranged from an average area of 2.4 square miles to the larger subbasins of 7.6 square miles. The 710 subbasins delineation can be

seen in Figure 5.2. The stream network is defined using ESRI ArcGIS and ArcHydro terrain reprocessing creating flow direction and accumulation. The stream network used is the same delineated stream network used as in the HEC-HMS Turkey River Watershed Model for Hydrologic Assessment of the Turkey River Watershed (*IFC*, 2014).
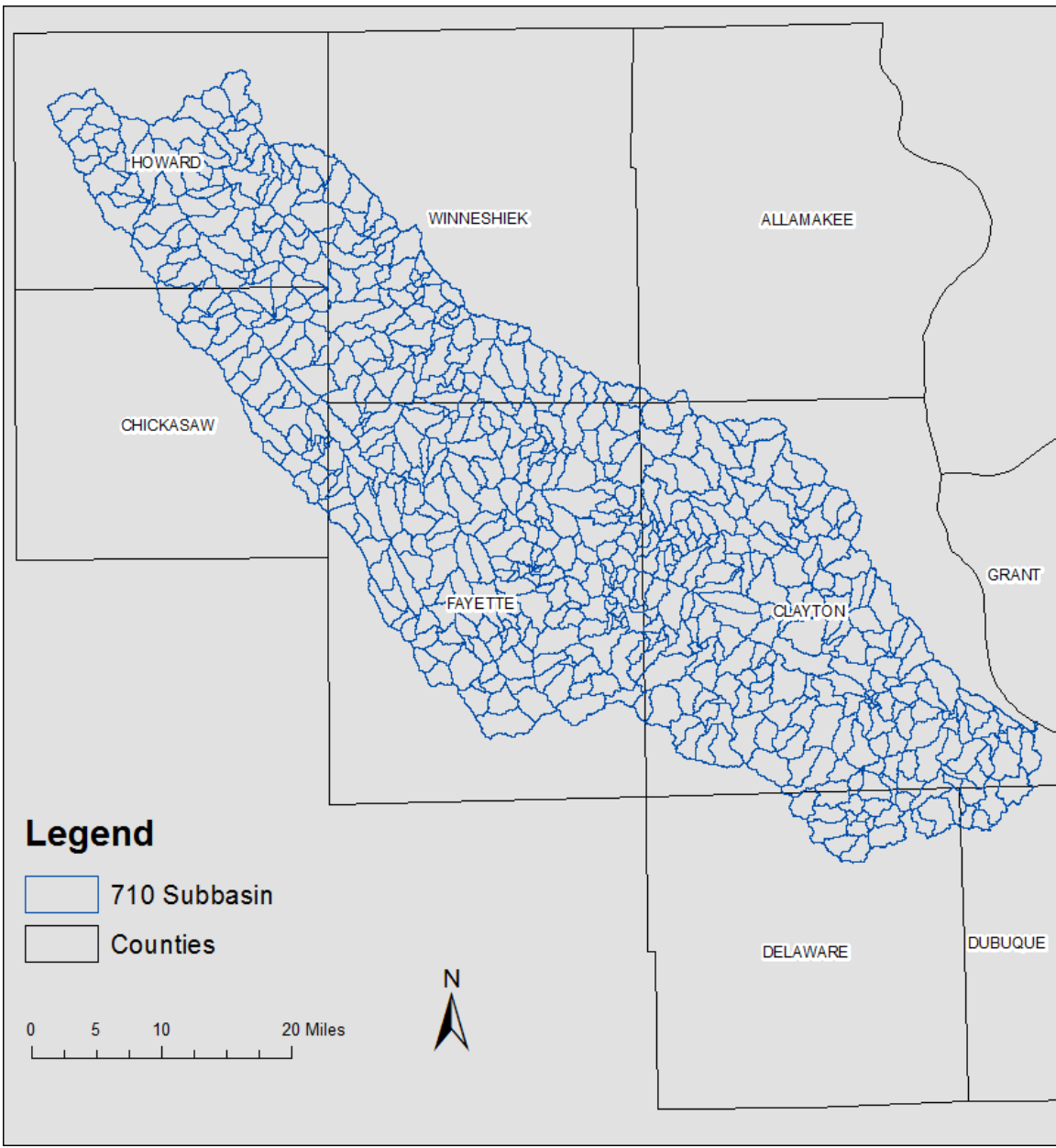
Figure 5.2: The delineated 710 subbasins for the Turkey River Watershed in blue outline (*IFC*, 2014).

5.4 HSPF Model Components

HSPF model was first released by the Environmental Protection Agency (EPA) in 1980. It was a descendant of the Stanford Watershed Model (modeled hydrology), the Non-Point Source (NPS) (modeled water quality), and Agricultural Runoff Management (ARM) (modeled water quality) models. HSPF is a conceptual watershed model where different LULCs are represent by land segments (PERLND & IMPLND) and runoff is routed through the river reach network (RCHRES). Land segments do not need to be homogeneous or contiguous elements. However, all areas are assigned to a unique land segment and are assumed to have a similar average response (*Donigian and Walter*, 1984). Operating HSPF, important modeling sections, and how river reaches are represented will be discussed further in the following sections.

5.4.1 Model Sections

Typically HSPF runs with one User Control Input (UCI) file. The UCI file is responsible for instructing the system to perform the necessary operations called by the user. The UCI file is made of a series of operations called operation blocks (*Bicknell et al.*, 1997). These blocks are broken into two basic categories, application blocks and utility blocks. Application blocks perform simulations of real world watershed processes like hydrologic and hydraulic processes and as well as water quality processes. The utility blocks perform operations that manipulate and analyze time series data created by the application blocks (*AquaTerra*, 2011). Application blocks create time series data for utility blocks used for analysis. An example of application

block is the PERLND block which performs all the pervious land segment hydrologic calculations. An example of utility block is the COPY block used to alter one or more time series data sets whether by adding the data together or multiplying it by a scalar.

The only three active application blocks/sections used within HSPF for the Turkey River Watershed are PERLND, IMPLND, and RCHRES. PERLND and IMPLND sections simulate runoff and water quality from pervious land segments and impervious land segments respectively. The third application block is RCHRES which simulates the movement of runoff and its associated water quality constituents through channels and mixed reservoirs (*AquaTerra*, 2011).

5.4.2 PERLND, IMPLND, and RCHRES Sections

PERLND is the primary application block which simulates snow accumulation, snow melt, the water budget, sediment transport, and water quality constituents on pervious land segments. To simulate these processes, PERLND models the movement of water along three paths. The three paths are overland flow, interflow, and groundwater flow. Each path experiences differences in both time delay and interactions between water and its dissolved constituents. PERLND also includes snow accumulation and snow melt to represent the full range of physical processes affecting the generation of water (*AquaTerra*, 2011; *Bicknell et al.*, 1997).

IMPLND on the other hand models the movement of water from impervious areas like urban landscapes where little to no infiltration occurs. Land processes

like runoff and pollutant runoff move laterally down slope to potentially pervious area, stream channels, or reservoirs. Although IMPLND deals with strictly impervious areas it shares physical processes like snow accumulation and snow melt with PERLND to account for the full range of physical processes affecting water generation (*AquaTerra*, 2011; *Bicknell et al.*, 1997).

RCHRES block is for routing the runoff simulated by the PERLND and IMPLND sections for a single reach. Possible processes that can be modeled in HSPF are hydraulic behavior, water temperature, scouring, inorganic nitrogen and phosphorous balances, pH, carbon dioxide, total inorganic carbon, and alkalinity (*AquaTerra*, 2011). The flow through the RCHRES are assumed to be unidirectional.

5.4.3   Subsections of PERLND, IMPLND, RCHRES

Pervious land segments are simulated in section PERLND and further broken down into the subsection or codes, ATEMP, SNOW, and PWATER. Impervious land segments, simulated in section IMPLND, are categorized into ATEMP, SNOW, and IWATER. Air Temperature for Elevation differences (ATEMP) and snow (SNOW) are sections used for both section PERLND and IMPLND. The only active section for RCHRES is HYDR, which simulates the hydraulic behaviors in a reach or mixed reservoir. Discussed below are the subsections ATEMP, SNOW, PWATER, IWATER, and HYDR for PERLND, IMPLND, and RCHRES.

ATEMP - Air Temperature for Elevation Difference: This section modifies the input air temperature to represent the mean air temperature over the

land segment using:

$$AIRTMP = GATMP - (LAPS)(ELDAT), \qquad\qquad (5.1)$$

where AIRTMP is the air temperature over the pervious land segment (PLS) at the start of the RUN (°F), GATMP is the air temperature at gauge (°F), LAPS is the lapse rate (°F/ft), and ELDAT is the elevation difference between the land segment and the gauge. A correction is used to modify air temperatures when the elevation of the land segment significantly differs from the elevation at the temperature gauge. If precipitation occurs, a wet lapse rate of 0.0035°F per foot difference in elevation is applied. If no precipitation occurs, a dry lapse rate that varies with the time of day is used. A table of hourly dry lapse rates varying between 0.0035°F to 0.005°F is built into the HSPF (*Bicknell et al.*, 1997). Equation 5.1 shows the corrected air temperature:

SNOW - Snow: The SNOW section deals with the runoff derived from snow fall, snow accumulation, and snow melt, which major hydrologic processes occur during the winter and spring months. The energy balance method is used for snow melt simulation. Five meteorological time series are used as input time series at the start of each simulation interval. Air temperature is the deciding factor for snow fall. Apart from air temperature the other four time series needed for each simulated land segment are precipitation, solar radiation, dewpoint, and wind velocity. Cloud cover input is also optional. Five major processes take place once snow accumulates on the

ground. The five are net radiation heat (RADHT), both longwave and shortwave, convection of sensible heat from the air (CONVHT), latent heat transfer by condensation of moist air on the snowpack (CONDHT), heat from rain (RNSHT), and conduction of heat from the underlying ground to the snowpack (GMELTR) (*Bicknell et al.*, 1997). During the simulation process these five have the most influence for melting snow. For more equations and calculations for section SNOW, see the HSPF 12 manual (*Bicknell et al.*, 1997).

PWATER - Simulation of Pervious Land Segment: PWATER is the most important section of PERLND because other sections depend on the outputs from this section. PWATER is used to calculate the components of the water budget primarily to predict the total runoff from the pervious areas. PWATER section is often part of the calibration process because it has a large impact on hydrologic processes and will be discussed further in Calibration Parameters section (*Bicknell et al.*, 1997). Figure 6.1 illustrates the hydrologic processes that are modeled by PWATER.

IWATER - Simulation of Impervious Land Segments: IWATER simulates retention, routing, and evaporation of water from impervious land segments in IMPLND section and is similar to section PWATER of PERLND section. Sections ATEMP and SNOW are both performed the same way for PERLND and IMPLND. However, IWATER does not simulate infiltration or subsurface processes making it a much simpler process than PERLND (*Bicknell et al.*, 1997).

HYDR - Simulation of Reaches and Reservoirs: HYDR section simulates hydraulic behavior in river reaches or reservoirs (RCHRES). The goal in this study is to route reach water throughout the watershed. HYDR section can also be used for studying reservoir behavior and analyzing constituents dissolved in the water but are not performed for this study. The way water is routed is it enters RCHRES through the surface or subsurface. The user assigns time series, such as total flow from previous land segments (PERO) or total surface runoff from impervious land segments (SURO) (PERO and SURO come from PWATER and IWATER), to RCHRES. Evaporation from RCHRES can also be considered when routing water throughout the watershed (*Bicknell et al.*, 1997).

5.5   FTABLEs

To accurately represent stream reaches and reservoirs in RCHRES, the HSPF model uses hydraulic function tables called FTABLEs. The FTABLEs describes the hydrology of a stream reach and/or reservoir by forming a functional relationship between water depth, surface area, water volume, and outflow. Within HSPF the FTABLEs can be automatically generated but often are inadequate in describing the reach or reservoir characteristics (*EPA*, 2007). Each reach will usually have its own FTABLE unless they share the same properties.

In order achieve the most accurate reaches, two regional equations are developed:

$$W_2 = K_w A_{drain}^{\alpha_w} \tag{5.2}$$

and

$$H_{full} = K_H A_{drain}^{\alpha_H}, \qquad\qquad (5.3)$$

where W_2 is the width of the water surface at bankfull, H_{full} is the height of the water profile at bankfull, A_{drain} is the area of the drainage basin, and α_W and α_H are exponents assumed to be 0.6 and 0.4 respectively. The equations are developed to describe the relationship between bankfull geometry and contributing drainage areas. Equations 5.2 and 5.3 take a power law form with an assumed exponent. The scalar coefficients are calibrated by passing a best-fit curve through observations of bankfull geometry made at available from USGS stream gauge data.

The curves are then validated with similar data from additional sites and then applied to the drainage basins of user-defined reaches to obtain channel height and width at bankfull. The Geometry characteristics of the Turkey River Watershed basin constituents can be derived from the regional power equations for a given drainage area. These bankfull geometries are used to create FTABLEs describing the discharge at certain depths in each reach.

5.5.1   Calibration of Geometric Assumptions

The channels are assumed to have a compound trapezoidal cross-section, as shown in the Figure 5.3, where the data below, including bankfull, is within the channel and data above bankfull is in the floodplain.
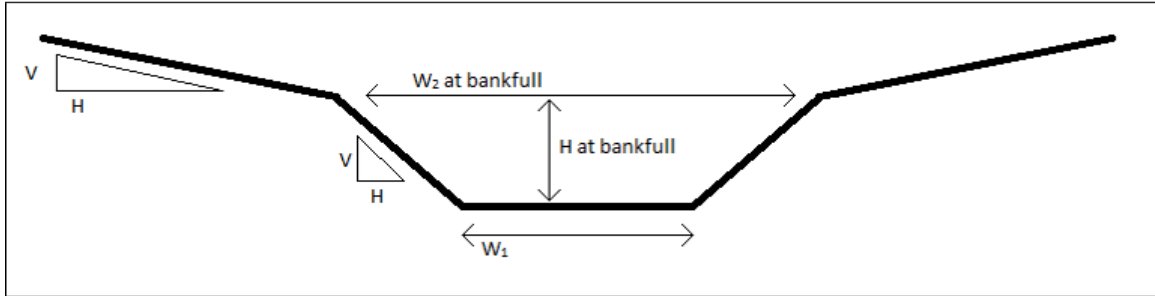
Figure 5.3: Geometric channel assumptions for FTABLEs.

The area of a trapezoid (A) is:

$$A = \frac{(W_1 + W_2)h}{2},$$

(5.4)

where W_1 is the bottom width, (W_2) is water level width, and depth of the water (h) in Equation 5.4. The top width of a trapezoidal channel can be be expressed as:

$$W_2 = W_1 + (2mh),$$

(5.5)

a function of the bottom width, where m is the vertical slope, or the inverse of $H : V$. In HSPF, an initial horizontal to vertical, $H : V$, bank slope ratio for the channel is assumed to be 1 for the channel and 0.1 for the floodplain.

Available historic and current discharge and channel properties are extracted from the USGS Surface Water Field Measurements database. Good calibration sites have more than 20 data entries and such sites tend to be well-maintained. The well-maintained sites tend to be closer to populated areas and in operation for more than

five years. Plots of Gauge Height vs. Width and Gauge Height vs. Cross Sectional Area (Figure 5.4 and Figure 5.5) are examined for graphical indicators to find bankfull characteristics using the USGS Surface Water Field Measurements database. For the site near Garber, Iowa in Figure 5.4, the linear region roughly from 150 to 200 feet is assumed to correspond to the side slope of the channel. The total width will be a function of the bank slope on both sides of the channel. Since the channel widens 50 feet in about 10 feet of stage (going roughly from 150 feet to about 200 feet on the x axis and about 5 feet to 15 feet on the y axis), the total horizontal gain from the bank slope is 50 feet (25 for each side of the channel). This means the side slope horizontal to vertical ratio, (H:V) is 2.5, not the assumed 1 in HSPF. The assumed horizontal to vertical ratio of 2.5 was also agreeable with other gauge sites. The gauge height vs. cross sectional area plot in Figure 5.5 has two distinct linear regions. These two regions are assumed to correspond with the change in side slope where the channel transition from bankfull to the floodplain. This change in slope causes the cross-sectional area to vary less with water depth in the floodplain because the land is not as steep. The intersection in these two regions indicate the depth at which bankfull occurs, which is roughly around 10 feet. The trend-line is shifted downwards for both regions. Theoretically at zero gauge height there should be zero channel area but this is not the case. This is partially due to measurement error (all data points are field measurements) and possibly bed-erosion of the channel over time. This is why the trend-line was shifted downwards to have a conservative estimate of bankfull conditions. Sites that had enough data to see trends but not enough to determine
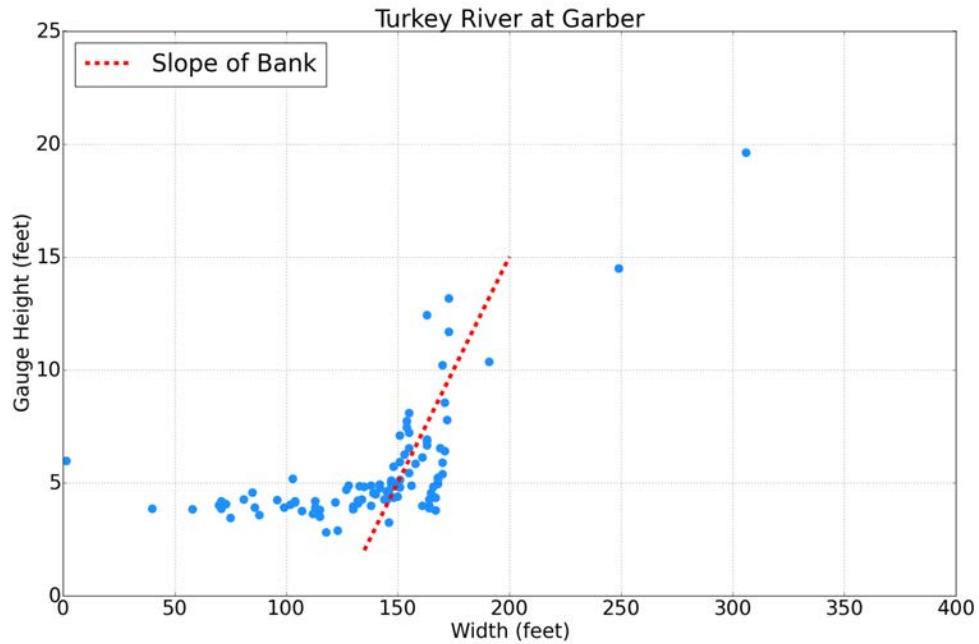
Figure 5.4: Turkey River at Garber, Iowa stage height vs. channel width.

the geometric characteristics were plotted and then later used to validate the final regional power relation.

5.5.2 Validation of Geometric Site Assumptions

Geometric properties determined graphically are validated by comparing a plot of the cross-sectional area vs. discharge to values determined through using the slope-area method, or Mannings open flow equation:

$$Q = \frac{1.49}{n} A^{5/3} P^{-2/3} S^{1/2}, \tag{5.6}$$
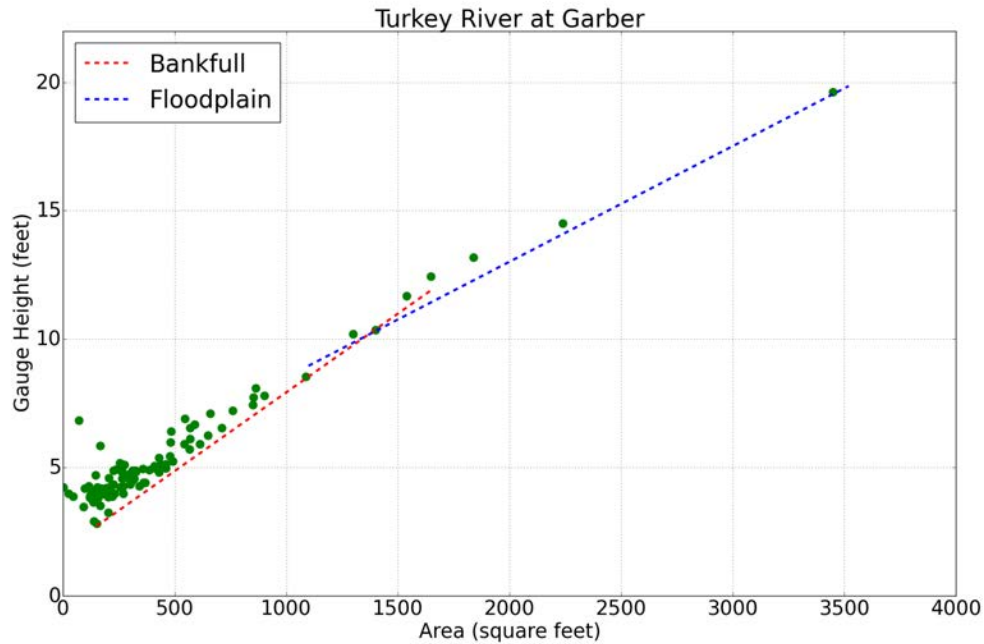
Figure 5.5: Turkey River at Garber, Iowa stage height vs. channel cross-sectional area.

where Q is the discharge, n is the Mannings coefficient of effective friction, A is the cross-sectional area, P is the wetted perimeter, and S is the slope of the free surface.

The Manning's (n) was assumed to be 0.035 both in-channel and in the floodplain to represent the mean value in a range of bed materials, vegetation, and meander within the region based on land use, geology, and topography. The value of 0.035 is within the range for multiple bed materials from sand to coarse gravel (*Phillips and Tadayon*, 2006). The trapezoidal channel characteristics of width at water surface, bottom width, and side slope are used as variables in an equation to relate wetted perimeter to stage (converted to an effective depth by subtracting the gauge height). The slope of the free surface is represented by the slope of the main channel. This

method assumes steady, uniform flow in order to meet the criteria of the Mannings equation. Manning's equation works for nonuniform flow but since the assumption is that the friction slope equals the channel slope it can be assumed steady uniform flow.

5.5.3 Calibration: Using Site Geometries to Fit Regional Power Relation

The process of collecting bankfull data is repeated several times to provide five sites through which to pass a curve describing the regional power relation between bankfull geometry and contributing drainage basin. In the calibration, values describing the expected geometry based on Equations 5.2 and 5.3 values are compared to the observed values. The expected geometry values are linked to variable values containing the scalar coefficients. A linear regression constant is calculated for the expected and observed values, and then maximized using a solver function that varies the scalar values. The final regional curves produced are shown in Figure 5.6 and Figure 5.7. The curves are compared to the prefabricated equations given in EPA BASINS Technical Note 2 (*EPA*, 2007).

5.5.4 Mannings Equation for Steady, Uniform Flow

The Mannings flow with respect to the cross-sectional area of the channel is then compared to the empirical flow with respect to the cross sectional channel. A good example of geometric validation using empirical data is shown in Figure 5.8. Given the high-value discharge, the Manning's equation underestimates the cross-
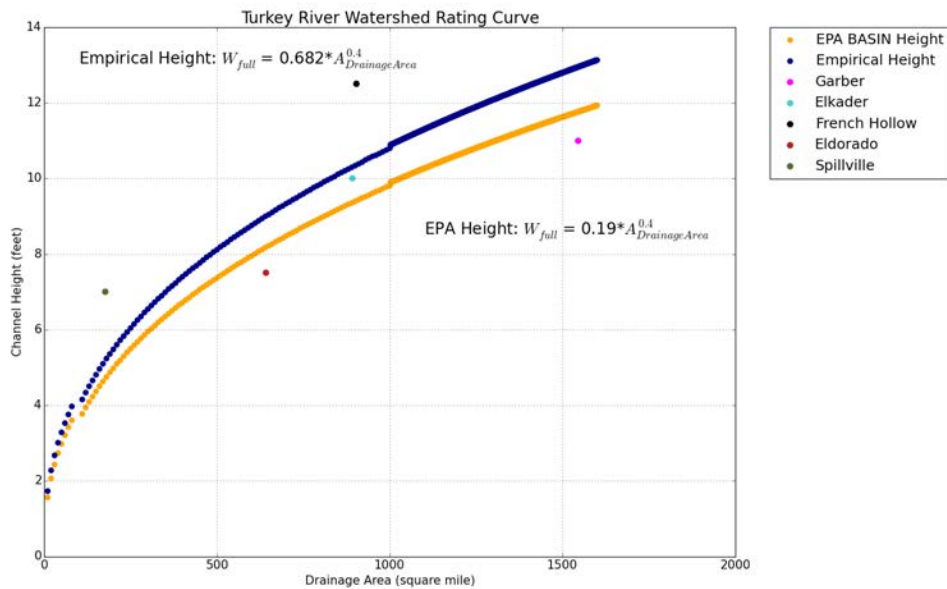
Figure 5.6: Bankfull Height Regional Rlation, $H = 0.687*A^{0.4}$.
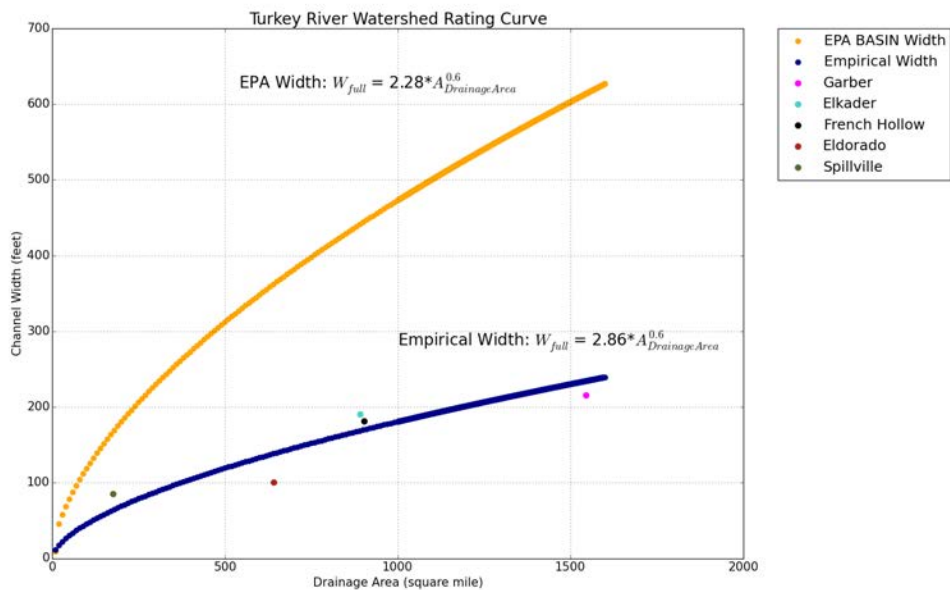
Figure 5.7: Bankfull Width Regional relation, $W = 2.86*A^{0.6}$.

sectional area. Inversely, for a given large cross-sectional area, the Manning's equation over-estimates the discharge. This is likely due to the uniform friction coefficient, and the assumption that the floodplain and the channel slope are the same.
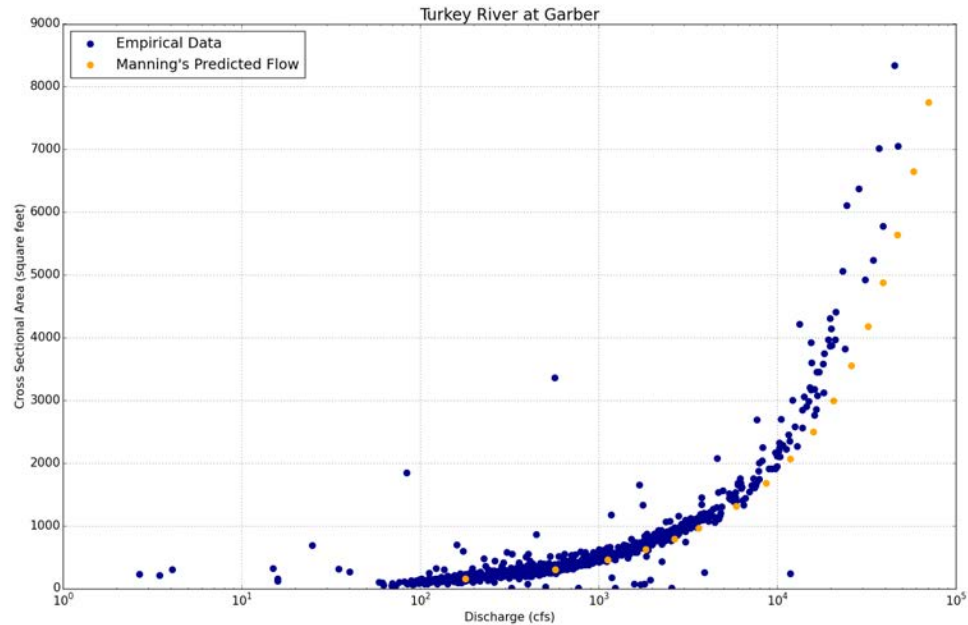
Figure 5.8: Cross-Sectional Area vs. Discharge at Garber, validating geometry through the Mannings equation.

5.5.5 Regional Power Relation Validation

Sites containing enough data to observe trends but insufficiently so for calibration are used in validating the power relation. The power relations are applied to the drainage area of the site to produce bankfull geometry. These bankfull heights and widths are then used with the same geometric assumptions in the Mannings equation
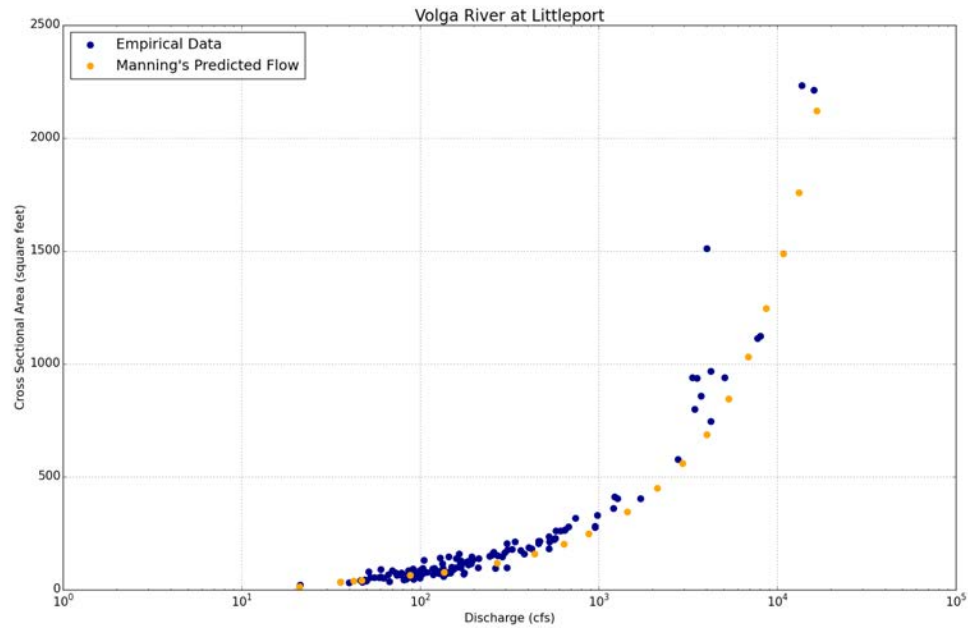
Figure 5.9: Cross-sectional Area vs. Discharge of the Volga River at Littleport, Iowa, calculated from modeled bankfull characteristics.

to produce a cross-sectional area vs. discharge plot. Figure 5.9 shows the Mannings equation prediction compared to the empirical data of the Volga River at Littleport, Iowa. The correlation coefficient is evaluated between the prediction and the empirical data for four sites. The sites used for calibration and validation are summarized in Table C.1 & C.2 in Appendix C. Note that a reasonable range of drainage basin areas are represented for good calibration.

5.5.6 Special Considerations

If the bankfull width is expressed in terms of bankfull height with a bottom width of 0, the two power relations can be set equal to one another with the width

scaled by 2.5 to reflect the H:V ratio. The resulting value of 0.3 mi^2 is a critical area below which the 2.5 H:V assumption does not hold, because the bottom width would have to be less than 0. Since this is not possible for a length, the bottom width remains zero as bankfull width decreases, increasing the H:V ratio from 2.5 as the drainage area decreases. The low correlation coefficient for Roberts Creek, whose channel slope is 0.005%, indicates the sensitivity of the Mannings prediction to the channel slope.

5.5.7 FTABLE Development

FTABLEs are developed for each reach. The drainage area is used with the regional power relation to give the bankfull width and height of each reach. Flow is assumed to be steady and uniform such that the slope of the free surface is the same as the bed slope. The floodplain slope is assumed to be 0.1 and the effective friction in the channel and floodplain are assumed to be 0.035. These parameters of reach length, upstream elevation, downstream elevation, bankfull width, bankfull height, floodplain slope, and effective friction are inputs into an executable file to create the FTABLEs. The FTABLE program is an executable that uses the Manning equation at each of 16 water level depths of interest to calculate the cross-sectional area, volume of the reach, discharge, and time to flow through the reach. An example reach can be seen in Figure C.1 in Appendix C, which has a drainage area of 8.35 square miles and length of 1.16 miles.

5.6 Turkey River Watershed Model Development

As mentioned before one UCI file is typically needed to perform all the necessary operations to simulate a watershed. Because of the high number of operations needed to simulate the 710 subbasins comprised in the Turkey River Watershed three UCI files are needed. In HSPF, an operation is an execution of code that transforms a set of input time series into a set of output time series (*Bicknell et al.*, 1997). The first file is for land segments which simulate runoff from pervious and impervious land segments. The second and third UCI files, which simulate stream flow, are for reach routing. After the land simulation, the output time series are stored on a WDM file and become inputs for the reach UCI files. Some of the output time series from the land simulation includes total outflow from pervious land segments (PERO), surface runoff (SURO), total simulated evapotranspiration (TAET), and active ground water outflow (AGWO). PERO and SURO output time series come from the land segment UCI file and are used as input time series for reach UCI files.

5.6.1 UCI File - Land Segments

For the land segment UCI file precipitation, air temperature, dewpoint temperature, wind, solar radiation, cloud cover, and potential evapotranspiration are all needed inputs time series. The six input time series are called from the WDM file to the external sources block in order to be used within the land segment UCI file simulation. The land segment UCI file output time series are then called in the external targets block which in turn writes the output time series in the WDM files.

The outputs called and computed are the total outflow from pervious land segments (PERO) and the surface outflow for the impervious land segment (SURO). PERO and SURO output time series are the two main input time series for the river reach UCI files. No reach routing is involved in the land segment UCI file.

5.6.2   UCI Files - Reach Routing

Because the land segment UCI file has the input time series for both of the river reach UCI files, it is simulated first. The second UCI file simulated is the Eldorado reach UCI file which simulates the water upstream from the stream gauge at Eldorado, Iowa. The input time series called in the external sources block are the PERO and SURO time series that comprise all the river reaches that flow into the Eldorado stream gauge reach. Each PERO and SURO output has a reach associated to it and there can be multiple PERO and SURO data sets per reach. The output time series called in the external targets block for the Eldorado UCI file is the total volume of outflow (ROVOL) from the Eldorado outlet, which is used as input for the third UCI file.
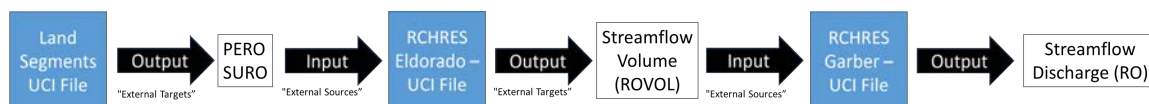
Figure 5.10: Flowchart of UCI files

The third file simulated is the Garber UCI file which simulates the water

downstream of from the Eldorado stream gauge and the water upstream at the Garber, Iowa stream gauge. In order for the Garber UCI file to be simulated correctly the Eldorado UCI file must be simulated before the Garber UCI. The ROVOL output time series from the Eldorado reach UCI file is called in the external sources block of the Garber UCI file to be used as an input time series for the reach just after the Eldorado outlet. The output from the Garber UCI file is the total stream flow (RO) in cfs from the outlet at the Garber stream gauge. The Garber stream gauge is used for the calibration site and will be explained further in the calibration section of this study. The PERLND and IMPLND section are not activated for the river reach UCI files because no land segments are being simulated; only the RCHRES section is activated. Figure 5.10 shows the flow chart of the order of UCI files and inputs/outputs for each UCI file.

5.7   Chapter Summary

Chapter 5 describes the hydrologic model development for the Turkey River Watershed. The weather information required for the continuous HSPF simulation are from the NCDC database and of that database eleven meteorological stations are used to give spatially varying representation of the Turkey River Watershed. The watershed is then delineated into 710 subbasins and assigned individual meteorological stations using TPM to give an accurate representation of the watershed. The HSPF model sections PERLND, IMPLND, and RCHRES are reviewed describing each sections contribution to the simulation process. Hydrologic function tables, FTABLEs,

are then defined and used to accurately define reaches within the model and calibrated to achieve accurate hydraulic relationships between water depth, surface area, water volume, and outflow. Finally, running the model is not conventional due to the high number of operations needed to simulate the 710 of subbasins. Three UCI files are needed to complete the simulation of the Turkey River Watershed. One for land segments and two for all the reaches up to Garber stream gauge. A third UCI file (total of four) will be needed to simulate the entire watershed for the watershed analysis portion of the study. In total, three UCI files are only needed for the calibration and validation process.

CHAPTER 6
CALIBRATION AND VALIDATION

6.1 Introduction

This chapter goes into the calibration and validation process and talks about each calibration parameter individually. Results for this chapter can be seen in Appendix A for both the calibration sites at the stream gauge at Garber and other validation sites within the Turkey River Watershed.

6.2 Calibration Parameters

HSPF's simulation of hydrologic processes often have many parameters, some of which are calibrated with observed stream gauge data. The stream gauge at Garber Iowa (USGS 05412500) is used for the calibration of model parameters. Model parameters have a high degree of interaction between other model parameters so that no single parameter controls a single aspect of the watershed simulation. For example increasing INFILT will move more water into the groundwater storage, but at the same time increasing LZSN will increase evapotranspiration from the groundwater storage. The net effect might be a negligible change in the amount of groundwater flow. As discussed earlier, PWATER calculates the components of the water budget primarily to predict the total runoff from pervious land segments, making PWATER an important and necessary section to calibrate. The parameters within PWATER and SNOW sections are the most associated with hydrologic processes and are calibrated. The calibrated model parameters are listed in Table 6.1 & 6.2. These parameters are

first estimated and then are calibrated over a 20 year period from October 1, 1992 to
September 30, 2012.

Table 6.1: Calibration parameters for PWATER.

CEPSC	Interception Storage Capacity
UZSN	Upper Zone Nominal Storage (Small Events Simulation)
LZSN	Lower Zone Nominal Storage (Annual Water Budget)
INFILT	Infiltration Index (Amount of Groundwater)
INTFW	Interflow Inflow (Flood Hydrography Shape)
IRC	Interflow recession constant (Shape of Interflow Recession)
KVARY	Groundwater Recession Flow Parameter
AGWRC	Groundwater Recession Rate
LZETP	Lower Zone E-T Parameter

Table 6.2: Calibration parameters for SNOW.

SNOWCF	Snow Catch Efficiency Factor
COVIND	Maximum Snowpack (Water Equivalent)
TSNOW	Critical Temperature
MGMELT	Maximum Rate of Snowmelt by Ground Heat

The PWATER parameters mentioned in Table 6.1 control many hydrologic

factors including the amount of water infiltrating the ground, the amount of storage available, and the amount of evapotranspiration occurring. There are many other parameters not mentioned in Table 6.1 & 6.2 such as the forest shade factor which accounts for transpiration during the winter months. In the following, parameters in Table 6.1 & 6.2 will be discussed. Figure 6.1 shows an illustration of the water storage's that are simulated within PWATER.
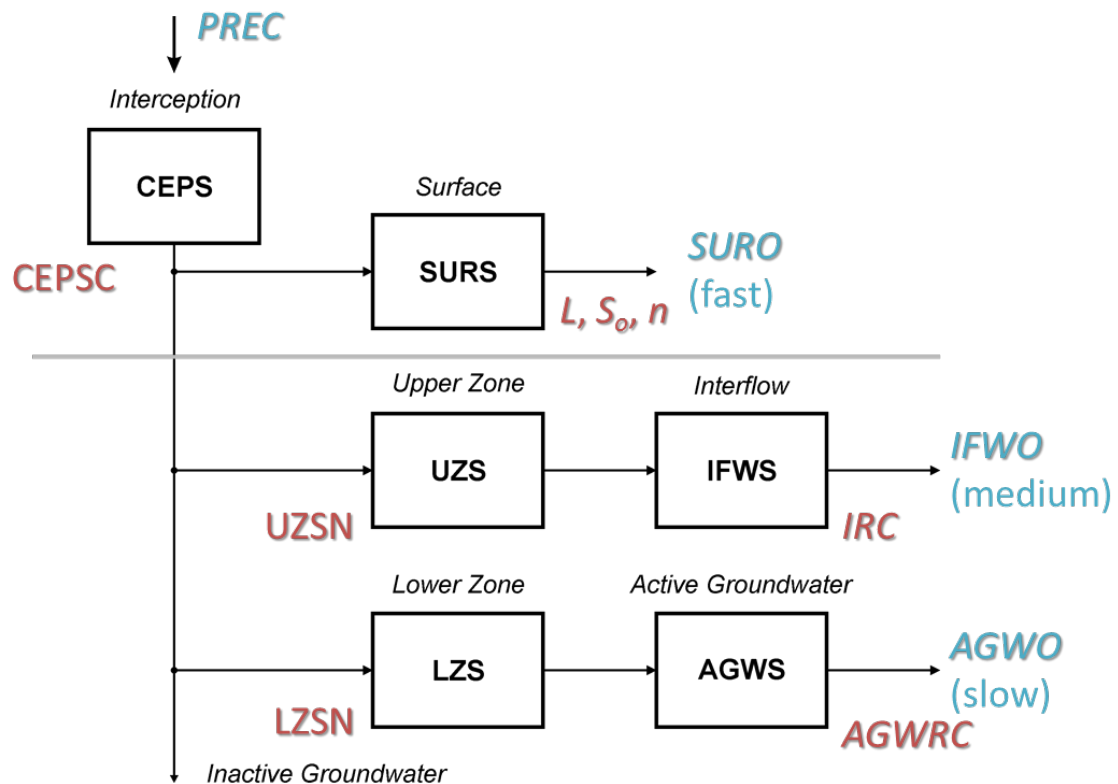
Figure 6.1: PWATER section precipitation is partitioned among several storage's of water. Runoff leaves from one of three storage's fast (surface), medium (interflow), or slow (active Ground Water).The L represents land segment length, S_o represents average land segment slope, n represents Manning's n, and $K_{interflow,groundwater}$ represent recession rates.

6.2.1   Storage Parameters

The Interception Storage Capacity (CEPSC) is a function of cover density. CEPSC is the amount of rainfall retained by vegetation never reaching the land surface and eventually evaporating (*EPA*, 2000). Table 6.3 has typical interception storage values for CEPSC for land surfaces. CEPSC is decided to vary by month over the growing season for all the land use and land covers. Cultivated crops and forest fall outside these ranges in Table 6.3 during August, September, and October months. These land uses and land covers can exhibit a wide range of interception rates. The Summary Table in BASINS Technical Note 6 has possible ranges of values for monthly distributed interception capacities, all of which fall within (*EPA*, 2000).

Land Cover	Range
Forest Cover, Heavy	0.20
Forest Cover, Light	0.15
Cropland	0.10-0.15
Grasslands	0.1

Table 6.3: Interception Storage Capacity.

Initial estimates of UZSN are made with approximate relations. For low depression storage, the recommended relation is:

$$UZSN = 0.06(LZSN) \qquad (6.1)$$

and for high depression storage, the relation is:

$$UZSN = 0.14(LZSN). \hspace{2cm} (6.2)$$

The equations account for low to high soil capacity storage, steep to flat surfaces, and limited to heavy vegetation (*EPA*, 2000).The low depression storage is used as initial UZSN for the Paleozoic Plateau portion of the Turkey River Watershed because it is more steep and hilly. The Iowan Surface portion of the Turkey River Watershed uses high depression storage as initial UZSN because it is flatter and dominated by agricultural lands. Initial UZSN range from 1.05 inches to 1.165 inches. After calibration it reduces to approximately 0.5 to 0.75 inches. Wetlands and forest lands have the largest UZSN storage capacity at approximately 0.80 inches for soil type B and 0.72 inches for soil type C. Agricultural lands have the smallest upper zone storage at 0.56 inches. Again, wetlands contribute only about 1% of total land cover but forest lands contribute a respectable amount of roughly 14% of the total area within the Turkey River Watershed. UZSN controls the water retained in the upper zone and the available water for evapotranspiration. The higher the UZSN the more it reduces the runoff and vice versa. UZSN has little effect on the annual water budget but a major effect on direct runoff.

The Lower Zone Nominal Storage (LZSN) depends on two factors, the water storage capacity of the soil and the frequency of water storage being used. The deeper and coarser the soil the larger the storage capacity and vice-versa. Other

factors such as precipitation and evapotranspiration may also control how large or small the storage capacity is for this parameter. LZSN is essentially the root zone of the vegetation. Approximate values for LZSN range from 2 to 20 inches for most parts of the United States (*EPA*, 2000). The empirical equation:

$$LZSN = 4 inches + 0.125(P) \qquad (6.3)$$

provides an initial estimate of LZSN based on the average annual precipitation P. For this study the initial LZSN range from 7.5 to 8.5 inches for the land surface and land covers. After manual and automated calibration LZSN is adjusted to approximately to 2.35 to 3.38 inches. Cultivated lands with corn and soy have a LZSN of 2.35 inches while wetlands have the greatest LZSN at 3.38 inches. Large LZSN like wetlands decrease flow rates by allowing the water to be stored and evapotranspiration to occur (*EPA*, 2000). Within the Turkey River Watershed wetlands only make up roughly 1% of the total area. Agriculture lands, which have the lowest LZSN, occupy approximately 56% of the Turkey River Watershed (largest land use within the Turkey River Watershed).

6.2.2 Other Parameters

LZETP is unit-less and controls the evapotranspiration opportunity from the lower zone which is the primary soil moisture storage. Technical Note 6 from BASINS offers typical values of LZETP and can be seen in Table 6.4 (*EPA*, 2000).

INFILT, a function of soil characteristics, is an index to the mean infiltration

Land Type	Range
Forest	0.6-0.8
Grassland	0.4-0.6
Row Crops	0.5-0.7
Wetlands	0.6-0.9
Barren Lands	0.1-.04

Table 6.4: LZETP typical values (unitless).

rate of a land segment. In turn, controlling the infiltration capacity of the soil also controls the amount of water that infiltrates and becomes groundwater. The INFILT values can be found through the hydrologic soil groups (SCS) classifications and in Table 6.5. INFILT rates higher than 0.1 inch per hour are found in places of high permeability and anything less than 0.005 inch per hour usually denotes impermeable areas like urban developments. Runoff timing and low flow volumes are affected most by INFILT (*EPA*, 2000). Initial values for INFILT were 0.1 for Iowan Surface and 0.05 for Paleozoic Plateau. After calibration the infiltration varied based on land cover and ranged from 0.07 to 0.30 inch per hour (in/hr). Wetlands are the greatest INFILT at 0.30 in/hr and agriculture lands are the lowest INFILT at 0.19 and 0.07 in/hour with soil types B and C respectively.

SCS Hydrologic Soil Group	INFILT Estimate (in/hr)	Runoff Potential
A	0.01+	Low
B	0.05-0.1	Moderate
C	0.01-0.5	Moderate to High
D	0.005-0.01	High

Table 6.5: Hydrologic soil groups (SCS) classifications.

INTFW is the coefficient that controls the amount of water entering the ground from surface detention storage becoming interflow. This parameter, the most effective in to controlling the shape of the hydrograph, controls the timing of runoff. It shifts and delays the flow to a later time, reducing flow peaks while maintaining the same volume. Increasing the INTFW increases the amount of interflow and thereby reducing the amount of surface runoff and vice-versa. INTFW has no effect on baseflow but can be used after calibration to better match flow peaks observed on the hydrograph (*EPA*, 2000). INTFW, which closely relates to LZSN, generally ranges from 0.5 to 5. The deeper the soil and the higher the precipitation the higher the value of INTFW. Initial value for interflow for the Turkey River Watershed was 3 but after calibrating agricultural lands, it fell to 1.47. Forest cover is 2.20. Grasslands and pastures is 1.76. Wetlands is 2.20. Pervious urban development is 1.76. These values fall within the range specified by BASINS Technical Note 6 (*EPA*, 2000).

IRC is the interflow recession constant, which affects the timing of the interflow outflow. Conceptually, IRC is related to a stormflow hydrograph by:

$$IRC = \left(\frac{Q_2}{Q_1}\right)^{\frac{24}{n}},$$

(6.4)

where Q_1 is the flow at time t_1, Q_2 is the flow at time t_2, and n is the number of hours from t_1 to t_2. It is similar to the active groundwater recession constant parameter AGWRC. AGWRC is the ratio of current groundwater discharge to the discharge from the previous 24 hours. In contrast, IRC is the ratio of the current daily

interflow to the previous day interflow discharge. IRC affects the hydrograph shape in the descending region between peak flow and baseflow. Typical range is from 0.30 to 0.85 with low values acting more like overland flow and higher values acting more like baseflow. IRC is first estimated using the equation and then calibrated (*EPA*, 2000). IRC for the Turkey River Watershed was estimated at 0.6 and calibrated to 0.607 per day, which falls within the range provided. AGWRC is a function of watershed conditions including climate, topography, soils, and land uses. It is estimated and calibrated to be roughly 0.98 per day.

KVARY, which is the groundwater recession flow parameter, describes non-linear groundwater recession rates. KVARY is usually one of the last parameters to be adjusted because it affects seasonal low flow and in general it is better to adjust INFILT and AGWRC for the behavior of the groundwater recession curves. It is only used if the observed groundwater recession demonstrates a seasonal variability with a faster recession, meaning higher slopes and lower AGWRC values, during wet periods and the opposite during dry periods.(*EPA*, 2000). KVARY was initial set to zero but after calibration it went to 0.75 per inch greatly improving the annual hydrographs.

In Table 6.2 the snow parameter Snow Catch Efficiency Factor (SNOWCF) is a factor by which precipitation data will be multiplied if the simulation indicates snowfall. This accounts for deficient catch efficiency of the gauge under snow conditions. COVIND is the maximum snowpack where the entire pervious land segment is covered with snow. TSNOW is the air temperature where precipitation turns into snow during saturated conditions. MGMELT is the maximum rate of snowmelt by

the ground heat. This value applies when pack temperatures are at freezing point (*Bicknell et al.*, 1997). The snow parameters were all estimated and then calibrated.

6.3   Calibration and Validation

The calibration period is restricted to the past 20 years, a period beginning on October 1, 1992 and ending on September 30, 2012 (20 water years). The past 20 years gives the best representation of the current LULC conditions, allowing the model to simulate the most accurate streamflow. The calibration site is at the Garber USGS stream gauge for the Turkey River Watershed (USGS 05412500). The two methods for calibration used in this study are a systematic manual approach and an automated approach. The systematic manual approach is used to improve the overall water balance and seasonal flow predictions. If there are large mismatches between simulated flows and observed flows the parameters are adjusted by hand. The manual approach is used to give better starting parameters for the second approach called Shuffled Complex Evolution-University of Arizona (SCE-UA).

The SCE-UA is an automated calibration program designed to find the optimal model parameters. It is an effective and efficient search algorithm used for conceptual hydrologic models (*Khakbaz et al.*, 2012). The SCE-UA is used to minimize two objective functions, which are measures of the model error. The first objective function is the root mean squared error (RMSE) and it measures the error between observed and simulated flows; the RMSE is most sensitive to errors in high flows. The second objective function is the relative squared error (RSE) and it measures

the error in a simulation between the logarithms of observed and simulated flows; the RSE is most sensitive to errors in low flows (*Duan et al.*, 1992). The SCE-UA is simulated three times, the first simulation focuses on minimizing RMSE objective function, the second focuses on minimizing RSE objective function, and the third, called the Multi Objective Calibration (MOC), focuses on minimizing both objective functions at the same time. The objective functions, RMS and RMSE, parameters either simulate high flows well and low flows poorly or low flows well and high flows poorly. The MOC is able to meet somewhere in the middle of the parameters and simulate both the high flows and low flows well. The parameters produced for the MOC run are verified in the validation period. *Vrugt et al.* (2003) also concluded that the SCE-UA method for calibration produced model parameters that better balanced the simulation of both high and low flows. It is also stated the SCE-UA is more efficient at establishing optimal parameters than other calibration processes like the adaptive random search (ARS) and the multistart procedure that are based on the simplex algorithm (MSX) (*Vrugt et al.*, 2003). *Wu and Zhu* (2006) provides a general description of the SCE-UA method steps. Accurately calibrated parameters will predict the components of the water cycle well and predict flows during periods other than the calibration period. The period when you can test the accuracy of the water cycle is called validation period. The validation period for this study took place from October 1, 1948 to September 30, 1992. Results from both the calibration period and validation period are shown below.

An important objective is to determine if the HSPF model for the Turkey

River Watershed is capable of representing the two geologic regions accurately, the Iowan Surface and the Paleozoic Plateau. The Turkey River Watershed is made up of all different kinds of soil groups ranging from A to D soil classes. To assign initial parameters for the model, it was assumed that the Iowa Surface, which has the majority of the agricultural land (59% of the total area for agriculture), is B soil group and for the Paleozoic Plateau C soil group. This is on the basis for what looked to be the majority for each region based on Figure 4.3. To determine whether a two soil group representation was necessary, a second calibration assuming both regions have the same soils properties (initialized with soil group C) was performed. After calibrating both the two soil groups and one soil group for the two regions there where small changes in the daily and monthly flows. The correlation between simulated and observed monthly flows for the one soil group (0.9327) was slightly better than that for two soil groups (0.9275), a difference of 0.005. For the monthly water balance both calibrations under-predicted. However, the two soil group calibration only under-predicted by 6.5% as where the one soil group under predicted by 7%. The differences may have been small between the two calibrations but the two soil groups calibration performed better for the monthly water balance and will be used for this study. The watershed could have been modeled with even more soil groups but due to the complexity of the model already, two soil groups is satisfactory.
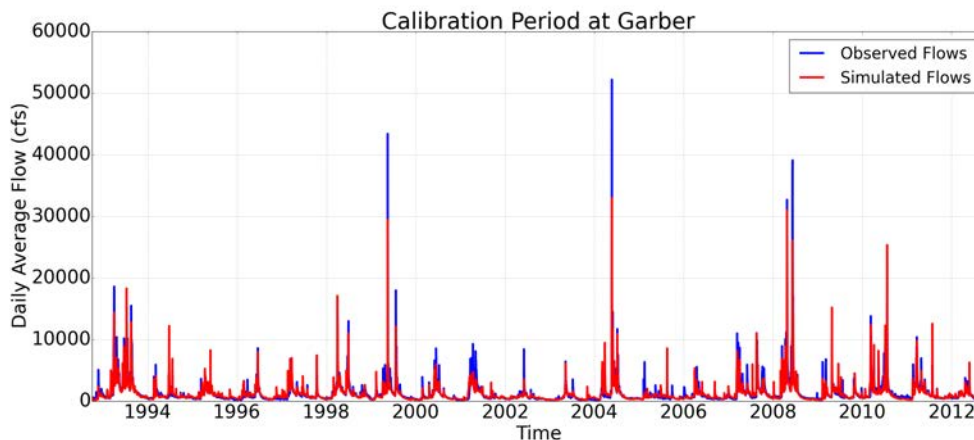
Figure 6.2: Observed and simulated daily flow time series for the Turkey River Watershed at Garber (USGS 05412500) for the calibration period from 1993 to 2012 water years.

6.4 Monthly Water Cycle

The Turkey River Watershed has distinguishable seasonal cycles for runoff. In Figure 6.3 the overall simulated runoff for the calibration period matches the observation runoff quite well. The largest discrepancies occur during the months of April, May, and June when the model underestimates the observed average runoff (streamflow). This could be due to the wet season that occurs during these months and of recent (since 2008) they have been quite moist. The model under-predicts the observed monthly runoff by roughly 6.5% during the calibration period.

Figure 6.4 shows the validation period for average monthly simulated and observed runoff. The model tends to over predict in all the months except March. In March the model is unable to produce the same amount of runoff as observed. This could be due to the snow melt during this time of year. The validation period

over-predicts by approximately 15% for a 44 year period starting from 1949 to 1992.
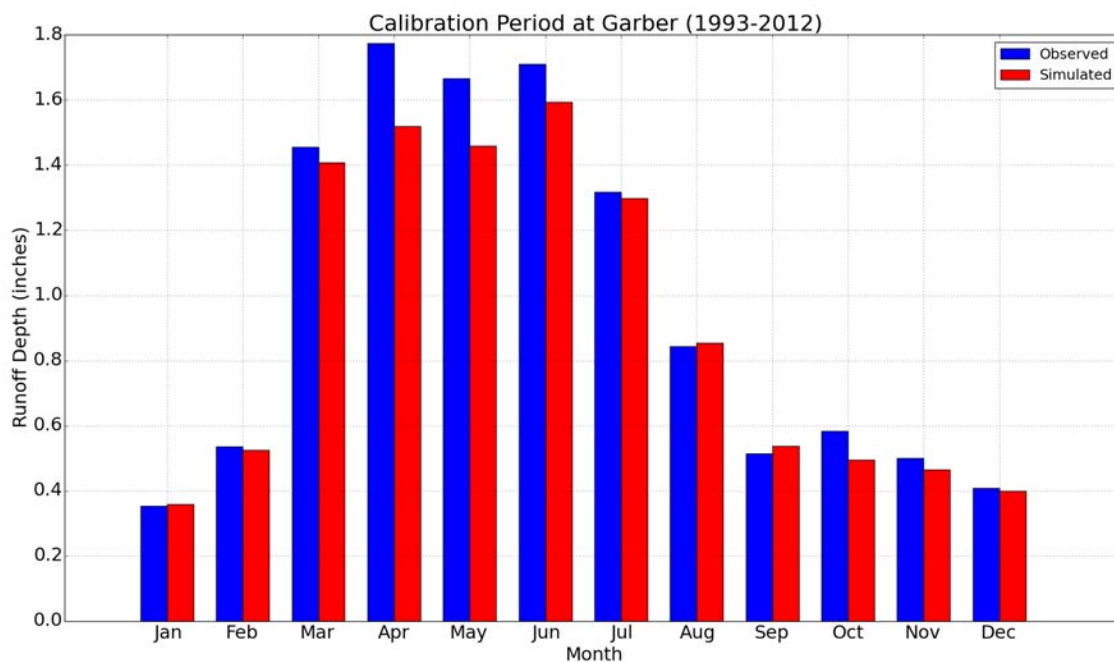
Figure 6.3: Average monthly water balance for the calibration period.
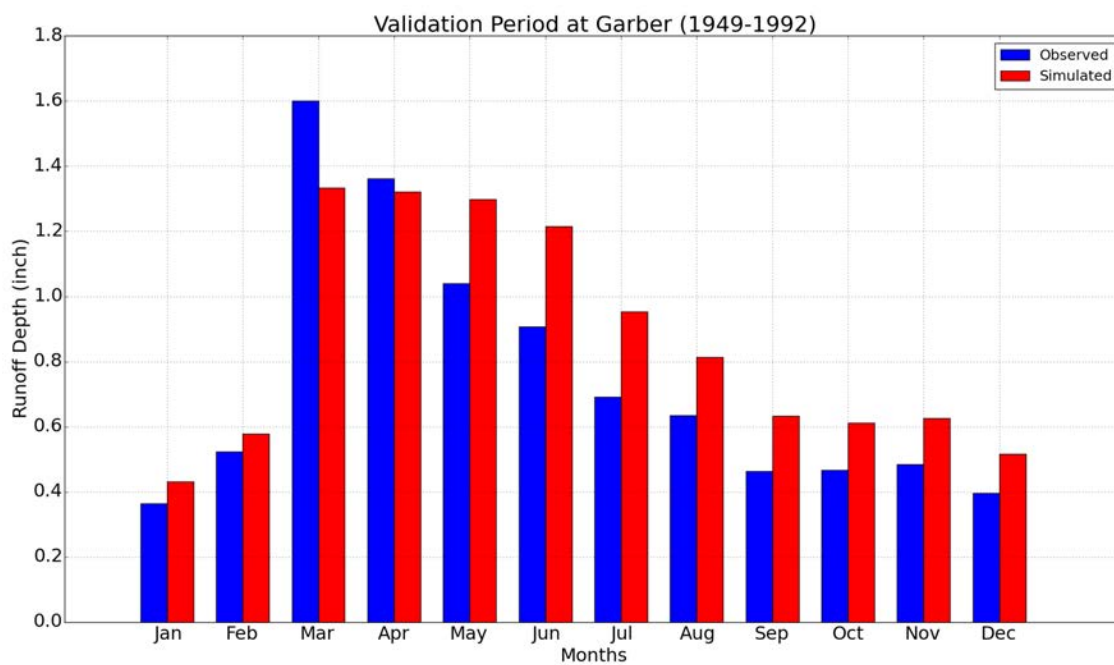
Figure 6.4: Average monthly water balance for the validation period.

The period of record's average monthly runoff can be seen in Figure 6.5 and the same trends for the validation period can be seen here. However, the model only over-predicts by approximately 7.8% during the period of record. The period of record contains both the calibration and validation periods. While the calibration period under predicted using calibrated parameters, the same parameters over-predicted for the period of record (including validation period). One factor that may have contributed to the over prediction of average monthly runoff is the use of fixed LULC conditions for the entire simulation. Changes in LULC, or changes in agricultural practices on these lands, are not reflected in the model simulation.
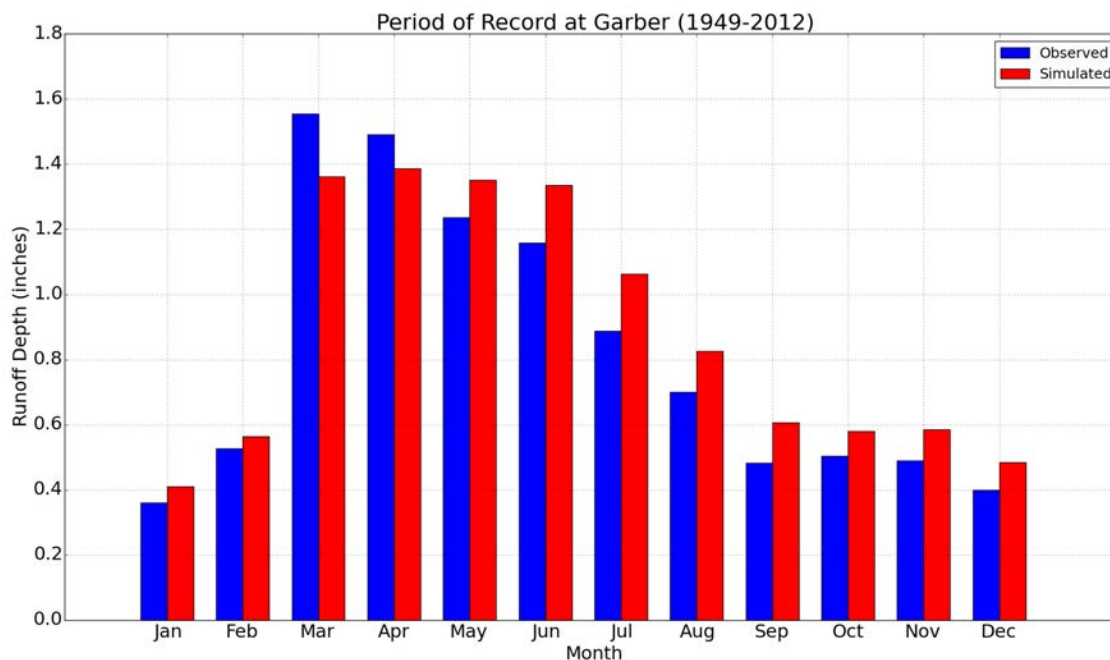
Figure 6.5: Average monthly water balance for the period of record.

6.5 Annual Runoff

If the model simulated the observed flows perfectly it would follow a one to one line if simulated flows and observed flows were plotted against each other. In Figure 6.6 this trend can be seen for the calibration period (green circles). The simulated annual flows for low runoff years are slightly over-predicted, just above the one to one line, as where the simulated annual flows for high runoff years are slightly under-predicted, falling just under the one-to-one line. Relatively, all the points hover right around the one-to-one line. The correlation between the simulated and the observed flows for the calibration period have a 0.971 correlation coefficient. This means the observed flows and simulated flows share a linear association with each other and vary each year. As where the validation period (purple triangles) show an overall over prediction for the average annual runoff. This could be partially due to this period having not as many high runoff years as the calibration period. The average annual runoff for the calibration period is roughly 11.64 inches and is roughly 8.92 inches for the verification period. The fixed LULC could also play a role in the over prediction for the validation period. The correlation between observed flows and simulated flows for the validation period is still good at 0.927. The entire period of record (64-year period) had a correlation coefficient of 0.932.
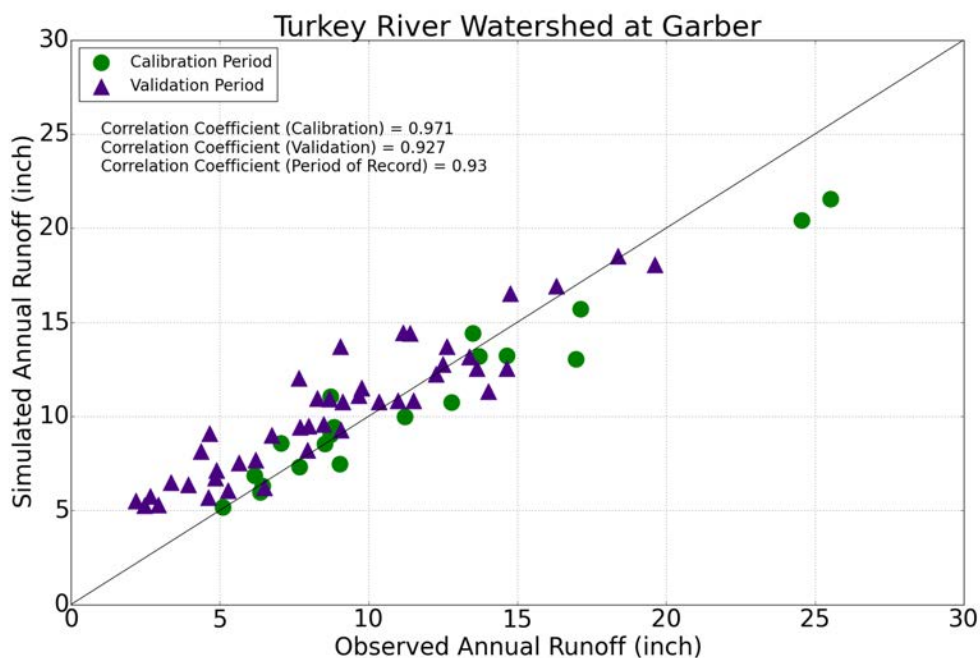
Figure 6.6: Annual Simulated and Observed runoff plotted against each for the calibration and validation periods.

6.6   Annual Maximum Peak Discharge

The model created for the Turkey River Watershed, using HSPF, simulated hourly flow predictions. These prediction are used to assess flood characteristics throughout the watershed. Figure 6.7 shows the calibration and validation period for simulated and observed annual maximum peak discharges. This shows the models ability to predict flood characteristics at the Garber stream gauge. There is a clear difference between the calibration period (Green circles - 1993 to 2012) compared to the validation period (Purple triangles - 1949 to 1992). For the calibration period there is some mismatch between individual simulated and observed peaks but for the

most part the points follow the one-to-one line fairly well. However, for the validation period there is a clear under-prediction for the flood peaks. The under-prediction could be due by the dramatic landscape conversion previously stated.
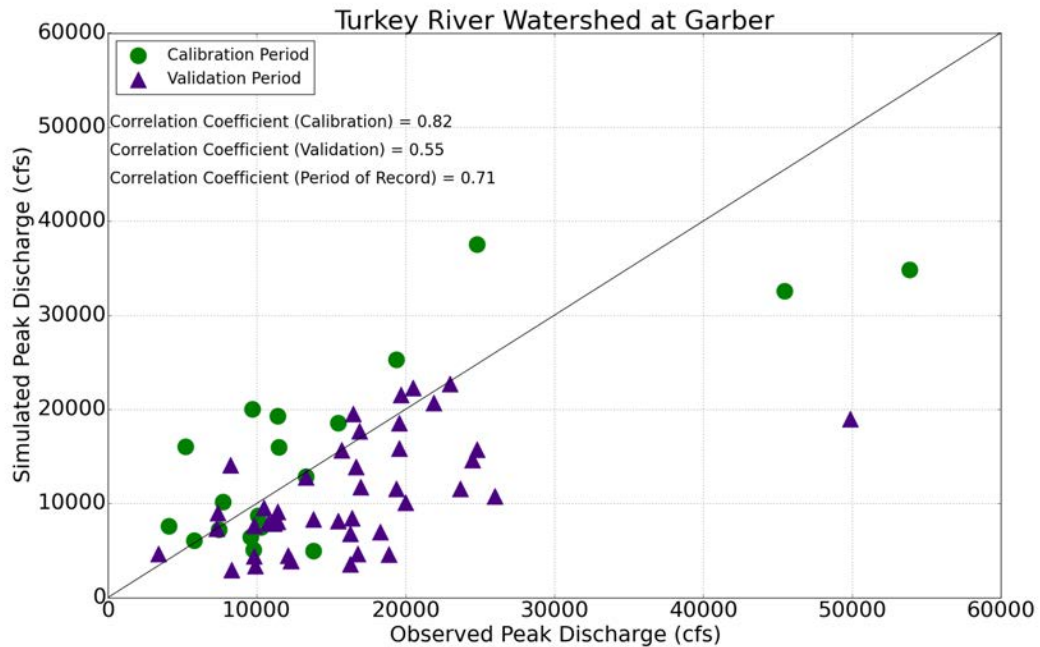
Figure 6.7: Annual Peak Simulated and Observed flows plotted against each for the calibration and validation periods.

An important factor for flood assessment is the model's ability to reproduce the statistical characteristics of flood peaks over the historical record. Figure 6.8 shows a flood frequency analysis ranking the annual maximum peak discharges, observed and simulated, from largest to smallest and plotting them against a sample estimate of their exceedance probability for the Turkey River Watershed. The Turkey

River Watershed model consistently under-predicts annual max peak flows for the entire period of record. The model does however carry the same general trend as the observed annual peak flows. With this known the HSPF model can be used but with the understanding there may be some biases.
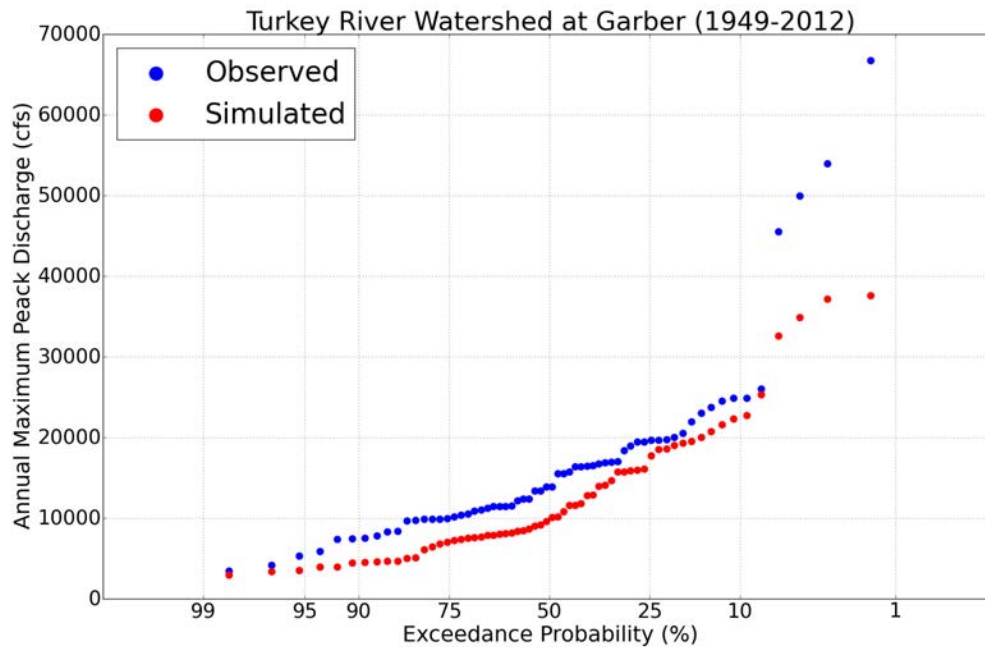
Figure 6.8: Flood frequency analysis of annual maximum peak discharges for simulated and observed flows for the Turkey River Watershed at Garber (USGS 05412500). The annual maximums are for the entire simulation period (1949-2012).

6.7 Chapter Summary

The chapter reviews calibration parameters and describes what they represent within the watershed. Total of 13 parameters are calibrated for the HSPF Turkey

River Watershed model. The automated SCE-UA calibration program is used to find the optimal model parameters using efficient search algorithms. It minimized RSE and RMSE object functions to find the model parameters. For the monthly water cycle the model simulated the observed runoff quite well, roughly under-predicting by 6.5% during the calibration period. During the validation period the model over predicts by 15% for monthly runoff. The correlation between the simulated and observed monthly flows for the calibration period is 0.971. This means the observed flows and simulated flows share a linear association with each other and vary each year. The validation period shows similar results with a 0.927 correlation coefficient, on average over predicting for the annual runoff. The annual maximum flows for the calibration had a correlation coefficient of 0.82 between observed and simulated flows as where the validation only had a 0.55 correlation coefficient. The under prediction could partially be due to the dramatic landscape conversion previously stated. Flood frequency analysis for the entire period consistently under predicts max peak flows at the Garber stream gauge, though the model carries the same general trend as the observed annual peak flows. Other gauge sites for flood frequency can be seen in Appendix A. The HSPF model can be used but with the understanding there may be some biases.

6.7.1 Brief Comparison between HEC-HMS and HSPF Models

Both HEC-HMS and HSPF are lumped parameter model. However, the way that lumping is done is different. With HEC-HMS, each different soil type and land

use is assigned a runoff curve number (CN). HEC-HMS represents a subbasin within a watershed by its area-weighted average CN, and uses that averaged (lumped) CN for the simulation period, making it fixed throughout the simulation process. HSPF represents a watershed with land segments associated with distinct soil types and land use conditions. For example, a forest land segment has a parameter sets that represents the average (or lumped) response of forested areas. The only thing that varies is the area of each land segment within each subbasin. The land segments are also fixed throughout the simulation period.

Another way HEC-HMS differs from HSPF is the simulation period. HEC-HMS is an event-based simulation model, and its simulation period is defined by the storm and runoff duration. For the HATRW report, most events took place over 24 hour period while applying a specific design storm such as a 25-year or 50-year storm event to the entire watershed. The simulation period extended out to three days to determine the resulting flood hydrograph at the downstream outlet. HSPF is a continuous simulation model, and its simulation period extends over many years; the availability of historical weather inputs often defines the simulation period. HEC-HMS is best for simulating large storm events, or specific design storm events. HEC-HMS simulates the runoff processes during a storm event, but not the groundwater processes in between events. In contrast, HSPF is a continuous soil moisture accounting model, and simulates the water balance for surface and subsurface zones at every time step.

Furthermore, the routing methods used for the Turkey River Watershed dif-

fered for the two models. HEC-HMS model used Muskingum routing, a lumped flow routing. The Muskingum method approximates the storage volume by combination of prism storage and wedge storage within a channel. Prism storage describes uniform flow in prismatic channels and wedge storage is generated by the passage of the flow hydrograph (*Shuttleworth*, 1993b). Two inputs are used for Muskingum routing in the HEC-HMS model, a flow wave travel time (K) and a weighting factor describing storage within a reach as the flow wave passes (X) (*IFC*, 2014). In contrast, HSPF uses storage routing, another lumped flow routing method. Within HSPF, inputs such channel slope and reach geometry are used to estimate the storage-discharge relationship for each each.

Flood frequencies are also estimated with different approaches with the two model. For HEC-HMS, a design storm approach is used. A return period is assigned to a design storm event and the resulting simulated peak flows at all locations are assumed to have the same return period. Design storm rainfall is based on an NRCS 24-hour Type II storm pattern, with rainfall depths (e.g., 50-year 24-hour accumulation) from the National Oceanic and Atmospheric Administration (NOAA) Atlas 14 Point Precipitation Frequency Estimates (*IFC*, 2014). HSPF calculated the 50-year return period based off the simulated annual maximums, performing a flood frequency analysis where the flows are ranked and assigned a probability (P = Rank/(N+1)). From the simulated flows the 50-year return period's probability, 0.02 (2% chance of occurrence in a year), is found by interpolating between the respect maximum annual flows rather than fitting a probability distribution to the sample data.

Lastly, the models are calibrated differently. The HEC-HMS model is calibrated for a single storm event occurring May 21, 2004 to May 23, 2004. The calibration's storm event produced severe flooding throughout the southern half of the Turkey River Watershed. Stage IV radar cumulative rainfall estimates and USGS discharge records are used to calibrate the model (*IFC*, 2014). The HSPF model is calibrated for a 20 year period from October 1, 1992 to September 30, 2012. Historical weather information from surrounding weather stations and USGS discharge records are used to calibrate the model.

CHAPTER 7
ASSESSMENT OF HYDROLOGIC TRENDS

7.1 Introduction

This chapter illustrates the Turkey River Watershed flood characteristics, high runoff areas, and flood indexes of past events. Understanding where high risk areas are within the watershed is the first step in preventing flooding.

7.2 Flood Characteristics of the Turkey River Watershed

In understanding how to prevent flooding, areas of high runoff within the watershed need to be identified. High floods areas are usually areas located downstream of areas of large runoff potential. The high runoff areas can provide relief to high flood areas by retaining more water from large rainstorms on the landscape and reduce downstream flood peaks. Within this chapter high runoff areas and high flood areas will be evaluated as well as intensity and extent of extreme floods that have occurred in the past.

7.2.1 High Runoff Areas

The HSPF model for Turkey River Watershed simulated runoff depths for each of its 710 subbasin areas. This is used to identify the high runoff areas from the 64-year simulation. The average subbasin runoff depth is roughly 10.54 inches. The range of simulated average annual runoff depths are shown for each of the 710 subbasins in Figure 7.1. There is variation between annual runoff depth for each

subbasin. The distribution of average runoff depth are classified into thirds. The first third, red triangles, are between 11.20 inches and 12.71 inches and classified as subbasins with high annual runoff depths. The second third, yellow circles, are between 9.96 inches and 11.20 inches and are classified as areas of medium annual runoff depths. The last third, green triangles, are between 7.94 inches and 9.96 inches and are classified as areas of low annual runoff depths.

Figure 7.1: The relationship between the mean annual flood and drainage area in the Turkey River Watershed. The mean annual flood computed for the HSPF RCHRES subbasin outlets from the 64-year simulations is plotted against the total upstream drainage area at the outlet; headwater subbasins are excluded from this analysis. A power-law mathematical model was fit to the sample data (solid black line). Comparing the distance of the sample mean annual flood from that predicted by the mathematical model (line), the top third is classified as a high annual flood (red), the middle third is classified as a medium annual flood (yellow), and the bottom third is classified as a low annual flood (green).

Figure 7.2 is a map showing annual average runoff depths for each subbasin. The annual runoff depth is calculated by summing the total annual runoff depth from within each subbasin and taking the average of the 64-year period. The subbasins of high annual runoff depths mostly occur in the Iowan Surface portion of the watershed, right above the Iowan Surface and Paleozoic Plateau divide, with more medium to low runoff depths occurring in the Paleozoic Plateau region. The high runoff areas in the Iowan Surface region could be partially due to the high agricultural area within the Iowan Surface portion of the watershed. The Iowan Surface region of the watershed has 59% of all agricultural lands. The medium to lower runoff areas that occur in the Paleozoic Plateau region could be due to the large majority of pastures, grasslands, and forests, which have higher storage and infiltration capacity than agricultural lands, within the watershed. Paleozoic Plateau region of the watershed has 83% of all pastures, grasslands, and forest.
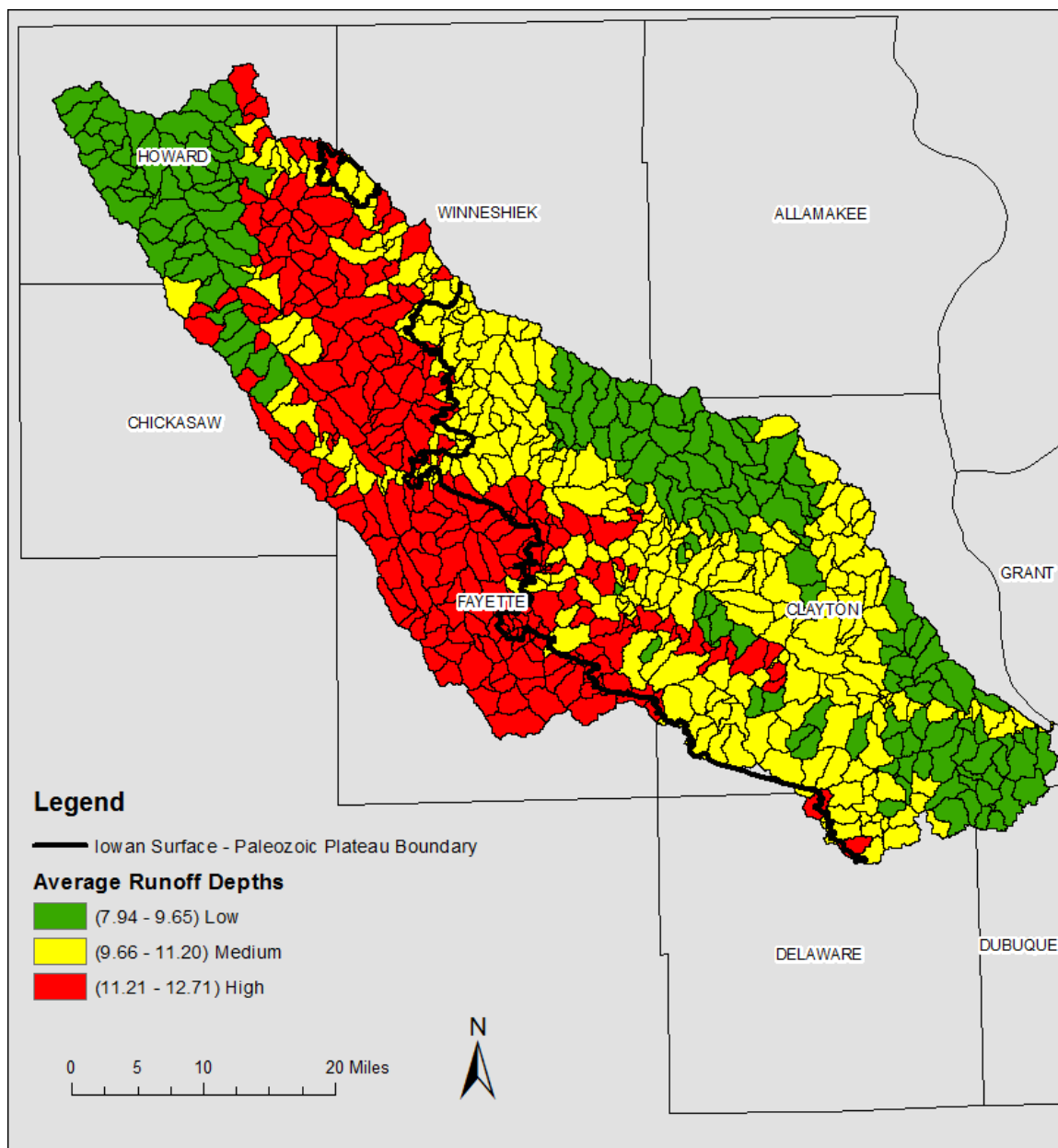
Figure 7.2: Average runoff depth in the Turkey River Watershed. The average annual runoff depth is computed for the HSPF RCHRES subbasins from the 64-year simulation. Higher average runoff depths are shown in red. The medium average runoff depths are shown in yellow. The lower average runoff depths are shown in green.

Another way to represent runoff is with the runoff coefficient. The runoff

coefficient is the fraction of precipitation that becomes runoff. Figure 7.3 maps the average annual runoff coefficient from the 64-year simulation across the Turkey River Watershed. The runoff ranges from as low as 19% of precipitation, to as high as 42% of precipitation (Discharge/Precipitation). Areas in the basin with high runoff are primarily located in the northern portion of the watershed, in Winneshiek, Chickasaw, and Fayette Counties.

Furthermore, Figure 7.4 shows the HEC-HMS model, from the HATRW report, output for runoff potential defined by the SCS Curve Number (CN). It shows the runoff coefficient as a percent of rainfall where it goes from 0% for no runoff to 100% where all rainfall is converted to runoff. HEC-HMS event based model applied a 25 year - 24 hour storm event. The two figures have some similarities where the higher runoff coefficient subbasins are located in the northern or upstream part of the watershed and the lower runoff coefficients are located in the southern or downstream part of the watershed. The results from both models have different runoff coefficient ranges. The HEC-HMS model range is from 31% to 72% contrary to the HSPF model range from 19% to 42%. The different values could be a result of the simulation periods. HSPF model is averaging over a 64 year simulation period opposed to the HEC-HMS models simulating over a 24 hour period for a 25 year storm event. The results for HSPF become averaged over the period of record for many different storm events versus the HEC-HMS results are for a single 25 year - 24 hour storm event.

From a hydrologic standpoint, implementing projects that can reduce runoff from the high runoff areas, like in the Iowan Surface region, should be a priority.
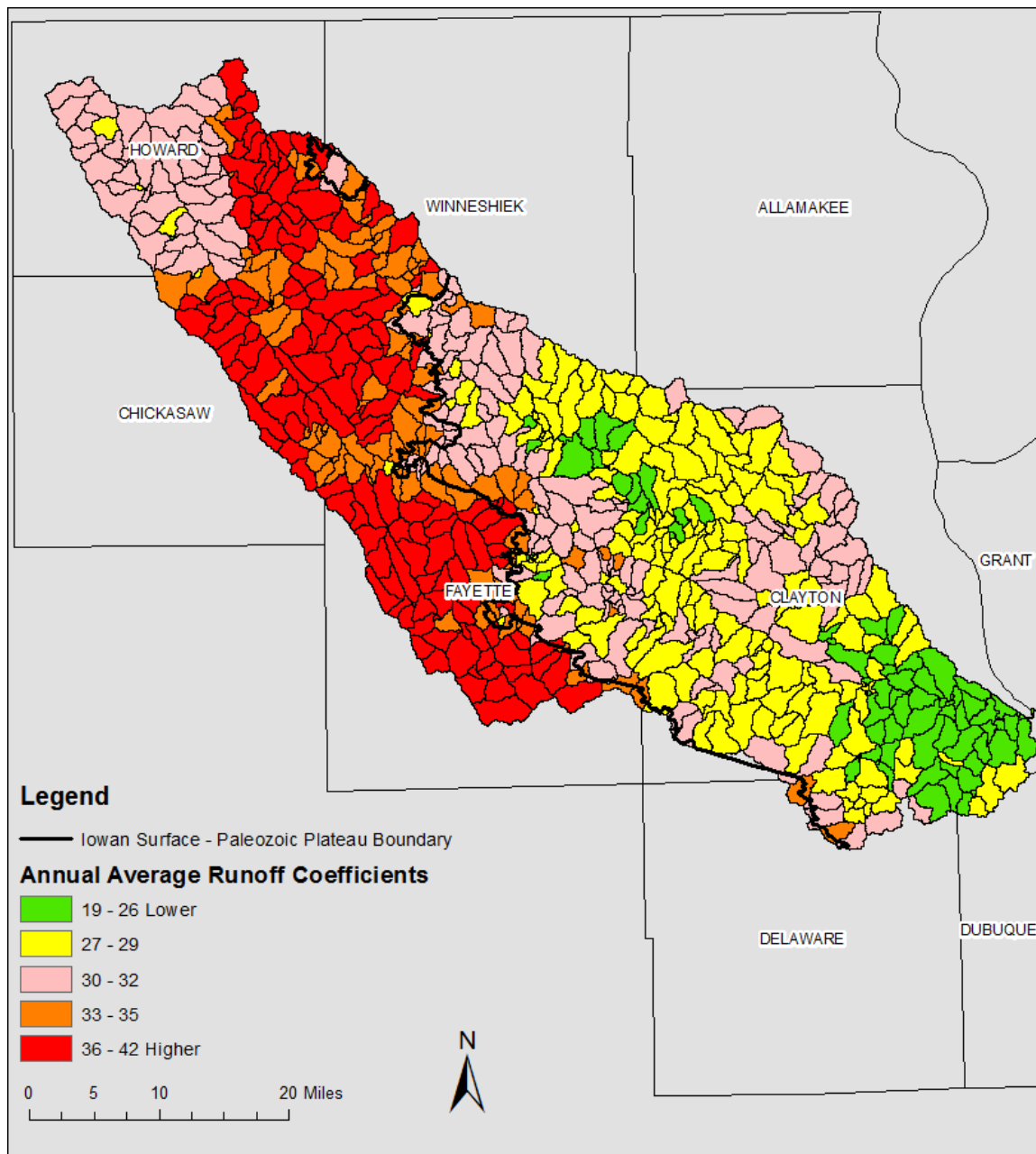
Figure 7.3: Average annual runoff coefficient in the Turkey River Watershed for the HSPF simulation. The average annual runoff coefficient is the fraction of precipitation that becomes runoff (reported here as a percentage). The runoff coefficient is computed for the HSPF RCHRES subbasins from the 64-year simulation.
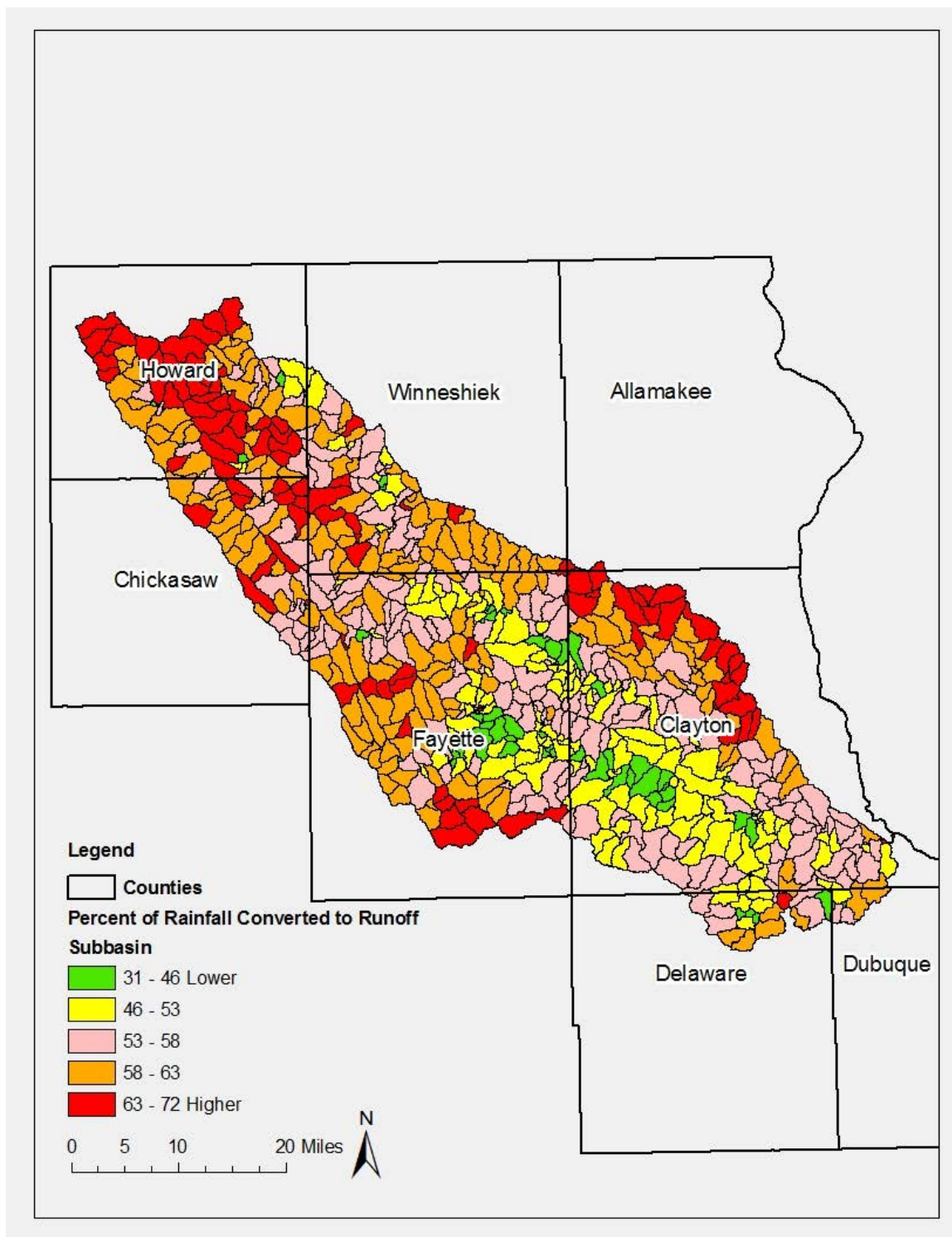
Figure 7.4: Design storm event runoff coefficient in the Turkey River Watershed for the HEC-HMS 25 year 24 hour storm (4.84 inches of rain) simulation (*IFC*, 2014). The runoff coefficient is the fraction of precipitation that becomes runoff (reported here as a percentage).

Conservation farming practices (Best Management Practices BMPs), the use of cover crops, and targeted land use changes can all promote additional infiltration and reduce runoff. Flood mitigation ponds are commonly implemented to store water temporarily, delaying the movement of excess runoff, and releasing it downstream at lower rates. Although if the area has flat terrain, which the Iowan Surface has compared to the Paleozoic Plateau, the use of flood mitigation ponds would be more challenging. Runoff would not travel as effectively on flat slopes compared to steeper slopes, making it difficult to transport the water to the storage ponds. Considering other factors like landowner cooperation, existing conservation practices already in place, or forested areas are things to consider when considering site selection for mitigation ponds.

Still, high runoff is but one factor in selecting locations for potential projects. Alone, it has limitations. For example, some of the highest runoff areas have very flat terrain. Flat terrain would make the siting of flood mitigation ponds more challenging. Of course, there are many factors to consider in site selection. Landowner willingness to participate is essential. Also, existing conservation practices may be in place, or areas such as timber that should not be disturbed. Stakeholder knowledge of places with repetitive loss of crops or roads/road structures is also valuable in selecting locations.

7.2.2 High Flood Locations

High flood locations are locations most impacted from areas downstream of high runoff subbasins. The HSPF model for the Turkey River Watershed calculated the flows at each of the 710 outlets by combining the runoff from upstream areas and routing the flow through the stream network. In identifying locations where the average flood magnitudes are relatively high, the largest peak discharges for each subbasin are evaluated for each year of the 64-year simulation.

At each of the subbasins outlet the annual maximum peak discharge is simulated. This is used in calculating the mean annual flood, calculated by taking the average of annual maximums for the 64-year simulation period. For a given subbasin, the mean annual flood tends to be larger for larger subbasin drainage areas and smaller for smaller subbasin drainage areas. In Figure 7.5 shows a relationship between the mean annual flood and drainage area for the Turkey River Watershed. The black line represents a mathematical model describing the actual mean annual flood for a given subbasin drainage area to determine which locations have a higher mean annual flood than predicted. All 311 headwater subbasins are excluded since the mean annual flood estimates are less reliable. This is because discharge estimates would be more heavily influenced by met stations differences in rain-rate for a few large storm events and would not reflect the routing effects through the stream network. Based on the difference between each of subbasin's mean annual flood and that predicted by the mathematical model for the outlets upstream drainage area, each subbasin is classified. The top third classifies as locations with high annual floods.

The middle third, closest to the mathematical model prediction, as locations with medium annual floods. The bottom third as locations with low annual floods.
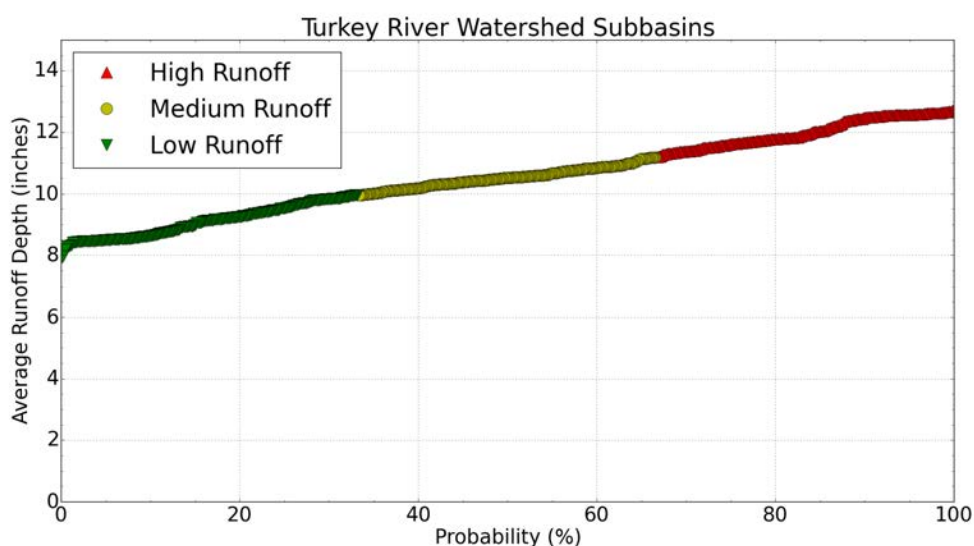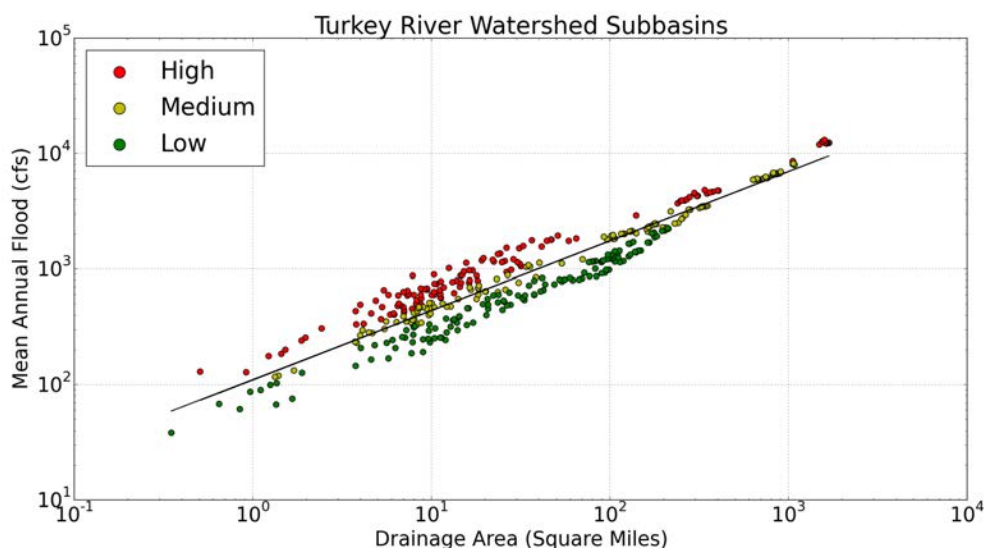

Figure 7.5: The relationship between the mean annual flood and drainage area in the Turkey River Watershed. The mean annual flood computed for the HSPF RCHRES subbasin outlets from the 64-year simulations is plotted against the total upstream drainage area at the outlets. Headwater subbasins are excluded from this analysis. A mathematical power-law model is fit to the sample data (solid black line). Comparing the distance of the sample mean annual flood from that predicted by the mathematical model (black line), the top third is classified as high annual flood (red), the middle third is classified as medium annual (yellow), and the bottom third is classified as low annual (green).

Figure 7.6 shows the locations of high, medium, and low mean annual floods for each subbasin in the Turkey River Watershed. This map differs from Figure 7.2 where some high runoff areas are low annual flood areas, particularly just north of the Iowan Surface and Paleozoic Plateau boundary. Although many of these subbasin areas

produce high runoff the upstream drainage area has an elongated shape which retards the water moving through the channels. This results in lower mean annual floods than similar-sized drainage areas with shorter channels and less elongated shapes. Again, it takes longer for water to flow down long narrow tributary helping reduce the flood magnitudes downstream. The land surface slopes of the two regions play a major role for mean annual floods. The Iowan Surface has flatter slopes causing the water to move slower through the drainage area in contrast to the Paleozoic Plateau which has steep slopes causing the water to move faster through the drainage area.

However, many high flood locations are low runoff areas but tend to be just downstream of a confluence where two stream networks join. An example of this is just south of the Iowan Surface and Paleozoic Plateau boundary. Here confluences join and timing plays a major role when determining whether the subbasin will be prone to high, medium, or low flooding. The arrival of water for two channels are such that the combined flows can result in higher annual flows. Higher annual floods can continue downstream for some distance.

From a hydrologic perspective, high annual flood locations should be a focus in flood mitigation planning. Since high flood locations are where upstream runoff combines to magnify flood magnitudes, projects that help reduce runoff by increasing soil infiltration should reduce peak flows downstream. This will hopefully disrupt the timing of flows at river confluences. If peak flows on the two tributaries arrive at same time, the combination increases peak flows downstream causing high annual floods. However, if the peak flows arrive at different times, the peak from one tributary

can pass downstream as the peak from the second tributary arrives, decreasing the overall peak flows downstream. Given the complex interaction of the timing of tributary flows, and their dependence on where and when it rains within the watershed, high flood areas make good locations for assessing the overall impact of upstream mitigation project.
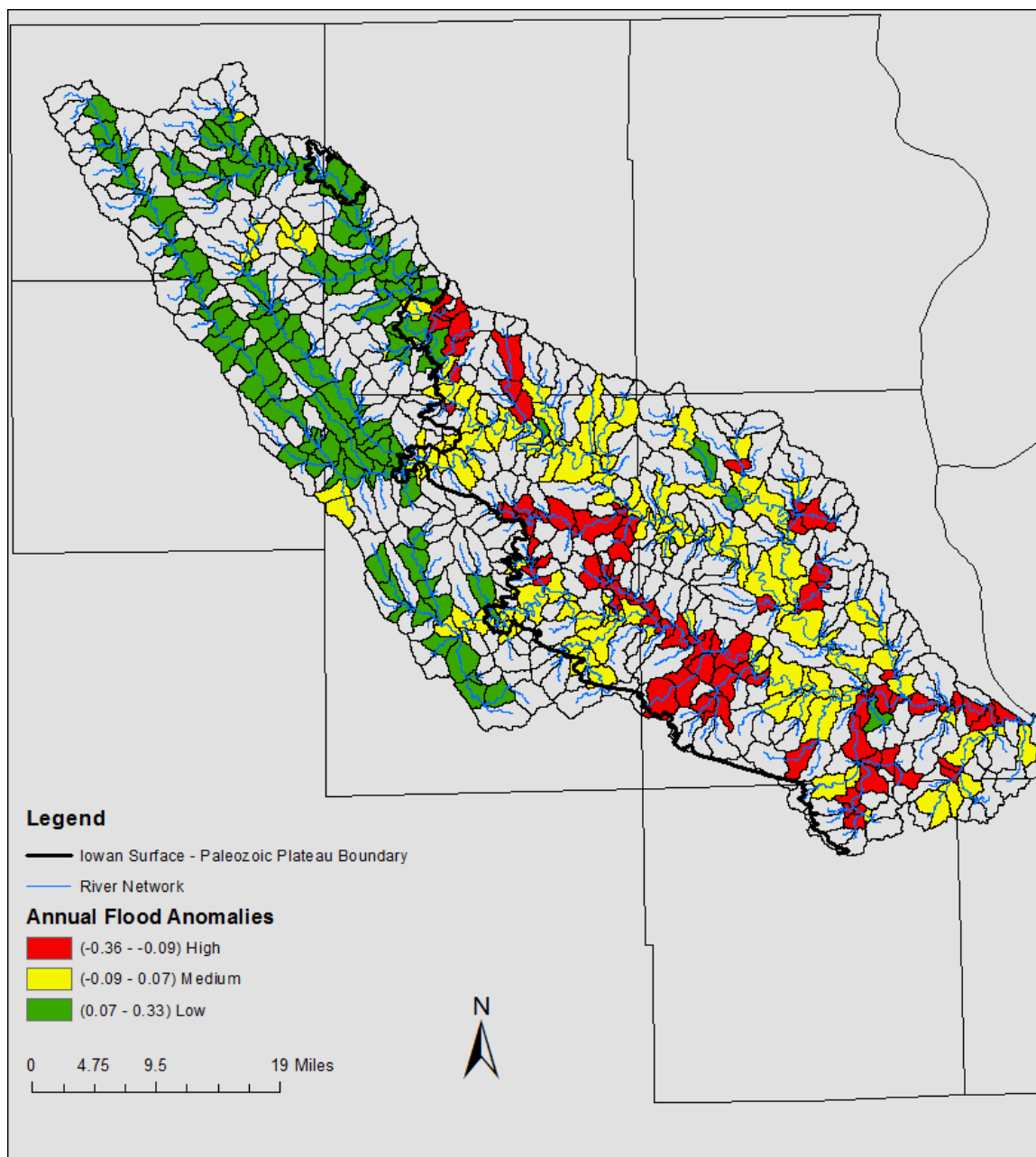
Figure 7.6: Mean annual flood anomalies for locations in the Turkey River Watershed. The mean annual flood computed for the HSPF RCHRES subbasin outlets from the 64-year simulations is compared against a mathematical relation of mean annual flood and drainage area for the entire basin. The headwater subbasins are excluded from this analysis. Locations with higher mean annual floods are shown in red. Location with medium mean annual floods are shown in yellow. Location with low mean annual floods are shown in green.

7.2.3 Intensity and Extent of Extreme Floods

Our examination of high flood areas summarizes the average flood characteristics over the 64-year simulation period. However, using the simulated peak discharges at the subbasins outlets, individual extreme floods can be examined in the watershed.

A Flood Severity Index will be used to better characterize severe flood events rather than peak discharge which depends on either a single rain event or the size of the subbasin's drainage area. The Flood Severity Index is the ratio of peak discharge to the mean annual flood at a given subbasin location. The mean annual flood is usually a rough measure when there are bankfull discharge conditions. An index of 1 or greater is a good indicator of flooding conditions. The top five Flood Severity Index for the annual maximum peak discharge at all outlets for each subbasin are ranked to identify the years when an extreme floods occurred. Table 7.1 shows the ranking of the top five years.

Rank	Water Year	Minimum	Maximum	Average
1	2008	0.47	8.61	3.25
2	2004	0.22	8.05	2.85
3	1993	0.69	11.30	2.61
4	1999	0.48	6.41	2.44
5	1991	0.23	7.07	2.27

Table 7.1: Ranking of the top simulated flood years in the Turkey River Watershed based on a flood severity index. The index is the ratio of annual maximum peak discharge (for the year) and the mean annual flood. The flood years are ranked below based on the average index at all 710 subbasin outlets. Also shown is the maximum and minimum index values at locations within the watershed.

The top severity flood index is in 2008 with an average index value 3.25 which means on average the peak discharge is over three times the mean annual flood across the watershed. Figure 7.7 shows each subbasins flood severity index for 2008. The maximum severity flood index reached 8.61. The flooding is widespread but only a few subbasins have a ratio below 1. They are located within the Winneshiek County near the north edge of the watershed by the Iowan Surface and Paleozoic Plateau divide with no color. The heaviest flooding occurrs in the mid section of the Turkey River Watershed. Although the intensity varies with location flooding is the most uniform across the watershed than for any other flood year.
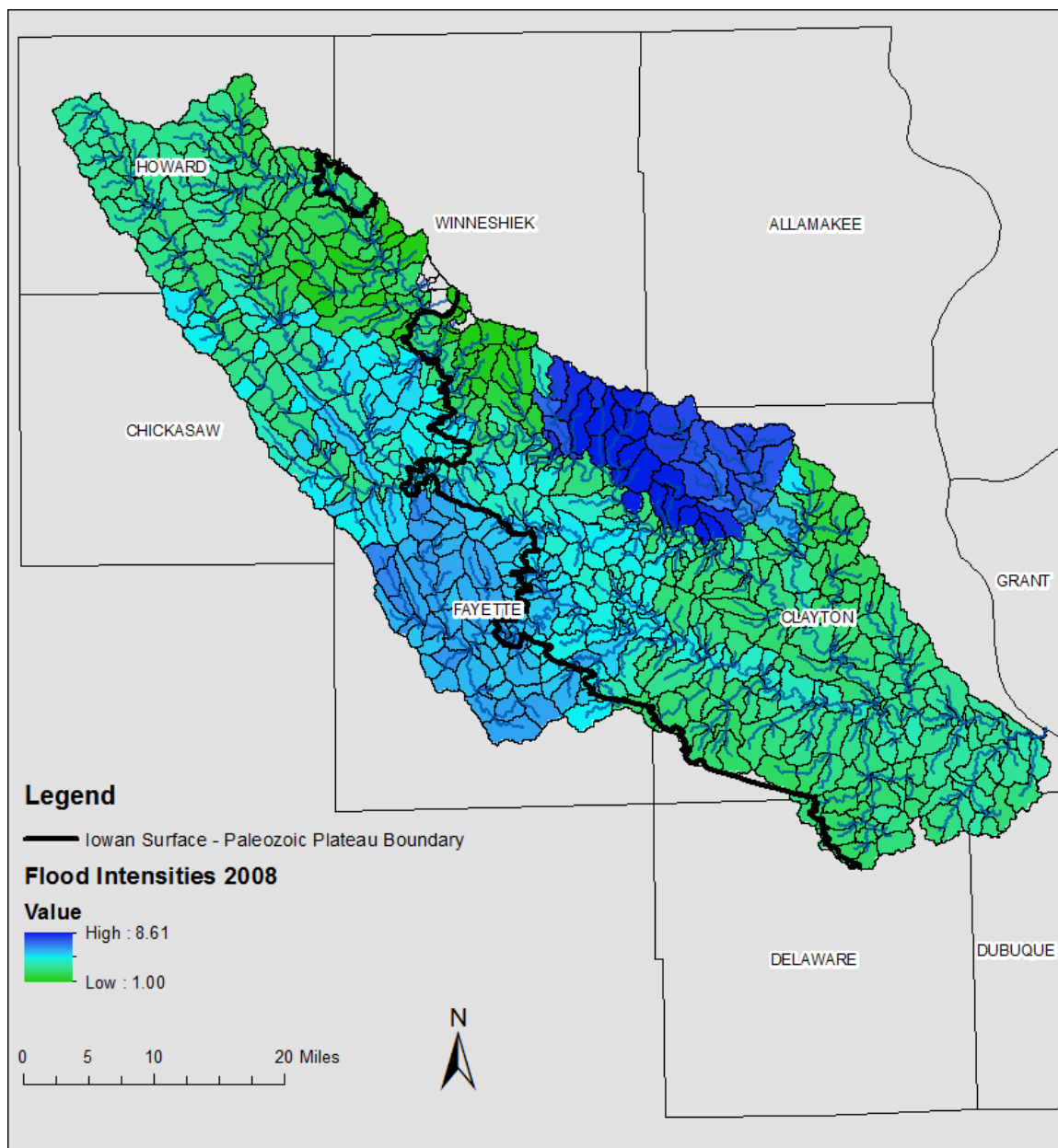
Figure 7.7: Flooding intensity and extent for the 2008 flood year. The map shows the estimated flood severity index at each subbasin outlet. Darker blue colors indicate a higher flood intensity. Areas below severity index of 1 are not shaded.

The rest of the flood years can be seen in Figure 7.8, 7.9, 7.10, & 7.11. Flood

years like in 2004 and 1993 had second and third highest average flood severity index,

with 1993 having the highest maximum at 11.30 out of all the water years. For all the years the flooding is more localized in certain portion of the watershed. Particularly in 1993, Figure 7.9, when the majority of the highest intestines of flooding occurs in the northern portion of the Turkey River Watershed. Each flood year experiences this trend of localization some more intense than others.
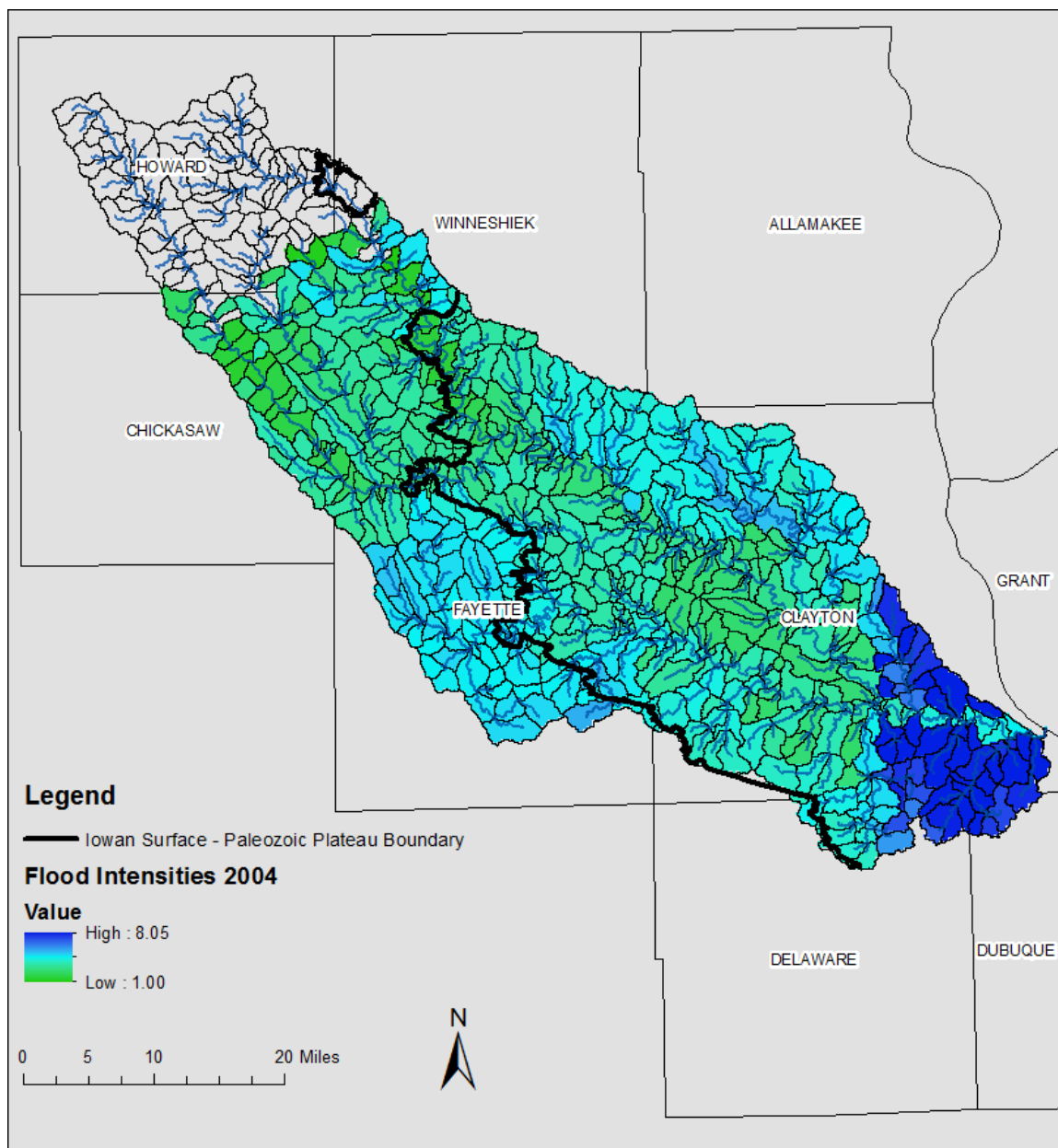
Figure 7.8: Flooding intensity and extent for the 2004 flood year. The map shows the estimated flood severity index at each subbasin outlet. Darker blue colors indicate a higher flood intensity. Areas below severity index of 1 are not shaded.
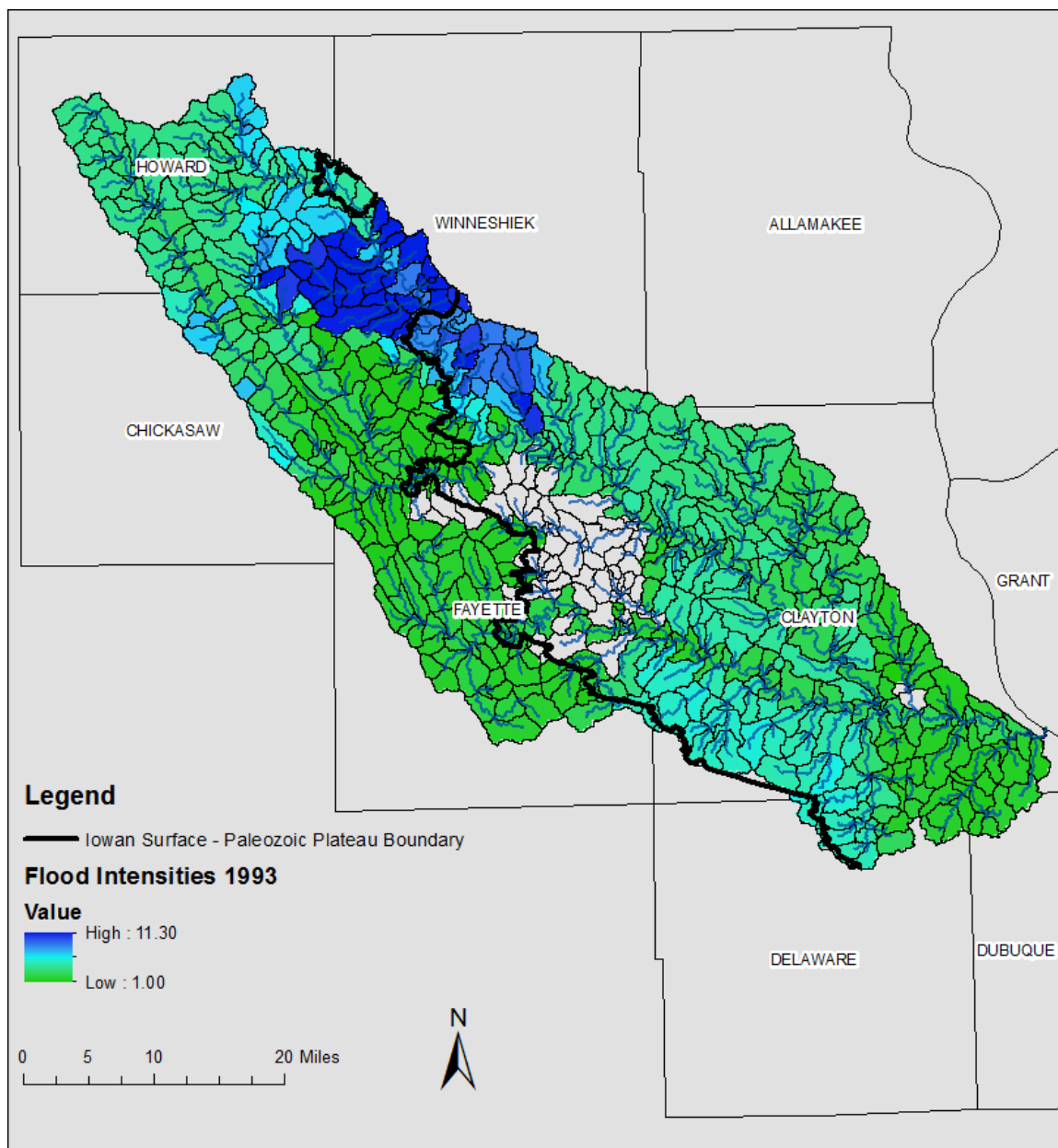
Figure 7.9: Flooding intensity and extent for the 1993 flood year. The map shows the estimated flood severity index at each subbasin outlet. Darker blue colors indicate a higher flood intensity. Areas below severity index of 1 are not shaded.
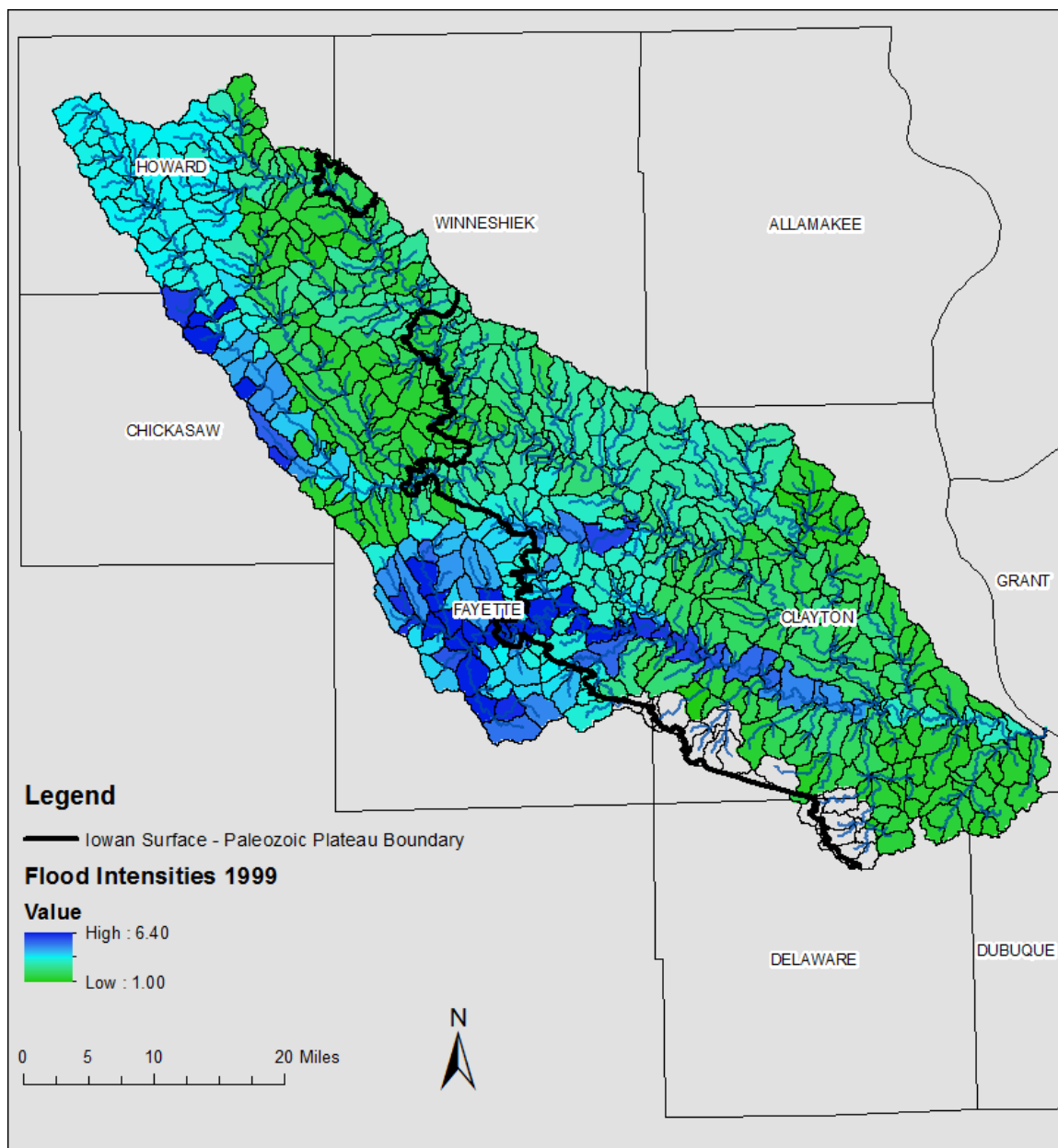
Figure 7.10: Flooding intensity and extent for the 1999 flood year. The map shows the estimated flood severity index at each subbasin outlet. Darker blue colors indicate a higher flood intensity. Areas below severity index of 1 are not shaded.
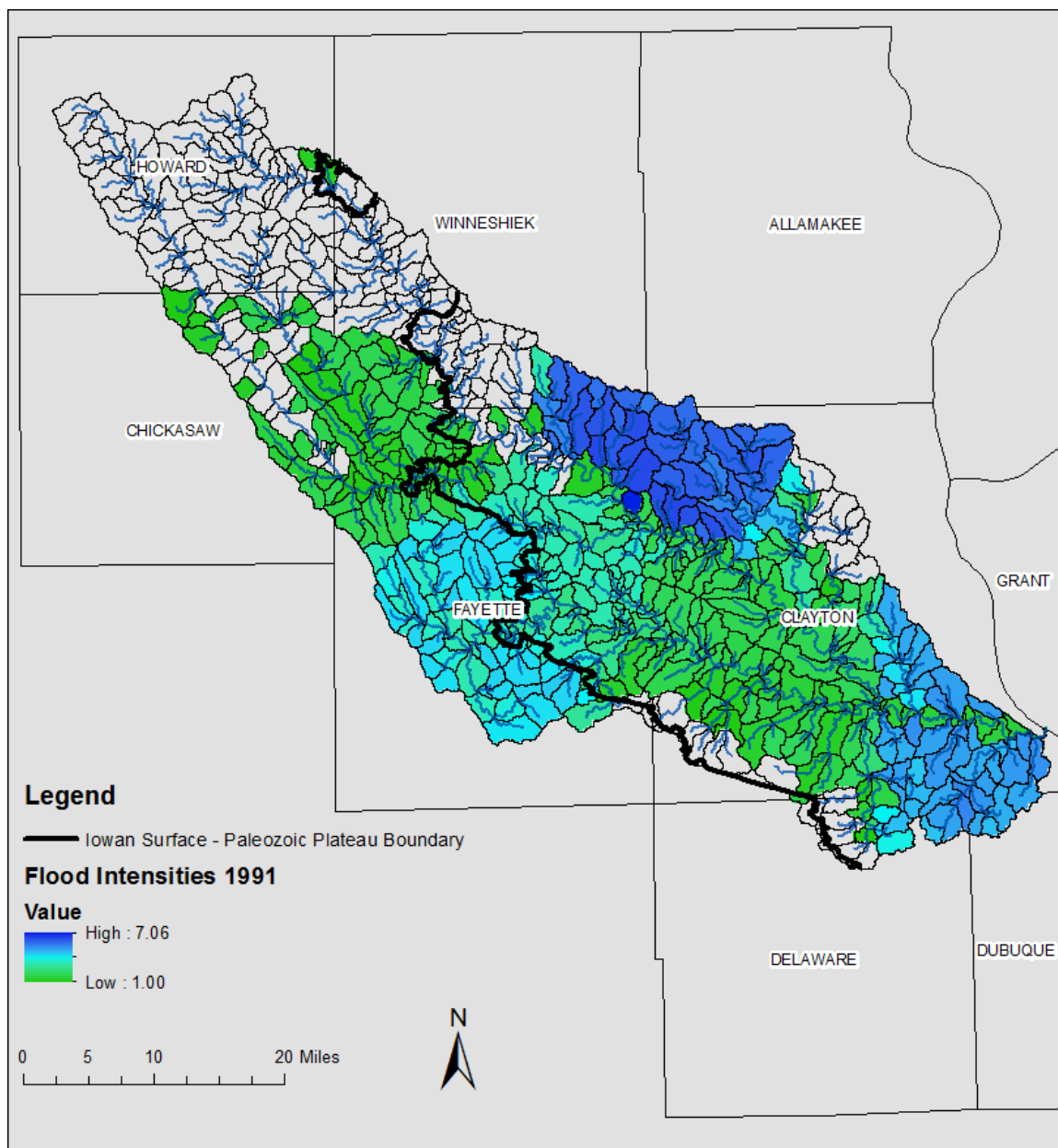
Figure 7.11: Flooding intensity and extent for the 1991 flood year. The map shows the estimated flood severity index at each subbasin outlet. Darker blue colors indicate a higher flood intensity. Areas below severity index of 1 are not shaded.

7.3   Chapter Summary

The examination of extreme flooding from the 64-year Turkey River Watershed HSPF model simulations provides a better understanding of the nature of extreme floods in the watershed. Some are quite localized in extent, and impact just a few tributaries severely. Other are associated with more widespread flooding, although the intensity may be less severe. From a flood mitigation planning perspective, it is important to recognize how different individual flood extremes can be. Often in engineering design of flood mitigation measures, a design storm with uniform rainfall across the basin is used to predict flows. One advantage of using a continuous simulation model (like HSPF) for planning is that the performance of flood mitigation measures over a range of potential flood conditions can be simulated and evaluated. In the remaining sections of this chapter, we use this approach to evaluate different hypothetical watershed scenarios.

CHAPTER 8
STREAMFLOW TREND IN THE TURKEY RIVER WATERSHED

8.1   Introduction

This chapter presents a hydrologic analysis of the Turkey River Watershed, providing insight on how streamflow has been increasing over the past 64 years. Increases in streamflow could be caused by land use changes or changes in climate. Trends in harvested agricultural area, both corn and soybean, and trends in precipitation, are also assessed. The results are used to speculate on the main cause of streamflow increases.

8.2   Streamflow Trends

Increased streamflow, which has a direct relationship to flooding, has emerged as an abiding problem for local communities in Iowa, many of which frequently flood. The Turkey River Watershed, in particular, has been subjected to this abuse and has been well monitored over the years, which makes it a good candidate to study. Understanding whether streamflow has increased naturally or due to human activity, such as increased cultivated lands, induced climate change, or a combination of the two, is an important aspect in this study.

Figures 8.1, 8.2, & 8.3 show observed annual minimum, observed annual median, and observed annual maximum flows for the Garber stream gauge within the Turkey River Watershed. Figures 8.1 & 8.2 show increasing trends and are significant to the 1% level. In contrast, Figure 8.3 did not show a statistically significant trend,
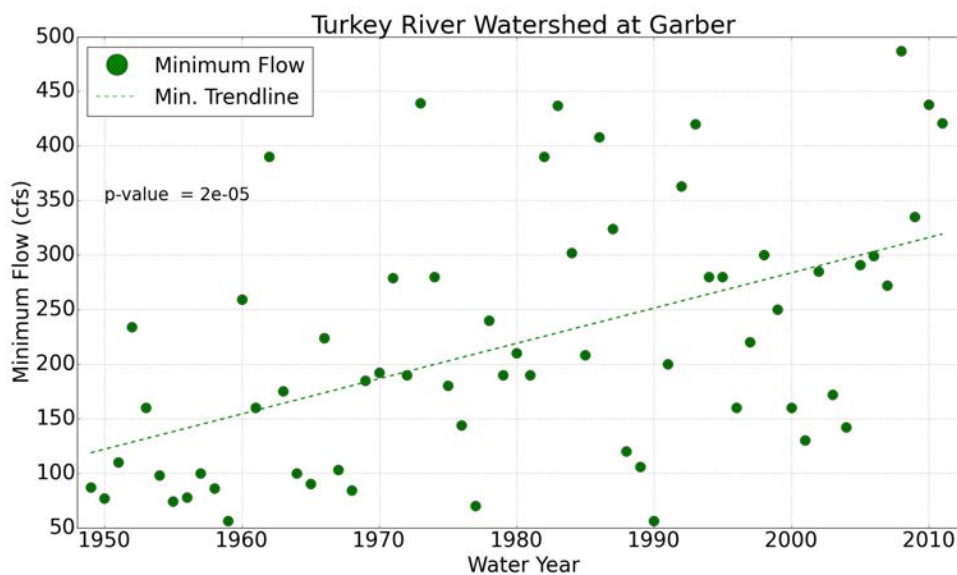
Figure 8.1: Minimum flows for the Turkey River Watershed at Garber.

even though there has been a slight increase in streamflow. Regardless, the median and minimum flows both showed significant increases in streamflow ever since the start of the study period (1948).

8.3 Precipitation Trends

Streamflow is obviously related to the amount of precipitation that falls. In Figure 8.4, annual precipitation and streamflow volume are plotted against each other for the 64 year period. Precipitation is calculated using an area weighted average using the eleven weather stations. In wetter years the streamflow is higher, and vice versa. The annual streamflow volume has a high correlation coefficient of 0.80 with annual precipitation. Figure 8.5 shows that annual precipitation is increasing with time. Therefore, increases in precipitation may be the cause of increasing streamflow.
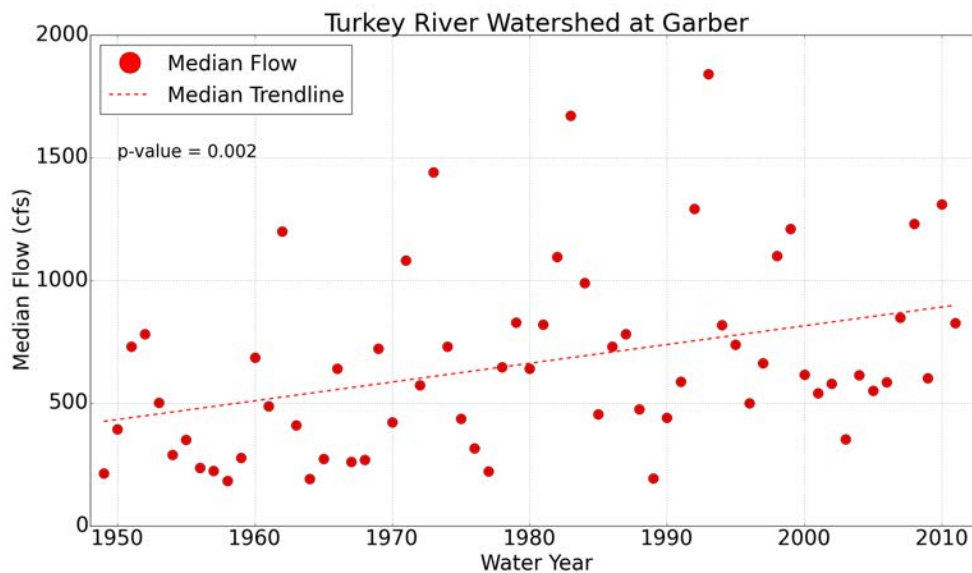
Figure 8.2: Median flows for the Turkey River Watershed at Garber.
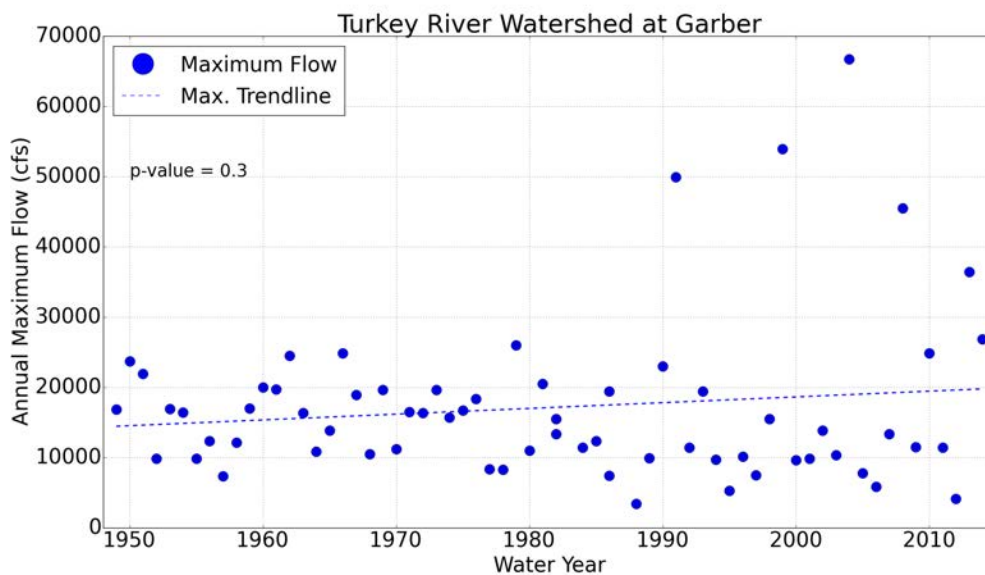
Figure 8.3: Maximum flows for the Turkey River Watershed at Garber.
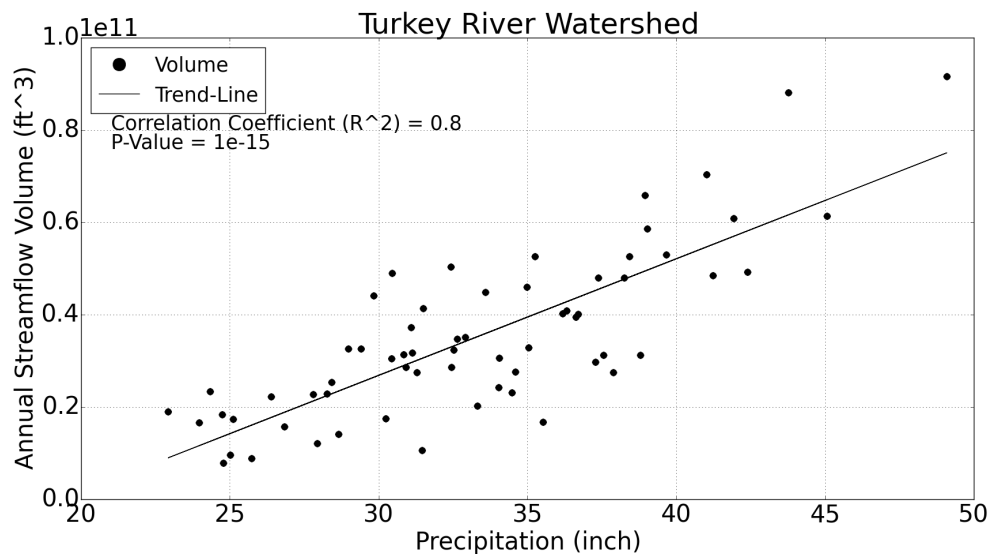
Figure 8.4: Annual stream volume plotted against annual precipitation, which shows an increasing trend.
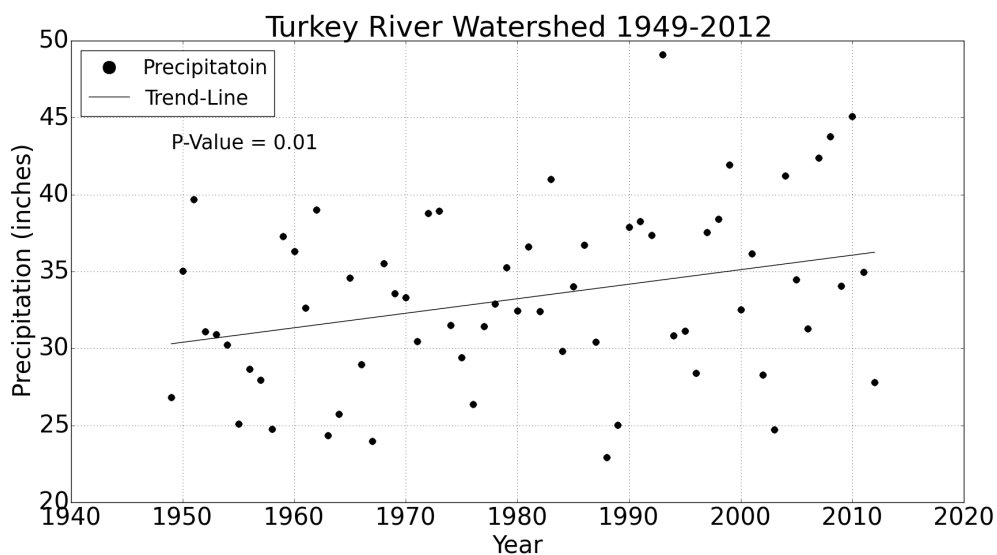
Figure 8.5: This plot shows the annual precipitation increases with time over the 64-year simulation period. It shows a statistically significant trend line to the 1% level.

8.4 Agricultural Trends

As stated previously, the Midwest has gone through an extraordinary transformation from perennial ecosystems to annual cropping systems ever since the mid 1800s. The Turkey River Watershed, located in the northeast part of Iowa, is no exception to this expansion of cultivated lands. These lands play an important role within the Turkey River Watershed, because they occupy the majority of the land cover. Agricultural lands, producing mostly corn and soybean, occupy 56% of the total watershed. The Turkey River Watershed falls across eight counties, five of which have the largest area harvested for both corn and soybean. The harvested area data comes from the United State Department of Agriculture (USDA) for Howard, Winneshiek, Chickasaw, Fayette, and Clayton counties. Figure 8.6 shows the sum of annual harvested areas, for both corn and soybean, in those five counties. It is calculated by taking the total annual harvested area (corn and soybean) and multiplying it by an area weighted factor based on the area of the county within the Turkey River Watershed. The harvested area is assumed to be evenly distributed throughout each county and assumed to be row crop agriculture. Figure 8.6 clearly shows an increasing trend in cultivated lands within the Turkey River Watershed (an increase of both corn and soybean) ever since the start of this study's period of record. However, corn and soybean harvested areas, as a whole, have been leveling off since the late 1990's. The lands that have been converted into agriculture for corn and soybean row crop were primarily pastures and grasslands.

In Figure 8.7 the annual streamflow volume is plotted with the agricultural
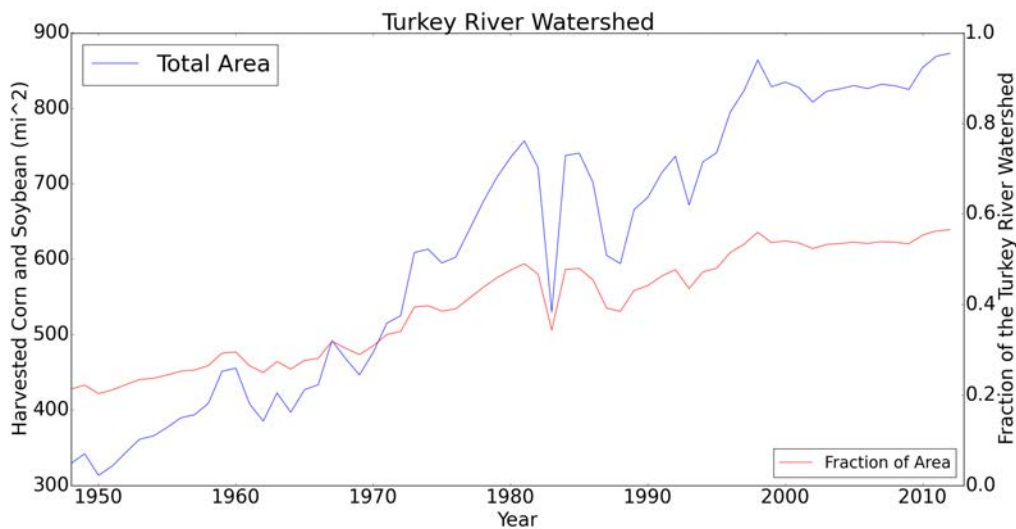
Figure 8.6: Total area (corn and soybean) harvested within the watershed is represented by the blue line. The red line is the fraction of both corn and soybean within the watershed. Both lines show increasing trends.

harvested area. Streamflow is also clearly related to the harvested area. When more land is in corn and soybean production streamflow tends to be higher, and vice versa. Streamflow has correlation coefficient of 0.3 with harvested area. Therefore, increase in harvested area may be the cause of increasing streamflow

8.5 Agricultural Impacts On Runoff

With such a rise in agricultural lands, LULC cover has dramatically changed within the Turkey River Watershed. A study by *Schilling et al.* (2010) showed evidence that LULC changes were a major contributor to the increase of discharge in the Upper Mississippi River Basin (UMRB). Daily streamflow was examined from 1890-2003 at the USGS stream gauge at Keokuk, Iowa. The study looked at each county upstream of the Keokuk stream gauge and quantified the amount of change between
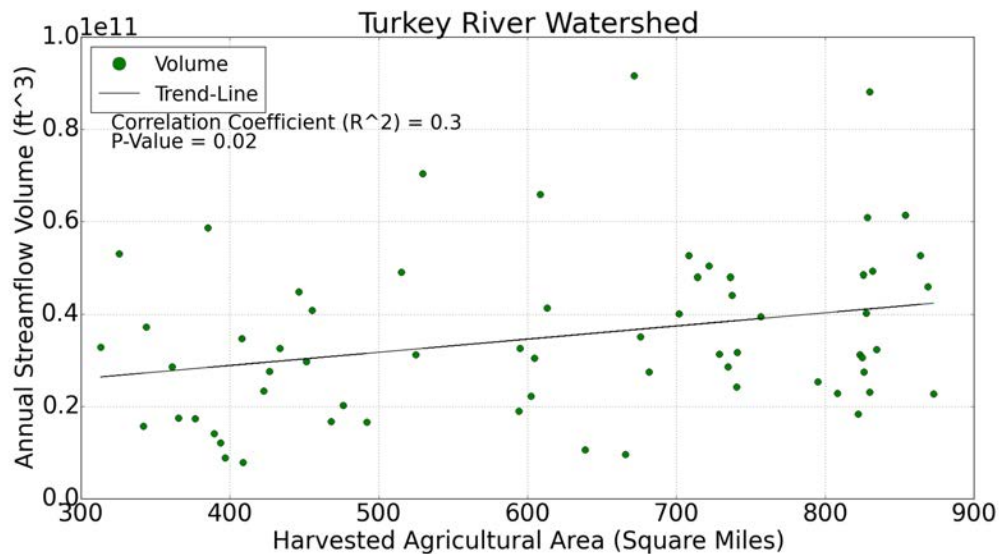
Figure 8.7: Annual streamflow volume and annual total harvested area versus time. The black line represents the increasing trend of annual streamflow volume and annual agricultural area.

discharge and precipitation due to increased soybean cultivation. It was determined that increasing soybean acreage increased the runoff coefficient (the ratio of discharge to precipitation).

The area of planted soybeans increased from practically nothing in the late 1930's to nearly 20 million acres in 2003 due to increase use of bio-fuels. By plotting the runoff coefficient and planted soybean area by time it was found that the runoff coefficient had increased significantly over a 65 year period from 1938 to 2003. Discharge (runoff) increased at a significantly higher rate than precipitation, implying runoff increased due LULC changes caused by the raise of soybean production rather than precipitation (*Schilling et al.*, 2010). In Figure 8.8 the runoff coefficient and soybean production relationship is seen for the UMRB. The yellow circles in
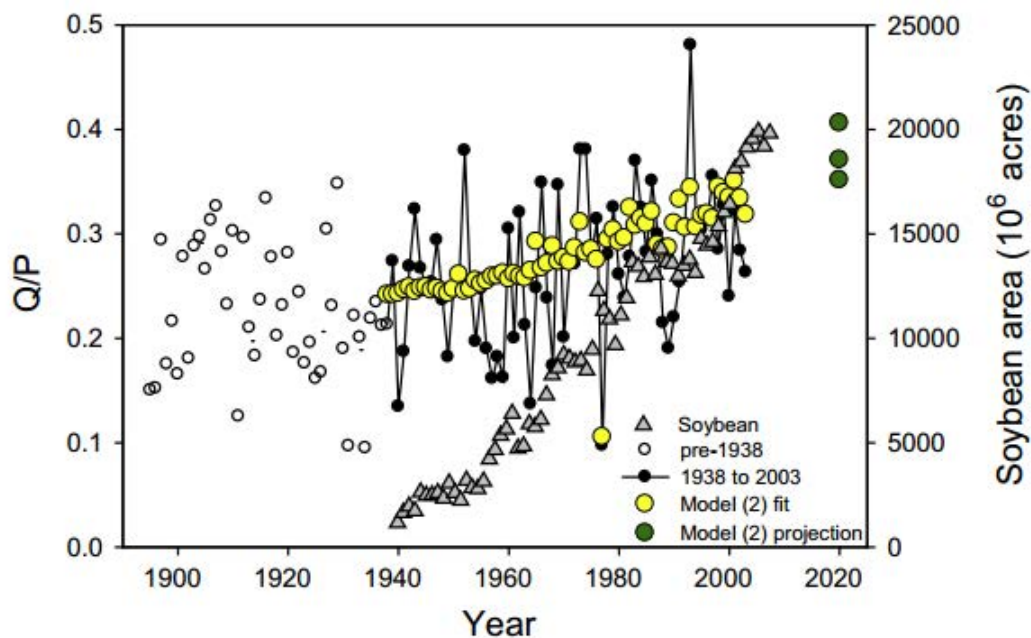
Figure 8.8: The relation of discharge (Q) to precipitation (P) for the UMRB at Keokuk stream gauge from 1890 to 2003. The total acreages for soybean area was from cultivation in Iowa, Wisconsin, and Minnesota from 1938 to 2003 in the gray triangles. The yellow is the model they used use to fit the discharge to precipitating relationship. The green circles represent a projection model using the same relationship (*Schilling et al.*, 2010).

Figure 8.8 represent the annual runoff coefficients since 1938. The gray triangles represent soybean production within the UMRB. This same relationship observed in *Schilling et al.* (2010) is seen in this study, noted in Figure 8.9 for the Turkey River Watershed. Both figures show increasing trends for the annual runoff coefficient and area harvested over time. This is a good indication that changes to LULC play an important role for increased streamflow.
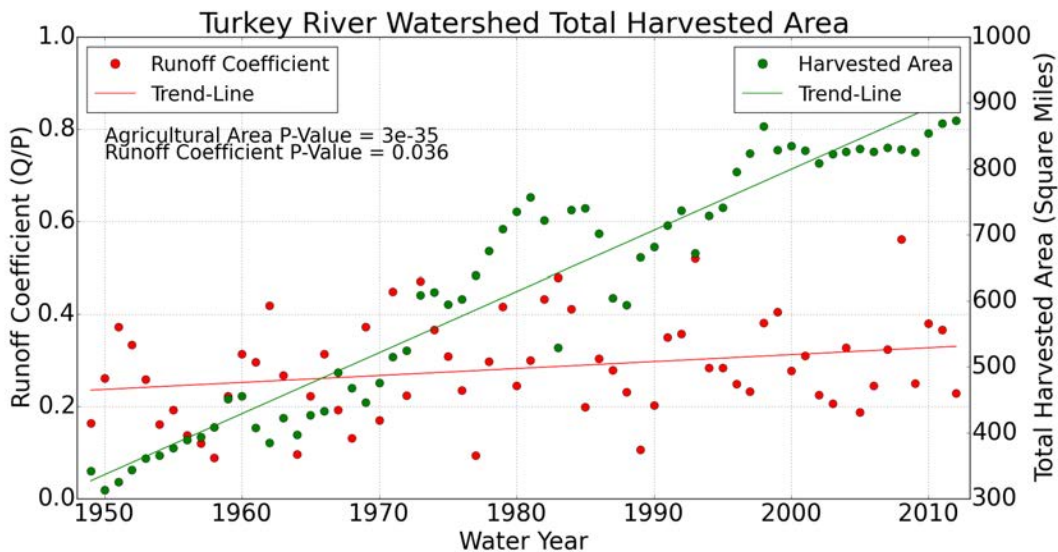
Figure 8.9: The scatter plot shows an increasing trend in harvested agricultural area and the annual runoff coefficient with time. The green solid line represents agriculture trend-line and the red solid line represents the annual runoff coefficient trend-line. Both show an increasing trend with respect to time.

8.6   Diagnostic Analysis of HSPF Simulation

To further examine the cause of streamflow increases, the Turkey River HSPF model is used to simulate the streamflow volume and runoff coefficient for the Turkey River Watershed. Figure 8.10 shows the simulated and observed runoff coefficients with time. For the simulated coefficients, the model assumes a fix LULC condition. Therefore, if increasing precipitation was the main contributor to streamflow increases, one might still expect a slight increasing trend in the model simulated runoff coefficient. However, virtually no trend is seen; simulated data (blue dots) shows a flat or even decreasing trend represented by the blue dotted trend-line (p-value of 0.74). The observed runoff coefficient (green dots) shows a statistically significant increase
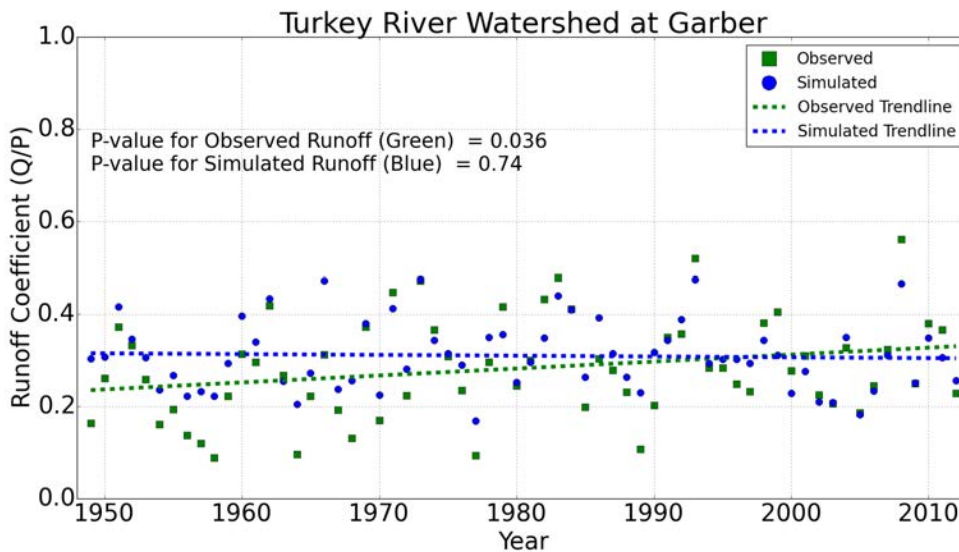
Figure 8.10: Annual runoff coefficients for simulated and observed flows for the Turkey River at Garber (USGS 05412500) versus time. The trend lines for the simulated and observed time series are evaluated with linear regression.

over the period of record as shown by the green dotted trend-line to the 5% level. The difference between the two trend lines is indication of the effect of increased agricultural corn and soybean production (which is not represented in the HSPF model). This outcome suggest that LULC significantly effects increased streamflow over the 64 year period of record; precipitation also increases but it is not the main contributor.

8.7   Chapter Summary

In conclusion, LULC changes do play an important role in the changes of the observed hydrologic response. Precipitation also plays a role, but not to the extent exhibited by changes to LULC. Due to the fact that LULC change is a major contributor and primarily caused by human activity, there are ways of preventing

increased streamflow and runoff. Prevention may include Best Management Practice's (BMP's), or returning some agricultural land back to grassland, forest lands, or native prairie vegetation. Therefore, in subsequent chapters, further investigation of flood prevention will be studied.

CHAPTER 9
MITIGATING THE EFFECTS OF HIGH RUNOFF WITH FLOOD STORAGE

9.1 Introduction

This chapter reviews a way to mitigate the effects of high runoff with flood storage. The most common type of flood storage is a pond. In agricultural areas, ponds usually hold some water all the time. However, ponds also have the ability to store extra water during high runoff periods. This form of flood storage can be used to reduce flood peak discharges. Also within this chapter, the HEC-HMS model, 50 year - 24 hour design storm event, from the HATRW report will be compared to the HSPF model, 50-year return period, for the pond scenario. This study using the HSPF model followed the same criteria as in the HATRW report for the pond scenario.

9.2 Storage Ponds

Unlike approaches for reducing runoff, storage ponds do not change the volume of water that runs off the landscape. Instead, storage ponds hold flood water temporarily and release it at a lower rate. Therefore, the peak flood discharge downstream of the storage pond is lowered. The effectiveness of any one storage pond depends on its size (storage volume) and how quickly water is released. By adjusting the size and the pond outlets, storage ponds can be engineered to efficiently utilize their available storage for large floods.

A system of ponds located throughout a watershed could be an effective strategy for reducing flood peaks at many stream locations. As an example, in the 1980s, landowners in southern Iowa came together to form the Soap Creek Watershed Board. Their motivation was to reduce flood damage and soil loss within the Soap Creek Watershed. They adopted a plan that included identifying the locations for 154 distributed storage structures (mainly ponds) that could be built within the watershed. As of 2014, 132 of these structures have been built (*IFC*, 2014).

In this section, the HSPF model simulates the effect of pond storage on flood peaks. For this hypothetical example, many ponds are distributed in tributary areas throughout the Turkey River Watershed. A prototype pond design that mimics the hydrologic impacts of flood storage is used because an actual storage pond design requires detailed site-specific information. Therefore, this example is not a proposed plan for siting a system of storage ponds. Suitable sites have not been determined available for locations within the simulation. Still, this hypothetical example does provide a quantitative benchmark on the effectiveness of distributed flood storage and the flood reduction benefits that are physically possible.

9.3   Prototype Storage Pond Design

Many ponds in Iowa have been constructed to provide flood storage. A pond schematic is illustrated in Figure 9.2. The pond is created by constructing an earthen embankment across the stream. A typical pond holds some water all the time (called permanent pond storage). However, if the water level rises high enough, an outlet

passes water safely through the embankment. This outlet is called the principal

spillway. As the water level rises during a flood, more water is stored temporarily in

the pond. Eventually, the water level reaches the emergency spillway. The emergency

spillway is constructed as a means to release water rapidly so the flow does not damage

or over-top the earthen embankment. The volume between the principal spillway

elevation and emergency spillway elevation is called the flood storage. FTABLEs are

developed and used for prototype ponds and can be seen in Figure 9.1.

```
FTABLE      991
rows cols                                       ***
  13    4
    DEPTH        AREA     VOLUME       DISCH  FLO-THRU ***
     (FT)     (ACRES)    (AC-FT)       (CFS)     (MIN)  ***
    00.00     001.00     000.00     0000.00
    01.00     006.10     006.10     0002.20
    02.00     007.45     014.90     0011.10
    03.00     008.40     025.20     0011.50
    04.00     009.10     036.40     0011.90
    05.00     009.72     048.60     0012.30
    05.50     010.11     055.60     0026.50
    06.00     010.48     062.90     0052.60
    06.50     010.82     070.30     0092.80
    07.00     011.10     077.70     0153.00
    07.50     011.39     085.40     0461.30
    08.00     011.64     093.10     0622.50
    09.00     011.31     101.76     1115.30
 END FTABLE991
```

Figure 9.1: Prototype pond FTABLE used for distributed flood storage analysis. If multiple ponds are used in a subbasin the variable columns of the FTABLE, VOLUME and DISCH, are multiplied by the respective number of ponds.

9.3.1 Prototype Pond Outlet and Emergency Spillway

Using information from ponds constructed in Soap Creek and NRCS technical references on pond design, a prototype pond outlet and emergency spillway were defined for the simulation experiments. A 12-inch pipe outlet was assumed for the principal spillway and a 20-foot wide overflow opening was assumed for the emergency spillway. The top of the dam was set two feet above the emergency spillway(*IFC*, 2014).

The elevation difference between the principal and emergency spillways was set to 5 feet. The amount of water released downstream by the pond depends on the water depth. The discharge from the principal spillway was determined using pipe flow hydraulic calculations. Once the water depth reaches the emergency spillway, releases also included contributions from both the 12-inch pipe and the emergency spillway. Discharge of the emergency spillway was determined using NRCS technical references assuming C-Type retardance on the spillway. This was determined to be a reasonable design assumption based on discussions with regional NRCS engineers(*IFC*, 2014).
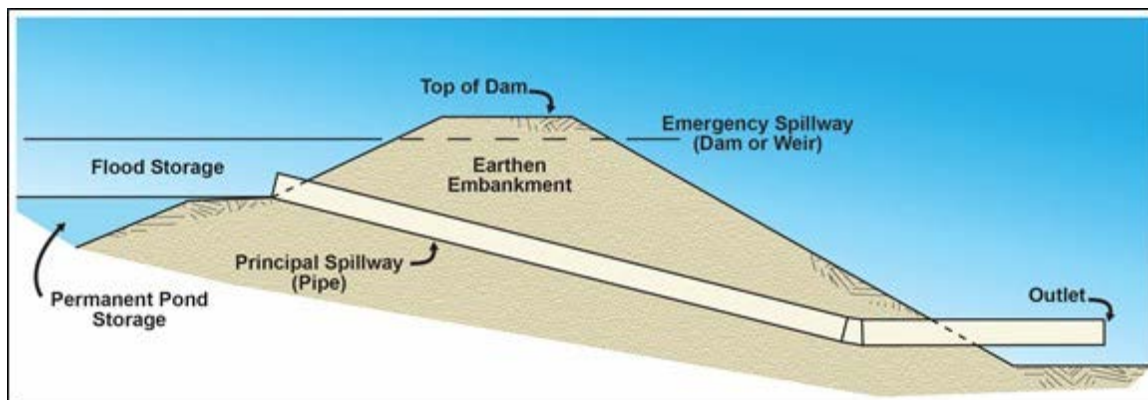
Figure 9.2: Prototype pond used for distributed flood storage analysis (*IFC*, 2014).

9.3.2 Prototype Pond Shape

Although pond design specifications and built ponds in Iowa provide a reasonable prototype for a pond outlet, the amount of water stored behind an earth embankment requires local knowledge of the topography. However, to represent a large number of ponds in our simulations, the effort to compute a precise relationship between pond stage (water level) and water storage for each would be enormous. The effort is also unwise, unless good sites for pond structures are selected in the first place (for each and every pond). As a compromise a prototype pond shape, developed in a recent study by the Iowa Flood Center (2014) for the Soap Creek Watershed, is utilized.

In the Iowa Flood Center (2014) study, pond sites in the Soap Creek Watershed were selected for topographic analysis; a total of 132 sites in Soap Creek, majority in headwater areas, were selected. The water volume impounded behind the dam

was computed as a function of water depth. The result, the storage volume in the pond for different water levels, is known as a stage-storage relationship. Since the stage-storage relationship differs at each site, an average fit to the relationship from all Soap Creek ponds that have a drainage area between 0.5 mi^2 and 1.5 mi^2 was developed and used as the prototype pond shape for all simulated pond locations.

9.3.3 Prototype Pond Hydraulics

The pond shape defines the stage-volume relationships as the water level changes in the pond. In contrast, the pond outlet defines the stage-discharge relationship for the pond. This information is combined to define the prototype storage-discharge hydraulic relationship needed for the pond simulation. One type of prototype pond is used; in this prototype, the emergency spillway elevation is set to 5 feet above the primary spillway. This results in a flood storage capacity of 48.6 acre-feet.

9.4 Siting of Hypothetical Ponds in the Turkey River Watershed

To examine the hypothetical impact that flood storage would have on the flood hydrology of the Turkey River Watershed, the prototype pond is placed throughout the headwater subbasins. In the Soap Creek Watershed, where flood storage is already used extensively, the average pond density is 1 pond for every 1.9 mi^2 of drainage area. Therefore, for the flood storage simulations for the Turkey River Watershed, pond structures are placed in headwater subbasins at a density of 1 pond for every 2 mi^2 of drainage area. In total 402 ponds are distributed throughout headwaters in the upper portion of the watershed, tallying to 250 headwater subbasins.

The 250 out of the 311 headwater subbasins in the Turkey River Watershed contain ponds ranging in size from 0.93 to 7.64 mi^2. If a subbasin drainage area was 6 mi^2, it would have 3 ponds. Furthermore, not all the area within a subbasin will drain to a pond; some water would flow into the stream below the ponds and not be temporarily stored. To handle these conditions in the HSPF model, it is assumed that half the subbasin area drains through a pond, and the other half does not. This step is most efficiently accomplished in the model by creating a single aggregate pond. That is, if there were 3 ponds in a subbasin, it has the same aggregate effect of a single pond that has three times the storage and three times the outflow. So from an HSPF modeling standpoint, the half of the subbasin that drains through a pond can more simply be routed through a single aggregated pond. In this way, the effects of the pond storage can be estimated, without having to specify the exact physical locations of any pond.

For the 250 headwater subbasins, a total of 402 prototype ponds are simulated. All the subbasins contained between 1 and 4 ponds. Figure 9.3 shows the 250 headwater subbasins, and the number of ponds assigned to each. In HSPF, the 402 prototype ponds are represented by 250 aggregated ponds, one for each of the 250 headwater subbasins. Overall, the ponds control flows from a total area of 392.7 mi^2; in other words, 23.2% of the watershed area drains through the simulated prototype ponds.
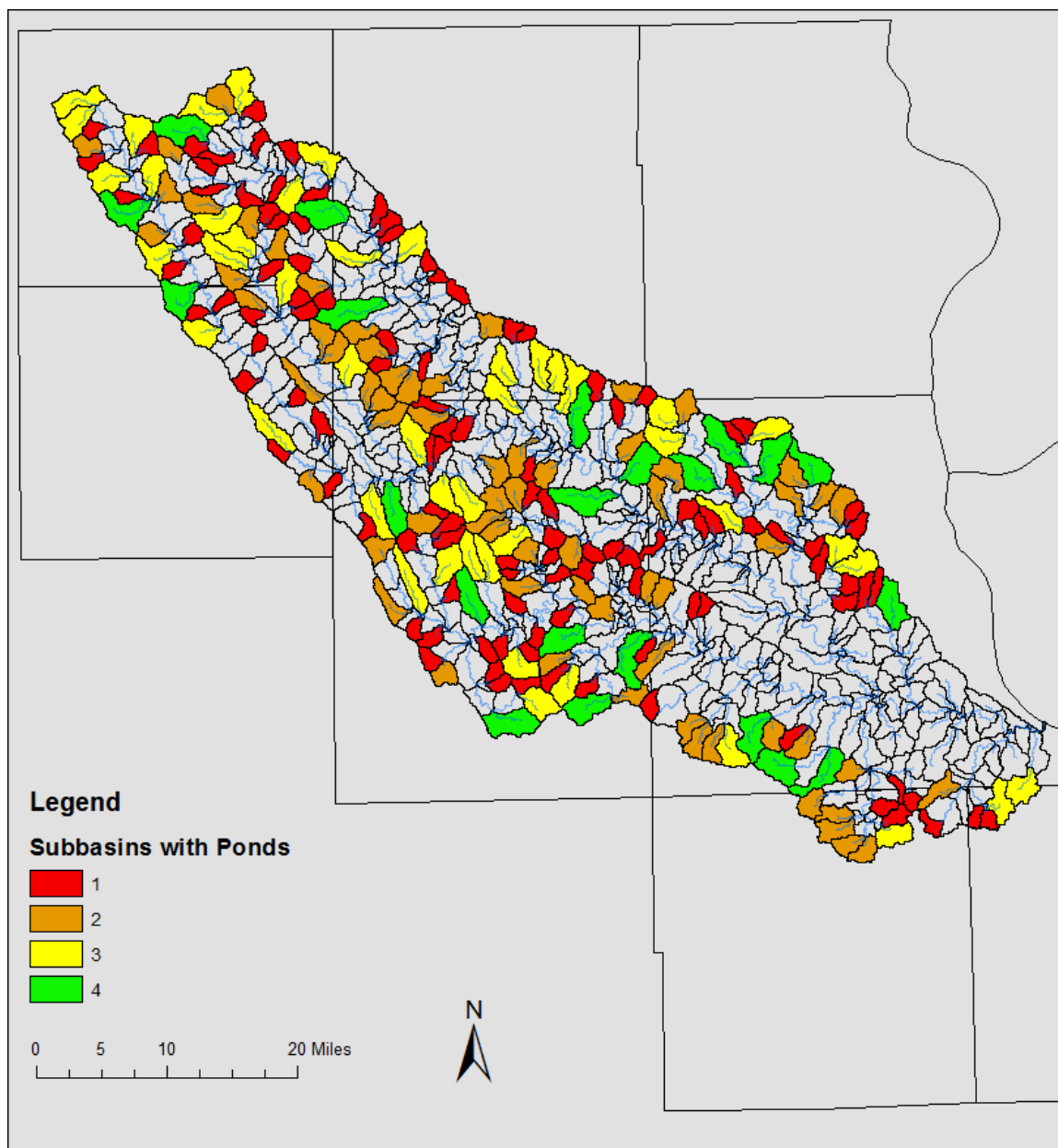
Figure 9.3: Shows the number of ponds for each subbasin in the Turkey River Sub-basin. Red color = 1 pond, orange color = 2 ponds, yellow color = 3 ponds, and green = 4 ponds.

The pond characteristics upstream of the nine index locations are characterized

in Table 9.1. Although 23.2% of the entire watershed drains through the prototype

ponds, this percentage varies for the index locations. The percentages are lower near the outlet of the Turkey River like Elkader (24.7%), Garber (24.5%), and the Volga River at Littleport (23.9%). The percentages are higher in the upper parts of the watershed like Otter Creek at Elgin (30.2%), Spillville (26.6%), and Crane Creek at Little Turkey River (26.0%).

From the 250 ponds representing the 402 theoretical ponds the available storage controlled by the pond is 19,537.2 acre-feet resulting in 0.47 inches water depth placed over the upstream drainage area (just subbasins with ponds). For the entire watershed, the ponds can temporarily store roughly 0.22 inches of runoff from a storm event.

Location	Drainage Area (mi²)	Number of ponds upstream	Upstream Area from Ponds (mi²)	Upstream Area from Ponds (%)
Otter Creek at Elgin	47	14	14.2	30.2
Spillville	177	55	47.1	26.6
Crane Creek at Little Turkey River	209	52	54.3	26.0
Eldorado	641	171	163.5	25.5
Elkader	903	253	223.0	24.7
Garber	1,545	388	378.5	24.5
Outlet at Mississippi	1,693	402	392.7	23.2
Volga River at Fayette	130	38	38.4	29.5
Volga River at Littleport	348	88	83.1	23.9

Table 9.1: Summary of pond characteristics at index locations for simulated prototype ponds. The upstream drainage area, the number of ponds, and the drainage area upstream of the ponds is indicated by index location.

9.5   Storage Pond Simulation

The Turkey River Watershed HSPF model runs for the 64-year simulation period for the flood storage pond scenario. The storage ponds do not alter the amount of runoff that is generated from the landscape, but instead the ponds temporarily store the runoff and release water downstream at a lower rate. Therefore, only the effect of the ponds on the simulated flood magnitudes are examined.

Figures 9.4 & 9.5 show the flood frequency analysis of simulated current conditions (baseline) and storage pond scenario (5 foot emergency spillway elevation). In this scenario, each pond provides 48.6 acre-feet of flood storage, resulting in a total of 19,537.2 acre-feet of flood storage for the entire watershed. Annual maximum peak discharges for the nine index locations are shown. At all locations, the pond scenario has lowered the simulated peak discharges. The average peak reduction effect is largest for the Otter Creek (21.3%); this locations also has the largest percentage of upstream area draining through the ponds (see again Table 9.1). The peak reduction effect tends to be greatest for larger simulated flood events (10- and 25-year return period). For example, again, the Volga River at Fayette peak reduction for the 10-, 25-, and 50-year return period is 25.5%, 19.8%, and 14.8% respectively for the largest flood, compared to the 15.2% average peak reduction.
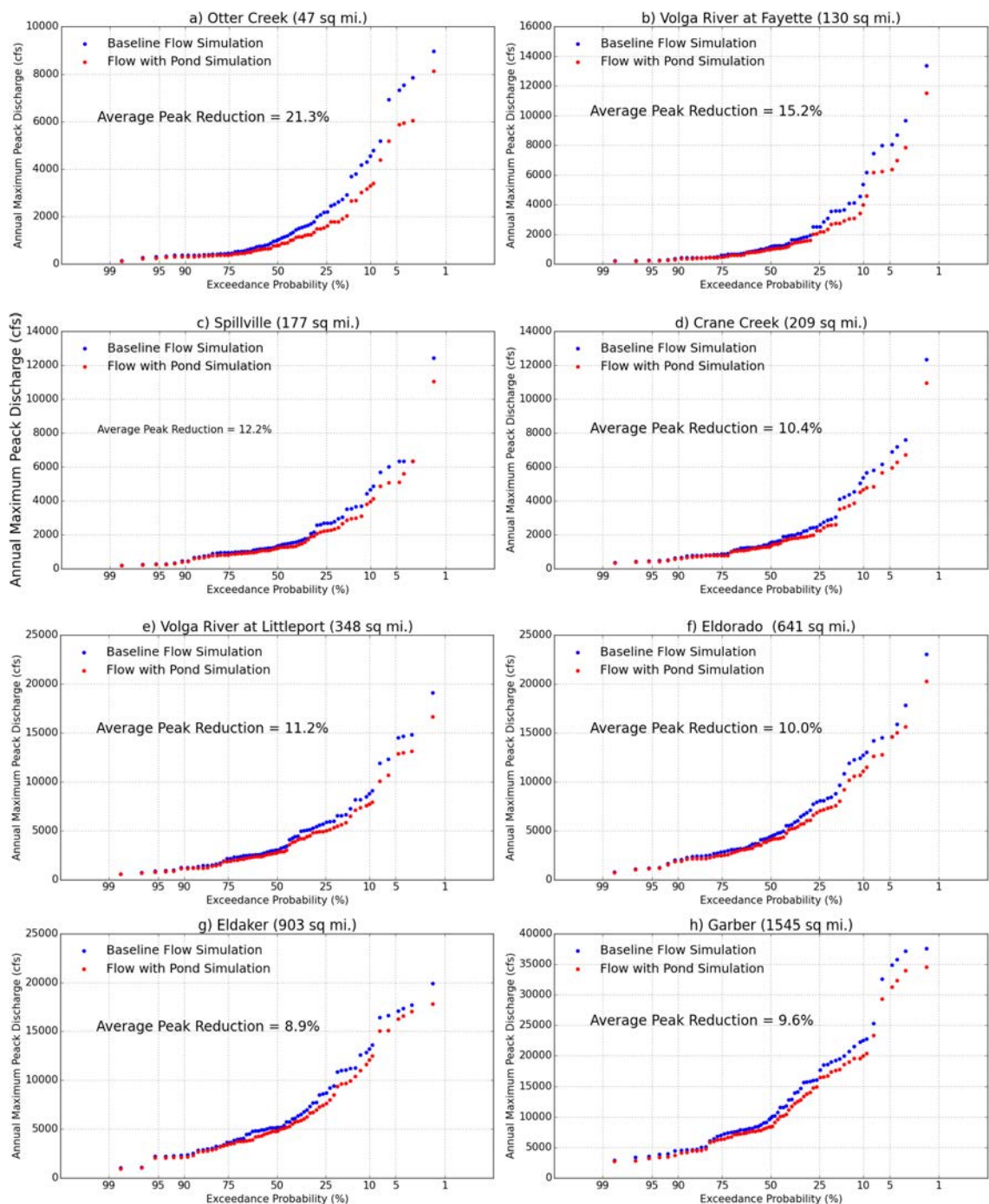
Figure 9.4: Sample probability distribution of annual maximum peak discharges for the baseline simulation and the flood storage pond scenario.
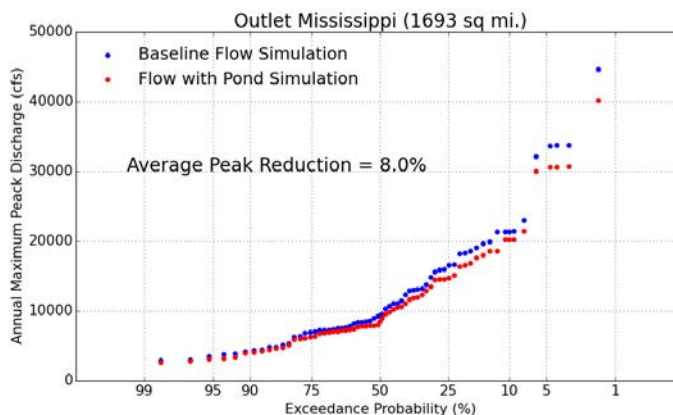
Figure 9.5: Sample probability distribution of annual maximum peak discharges for the baseline simulation and the flood storage pond scenario for the Mississippi Outlet.

By design, ponds store a greater volume of water as flows increase; after the water level raises above the emergency spillway elevation, the flood storage volume is exhausted and the peak reduction diminishes. Therefore, the flood storage is most effective in reducing peak discharges for a targeted range of flows (up until the storage is filled). Figures 9.4 & 9.5 display the largest reduction towards the lower exceeding probabilities, which indicates larger return periods. These effects explain the results in Table 9.2 for the flood storage pond scenario. The table summarizes the average peak reduction at the nine locations. Table F.1 in Appendix F displays baseline flows from the HSPF simulation.

This effect is more clearly seen by looking at the peak reduction for the 2-, 10-, 25-, and 50-year return period peak discharge levels (also shown on Table 9.2). At nearly all location the largest peak reduction occurs at the 10-year, 25-year, or

		Return Period (%)				HEC - 50 year 24 hour storm (%)
Location	Average (%)	2-year	10-year	25-year	50-year	
Otter Creek	21.3	22.9	27.9	21.1	13.0	34.1
Spillville	12.2	8.5	14.7	11.8	9.3	22.3
Crane Creek	10.4	12.3	13.1	12.7	11.2	17
Eldorado	10.0	6.9	12.8	5.7	12.2	11
Elkader	8.9	6.9	8.6	4.3	8.5	8.3
Garber	9.6	14.5	11.3	9.6	8.2	4.7
Outlet at Mississippi	8.0	9.5	5.5	9.2	9.7	4.6
Volga at Fayette	15.2	14.5	25.5	19.8	14.8	19.1
Volga at Littleport	11.2	8.0	12.1	11.5	12.6	12.6

Table 9.2: Peak reduction effect for the storage pond scenario (relative to the baseline simulation). The average reduction is shown (in %) for the 64 annual maximum events. Also shown are the reductions (in %) for the 2-, 10-, 25-, and 50-year return period events and the HEC-HMS 50 year - 24 hour design storm event (5.67 inches of rain in 24 hours). The reductions are evaluated at the nine index locations.

50-year return period level. The only exception is Elkader with an average peak reduction of 8.9%. The 10- and 25-year return periods have larger reduction because the ponds are utilizing their storage for rarer large flood events. In most cases the 50-year return period will see a diminished reduction. When flows exceed the ponds emergence spillway the storage pond loses its ability to store water and reduce peak flows.

HSPF, 50-year return period, and HEC-HMS, 50 year - 24 hour design storm event (5.67 inches of rain in 24 hours), compute different results for the pond scenario. Figure 9.6 shows both the HSPF (green bars) and HEC-HMS (blue bars) peak flow reduction results. The HEC-HMS results show a dramatic and rapid decrease in peak flow reduction going from smaller drainage areas to larger drainage areas (Otter Creek's 34.1% reduction (47 mi^2) to the Outlet at the Mississippi 4.6% reduc-
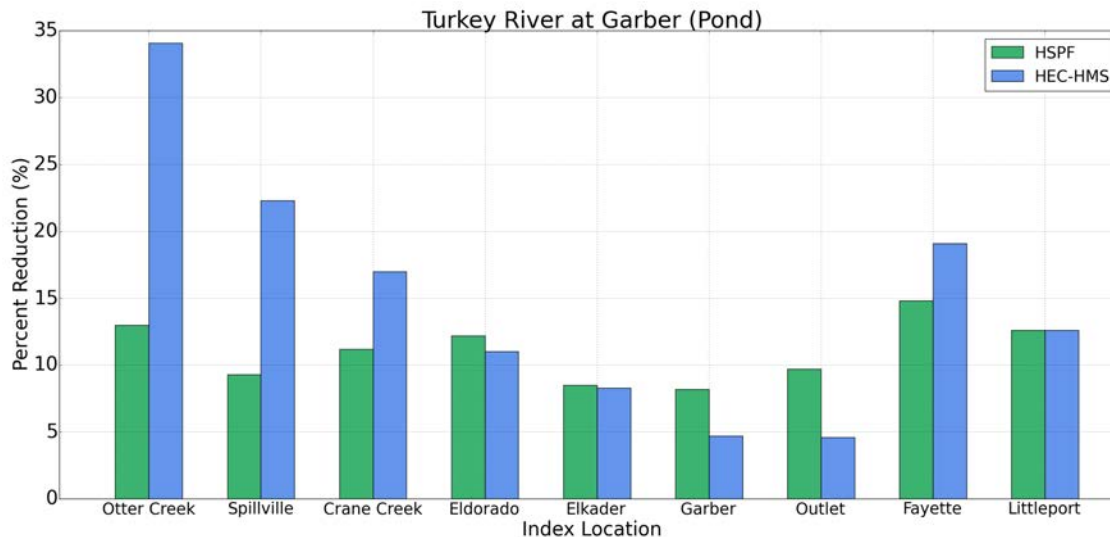
Figure 9.6: HSPF, 50-year return period, and HEC-HMS, 50 year - 24 hour design storm event, results comparison.

tion (1,693mi^2)). In contrast, the HSPF results show a relatively consistent percent reduction at every location. The difference in results from both models are related to their simulation approach. HEC-HMS is a single storm event of a duration of 24 hours, where rainfall is uniform and all the ponds have their maximum flood storage capacity available. HSPF simulates the flows and pond storage levels continuously over a 64-year period. The results for HEC-HMS are based on the simulated peak flows for the one event. The results for the HSPF are based on the top ranked simulated peak flows, and are associated with different storm events at each and every site.

To better understand how the flood storage scenarios change simulated flood peaks, Figure 9.7 displays the average peak reduction effect at subbasin outlets throughout the watershed for the ponds. Notice that some outlets have very high

peak reductions, approaching almost 47%. The high peak-reduction locations (red or orange) are only observed for the headwater subbasins, where the 402 storage ponds are located. Indeed, flood storage is most effective immediately downstream of a pond. As one moves downstream from a pond, the peak reduction effect diminishes rapidly. For subbasins immediately downstream of headwater subbasins, the peak reduction effect often drops to half (or less) than that observed upstream. The effect continues to diminish downstream of large tributaries and the main stem, reaching the lowest peak reduction, and can be seen at the downstream outlet where the Turkey River empties to the Mississippi River.
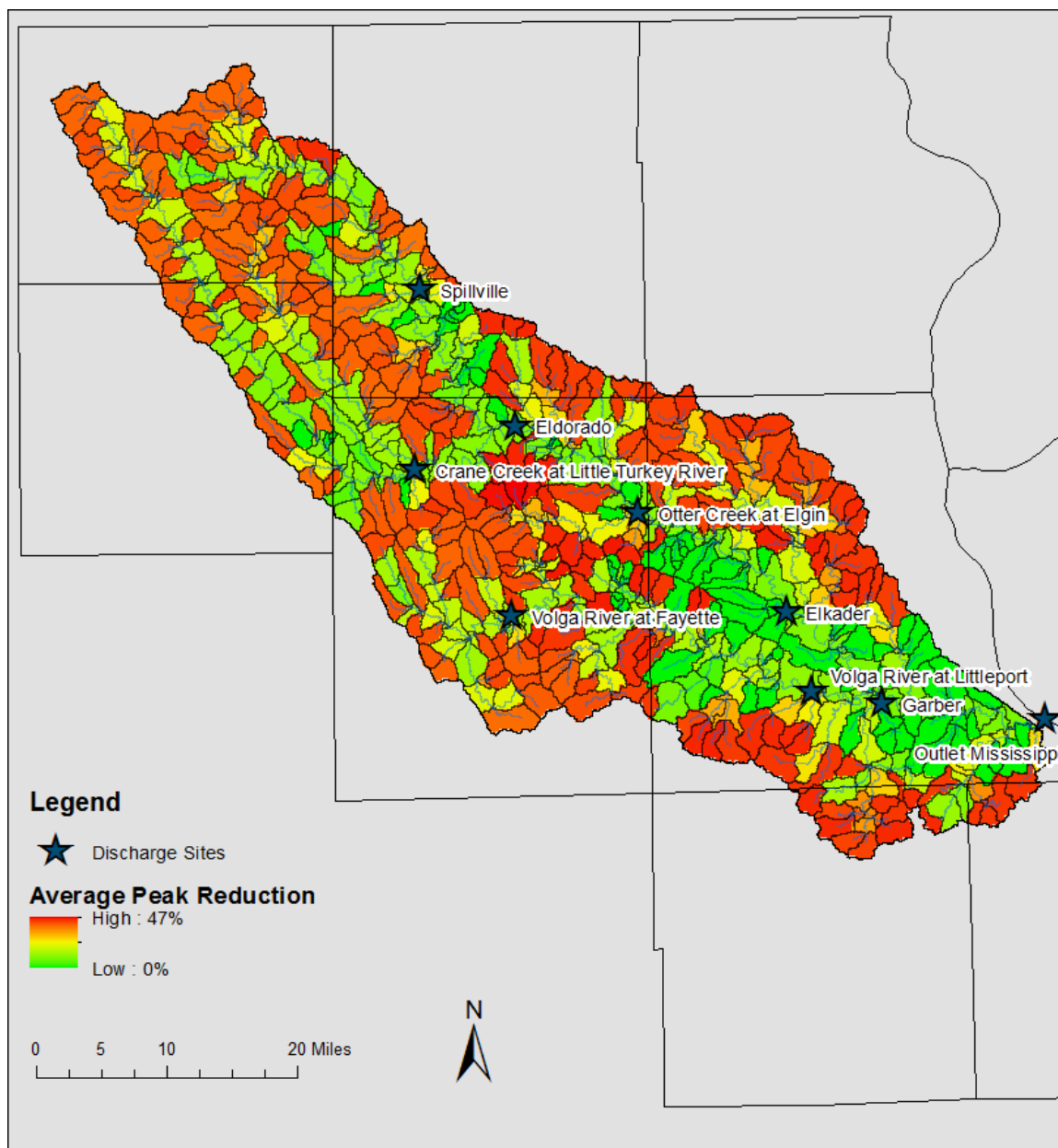
Figure 9.7: Average annual peak discharge reduction (in %) for locations in the Turkey River Watershed for the large flood storage pond scenario. The annual maximum peak discharge for the subbasin outlets from the 64-year simulations are compared for the pond scenario and the baseline simulation. The average peak reduction effect is computed from the 64 ranked annual events.

9.6   Chapter Summary

In this chapter prototype storage ponds are implemented into watershed reducing runoff. The prototype ponds are based on the Iowa Flood Center (2014) study in the Soap Creek Watershed. The average pond density is 1 pond for every 2 mi^2. In total 402 ponds are distributed throughout the watershed equating to 250 prototype ponds. If multiple ponds are within a single subbasin, the pond is multiplied by the respective amount of ponds representing one big pond. FTABLEs are used to represent the ponds. In a similar fashion if multiple ponds are located within a subbasin the FTABLE is multiplied by the respective amount of ponds. Ponds control 23.2% of the watershed drainage area. This results in a total of 19,537.2 acre-feet (0.22 inches) of available storage control by the ponds throughout the entire watershed. The largest reduction are seen in the smaller drainage areas like in Otter Creek (Drainage Area 47 mi^2) with a average peak flow reduction of 21.3% or Volga River at Fayette (Drainage Area 130 mi^2) with an average reduction of 15.2%. The outlet at the Mississippi saw an average of 8% in peak flow reduction from baseline conditions. This pond scenario shows potential benefits of using storage ponds. Storage ponds could potentially help on a localized level upstream where the flows are not as great. A major factor is land owner willingness, the owner would have to give a potion of land for the storage pond or ponds to help reduce peak flows downstream. Already within the Turkey a plan is set to build 300 water and sediment control basins (ponds), create or re-establishing 50 wetlands, and install 10 linear miles of riparian buffers. Flood mitigating measures already are being utilize within the Turkey River Watershed basin and will be

complete over the next 20 years (*Love*, 2015).

CHAPTER 10
REDUCING HIGH RUNOFF WITH INCREASED INFILTRATION

10.1 Introduction

Reducing runoff from areas with elevated runoff may be accomplished by increasing how much rainfall infiltrates into the ground. Changes that result in higher infiltration reduce the volume of water that drains off the landscape during and immediately after storms. The extra water that soaks into the ground may later be evaporated, it may slowly travel through the soil, either seeping deeper into the groundwater storage, or traveling beneath the surface to a stream. Increasing infiltration has several benefits; one benefit is that infiltrated water reaches a stream at a much later time, long after the storm ends, and by arriving late, the water keeps rivers running during long periods without rain.

In this chapter, one alternative is examined for reducing runoff through LULC changes and soil quality improvements. The hypothetical land use scenario is the conversion of row crop agriculture (corn and soybean) back to the Turkey River Watershed's native tall-grass prairie. The hypothetical example is meant to illustrate the potential effects on flood reduction. However, the example is not a project proposal; it would neither be recommended or practically feasible. Still, the hypothetical example does provide valuable benchmarks on the limits of flood reduction that are physically possible with runoff reduction. Also within this chapter, the HEC-HMS model, 50 year - 24 hour design storm event, from the HATRW report will be compared to the

HSPF model, 50-year return period, for the prairie scenario at Otter Creek location.

10.2 Tall-Grass Prairie in Row Crop Areas Scenario

Much has been documented about the historical water cycle of the native tall-grass prairie of the Midwest. Some evidence suggests that the tall-grass prairie could handle several inches of rain without having significant runoff. The deep, loosely packed organic soils, and the deep root systems of the prairie plants, allow a high volume of the rainfall to infiltrate into the ground. The water is then retained by the soils instead of rapidly traveling to a nearby stream as surface flow. Once in the soil, much of the water is actually taken up by the root systems of the prairie grasses and transpired back into atmosphere.

HSPF is used to simulate the hydrology of a native tall-grass prairie landscape for the Turkey River Watershed. In this simulation, all current cropland is replaced with native tall-grass prairie with its much higher infiltration characteristics; all other land uses (including urban) are unchanged. Obviously, converting all croplands to this pre-settlement condition is not a viable watershed plan. Still, this scenario is an important benchmark to compare with any watershed improvement project being considered.

To simulate a native tall-grass prairie with the Turkey River Watershed HSPF model, the calibrated model parameters for row crops are adjusted to reflect the tall-grass prairie condition. Specifically, existing corn and soybean land segments, which account for 56% of the watershed area, are redefined as tall-grass prairie. Using the

guidance outlined by *Donigian and J. Kittle* (1983), several model parameters are readjusted. Table E.1 in Appendix E summarizes the parameter adjustments. Note that the resulting parameters are just an approximation of prairie conditions, using best judgment based on experience with the HSPF model. The resulting simulations should also be considered an approximation, and are not as reliable as the calibrated HSPF model is for current (baseline) conditions.

10.3 Prairie Effect on Simulated Runoff

Following the assignment for the HSPF tall-grass prairie land segments parameters, which can be seen in Appendix E, a simulation is performed for the 64-year period. As expected, replacing row crops with tall-grass prairie has a significant effect on the simulated watershed hydrology. The average annual runoff depth for the prairie scenario (8.2 inches) is 2.3 inches less than that for the baseline (current conditions) simulation (10.5 inches), a reduction in runoff by 22%.

Figure 10.1 compares the simulated monthly water cycle for the baseline and the prairie scenario for the Turkey River at Garber. The runoff is lower for the prairie scenario for all months. The decrease in runoff for the prairie scenario is largest at the beginning of the year, and continues into the early summer. During the late summer and fall, the decrease is less. The seasonality also shifts for prairie condition where the peak average monthly runoff comes later in April compared to March for baseline conditions.

Figures 10.2 & 10.3 show the top 38% of peak flows for both simulated (baseline
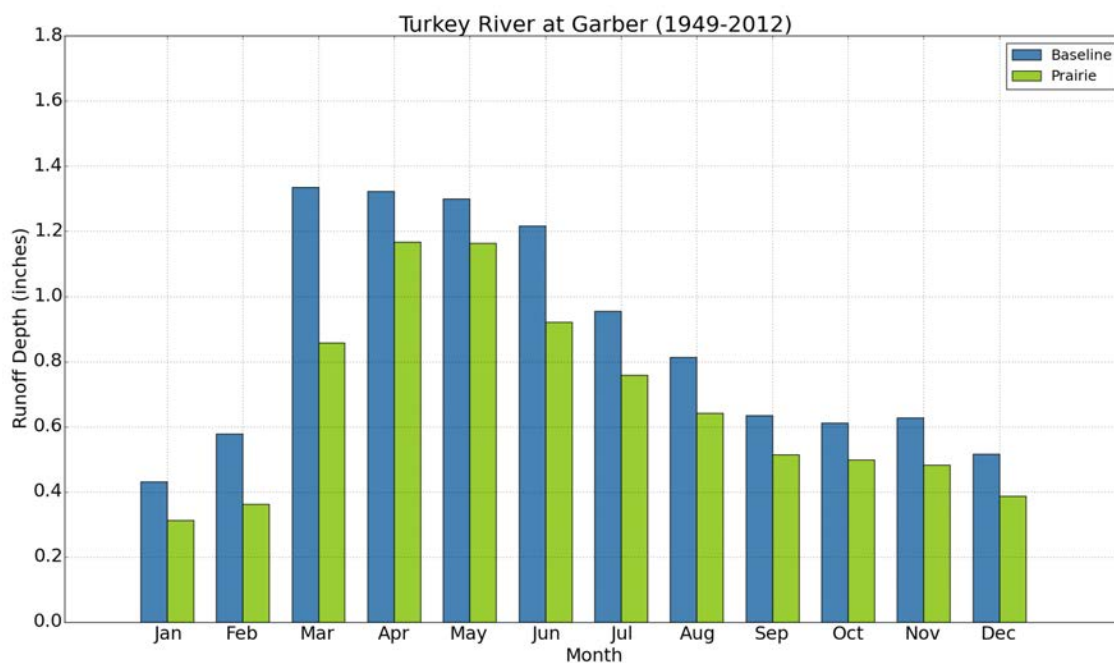
Figure 10.1: Simulated average monthly runoff depth (in inches) for the Turkey River at Garber for the baseline simulation and prairie scenario. The baseline is the calibrated HSPF model representing current conditions; the prairie scenario replaces row crops with tall-grass prairie. Results are shown for the 64-year simulation period (from 1949 to 2012).
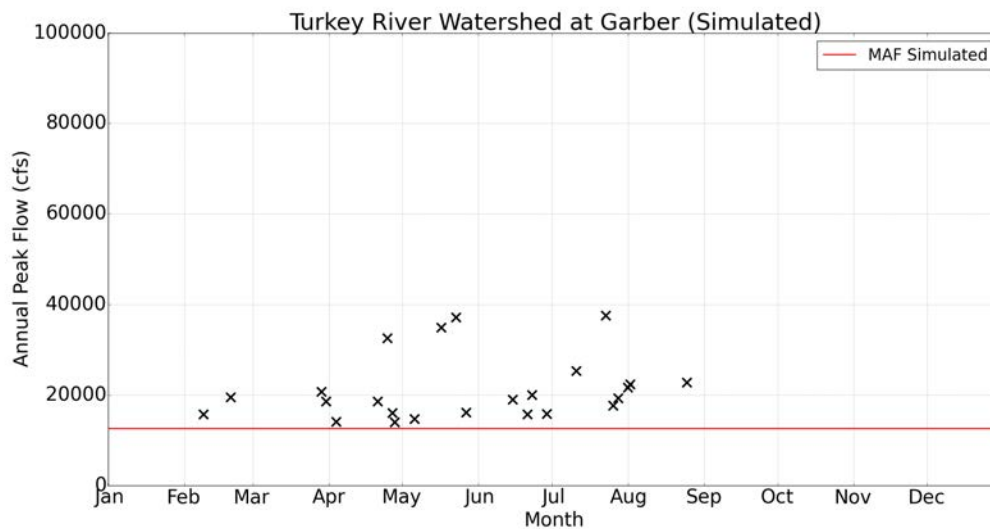
Figure 10.2: Simulated annual maximum peak discharges and the calendar day of occurrence for the Turkey River at Garber. The plots show all annual maximums greater than the mean annual flood (red horizontal line). The annual peaks are for the period of record from 1948 to 2012.

conditions) and prairie simulated scenario at Garber. It describes the models timing for peak flows during the 64 year period for baseline and prairie conditions. Like previously stated the seasonality shifts to later in the year. In Figure 10.4 this slight shift in the timing of peak flows can be seen for the top flow events. The average calender date for when peak flows occur for simulated baseline flow condition is May 27th in contrast with the prairie scenario average calender date for peak flows is May 30th. It should be noted the model has trouble capturing snow related peaks in March when comparing to observed flow in Figure 3.2 & Figure 10.4 in gray.

The average annual runoff coefficients for the prairie scenario are shown in Figure 10.5 for each subbasin. There is a significant difference in runoff coefficient from baseline condition (Figure 7.3) and prairie conditions. The entire watershed is green
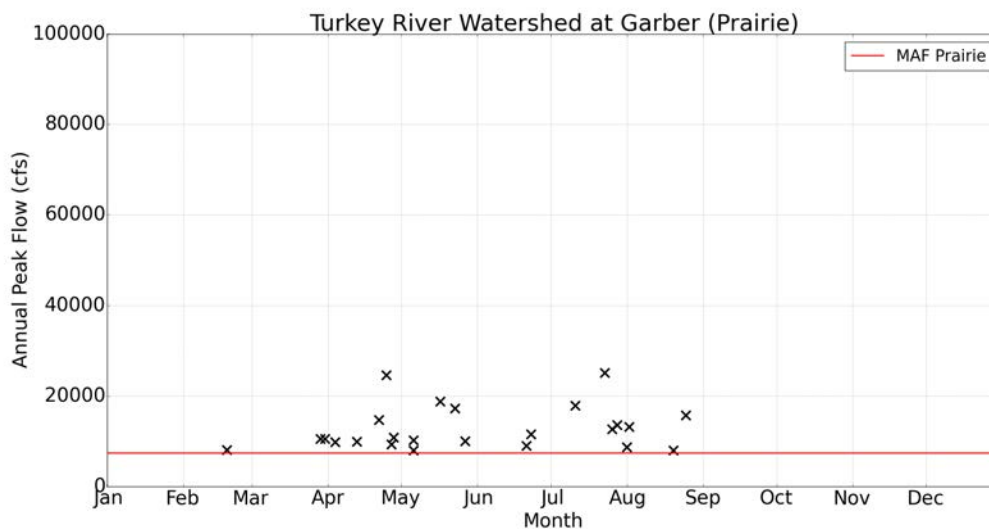
Figure 10.3: Prairie simulated annual maximum peak discharges and the calendar day of occurrence for the Turkey River at Garber. The plots show all annual maximums greater than the mean annual flood (red horizontal line). The annual peaks are for the period of record from 1948 to 2012.
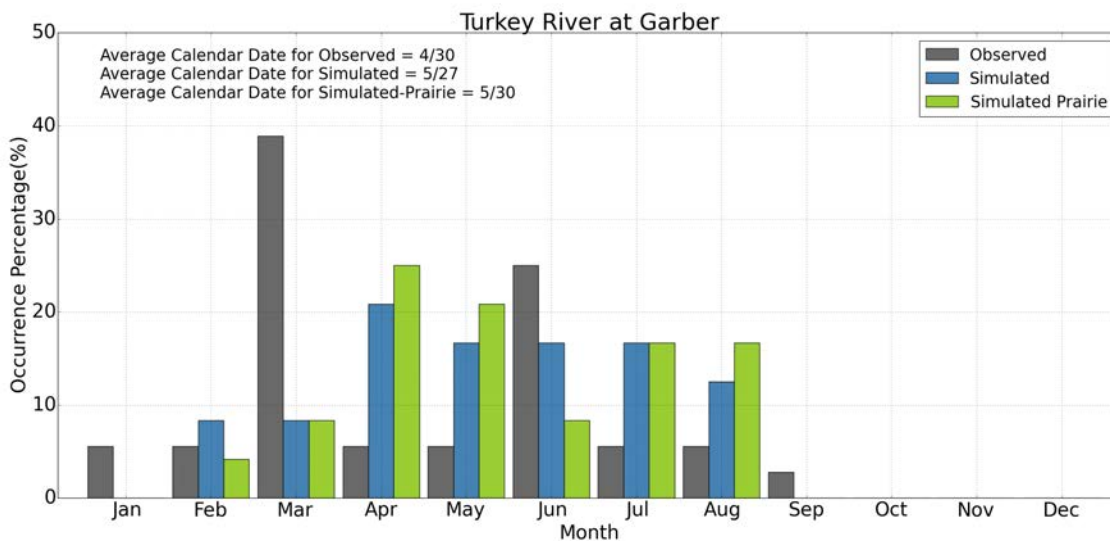
Figure 10.4: Top percentage of peak flow occurrences (in %) for each month comparing observed, simulated, and prairie simulated.

having the lowest runoff coefficients. Very few areas are over 27% of precipitation and the large majority range from 17% to 26% of precipitation.

Figure 10.6 shows the change in the average annual runoff depth of the prairie scenario from baseline conditions. The reduction in runoff ranges from 0% to a maximum of 42%. As one would expect, subbasin areas that currently have the highest percentage of row crops, some with as much as 90% row crops or more, also have the largest reductions when replaced by tall-grass prairie. Subbasins with 0% reduction are headwater subbasins with no agricultural lands. Indeed, subbasins with large reductions are now low runoff areas for the tall-grass prairie scenario, with average annual runoff depths of 7.7 inches or less; subbasins with small reductions are now high runoff areas, with average depths of 8.7 inches or more.

10.4   Prairie Effect on Simulated Floods

The nine locations in the watershed are the same as in Figure 9.7 for comparing simulated floods for watershed scenarios to current conditions. Figures 10.7 & 10.8 show the flood frequency analysis for the prairie scenario and the baseline simulation for all nine locations. Annual max peak discharges for the nine locations are shown on each locations graph. The annual maximum peak discharge is ranked smallest to largest for the 64-year simulation period. The same procedure was done for the pond scenario in Chapter 9.

Figures 10.7 & 10.8 show the flood frequency analysis for the prairie scenario and the baseline simulation. Annual maximum peak discharges for the nine index
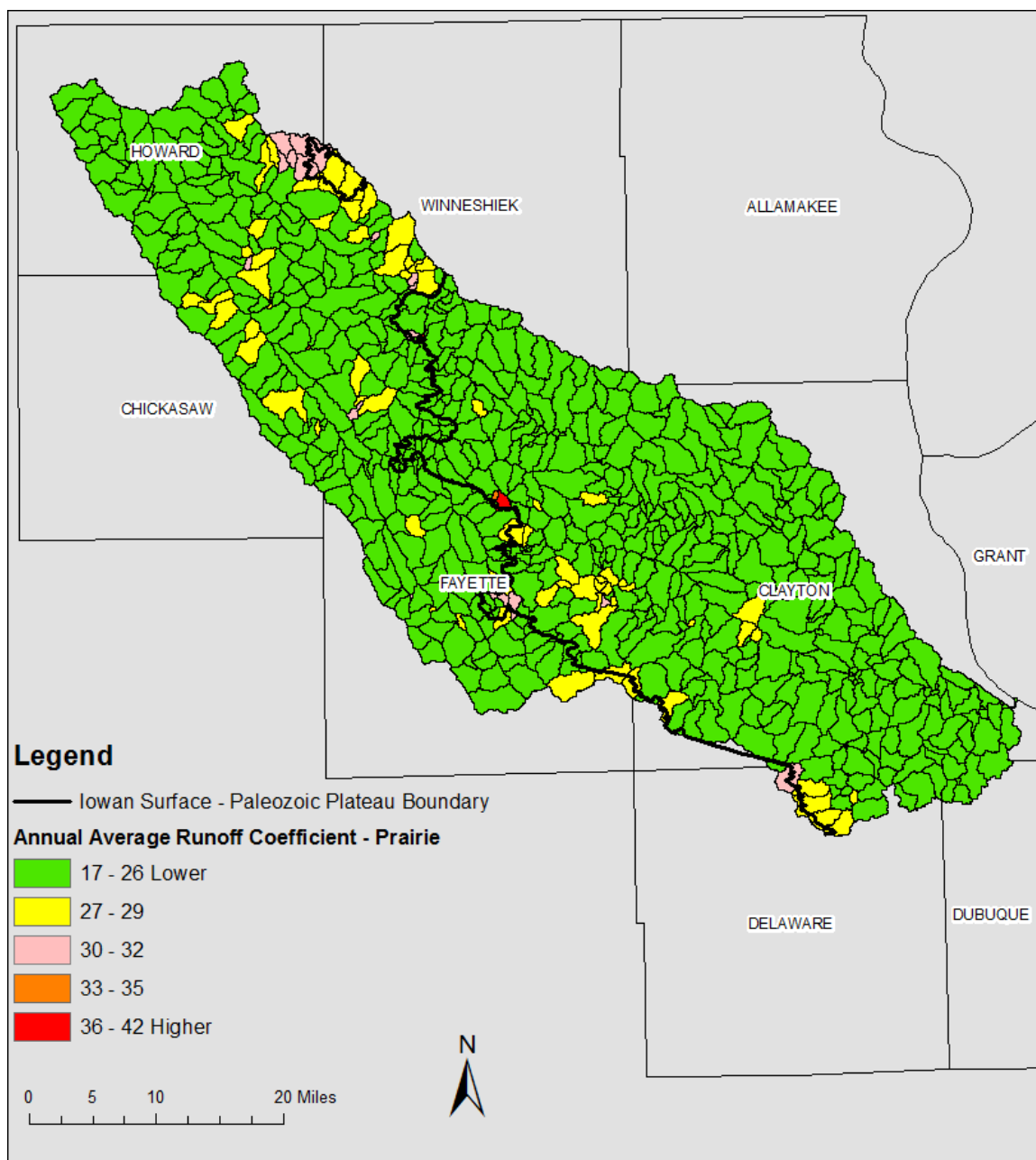
Figure 10.5: Average Annual Runoff Coefficients for each subbasin for the prairie simulation.
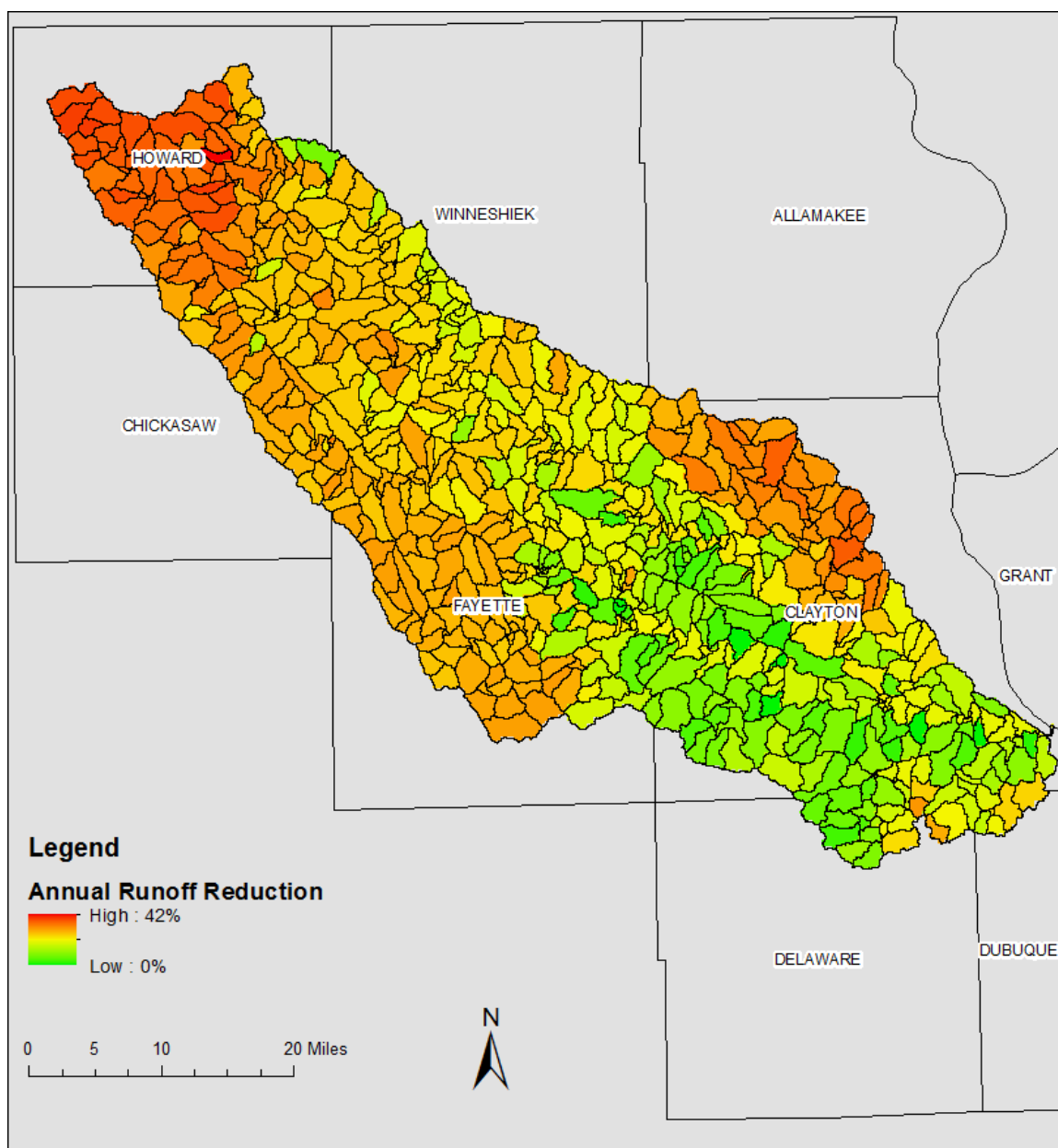
Figure 10.6: Change (in %) of the average annual runoff depth in the Turkey River Watershed for the prairie scenarios. The change is based on the average annual runoff depth from the prairie scenario and the baseline simulation for each subbasin from the 64-year simulation.

locations are shown. For the 64-year simulation period, the annual maximum peak discharges are plotted versus a sample estimate of their exceedance probability. At all the locations, the prairie scenario has lowered the simulated peak discharges greatly. One measure of the change is the peak reduction effect; the percentage reduction in the scenario peak discharge relative to that for the baseline simulation. Table 10.1 summarizes the average peak reduction, 2-, 10-, 25-, and 50-year return period peak discharge reductions. Table F.1 in Appendix F displays baseline flows from simulation. For smaller drainage areas, Otter Creek, Spillville, and Volga at Fayette have a large average peak reduction between 48% and 66%. The mid size drainage areas like Crane Creek, Volga at Littleport, and Eldorado are somewhere between 37.2% and 66.4% average peak reduction. The larger drainage areas like Elkader, Garber, and the Outlet at the Mississippi are between 43% and 50% average peak reduction. Similar results are found in a study by *Gerla* (2007); the Red River of the North had on average for the 5-year and 25-year rainfall events a 50-55% and 40-45% respectively average peak reduction when converting from cropland to grassland (*Gerla*, 2007).

These larger drainage areas have a greater average peak reduction than the larger return periods. The reduction percentage can depend on the amount of agricultural lands converted to prairie within the drainage areas. The more agricultural lands, the more percent reduction in peak discharge and vise-versa. The index locations at the most upstream portions of the watershed (Spillville, Crane Creek, Edorado, and Volga at Fayette) have greater peak discharge reductions because their drainage area incorporates a larger percentage of agriculture. Most of their drainage

areas are within the Iowan Surface region and have more agricultural lands.

The diminished peak reduction seen for the largest events for the large drainage areas are related to the nature of floods at different scales. For smaller drainage areas, floods are caused by local high rainfall intensities; for larger drainage areas, floods are caused by widespread high rainfall accumulation. For the largest events, rainfall accumulation upstream is so large that the storage in the soils is overwhelmed (even in a prairie landscape). Hence, one might anticipate that major floods, on the order of a 100- or 500- year return period, will saturate the soil, thus the peak reduction effect may be even more diminished for larger drainage areas.

To better understand how the prairie scenario changes simulated flood peaks, Figure 10.10 maps the average peak reduction effect at each subbasin's outlet throughout the watershed. The peak reduction effect is fairly large everywhere, ranging from 70% - 80% in certain headwater subbasins, to around 60% along the lower main-stem of the Turkey River, to as high as 85% for subbasins that currently have a high row crop percentage (and are replaced with prairie for this simulation). The largest peak reductions occur in headwater subbasins; the peak reduction effect tends to slowly diminish as one moves downstream. *Schilling and Drobney* (2014) found similar results with 12 catchments in Walnut Creek between watersheds that are 100% prairie versus watersheds that are 100% cropland. The average annual runoff from the prairie watersheds are 70% lower than the cropland watersheds (*Schilling and Drobney*, 2014). This proves prairie can have a significant impact on reducing runoff.

The HEC-HMS model from the HATRW report ran a single 50 year - 24
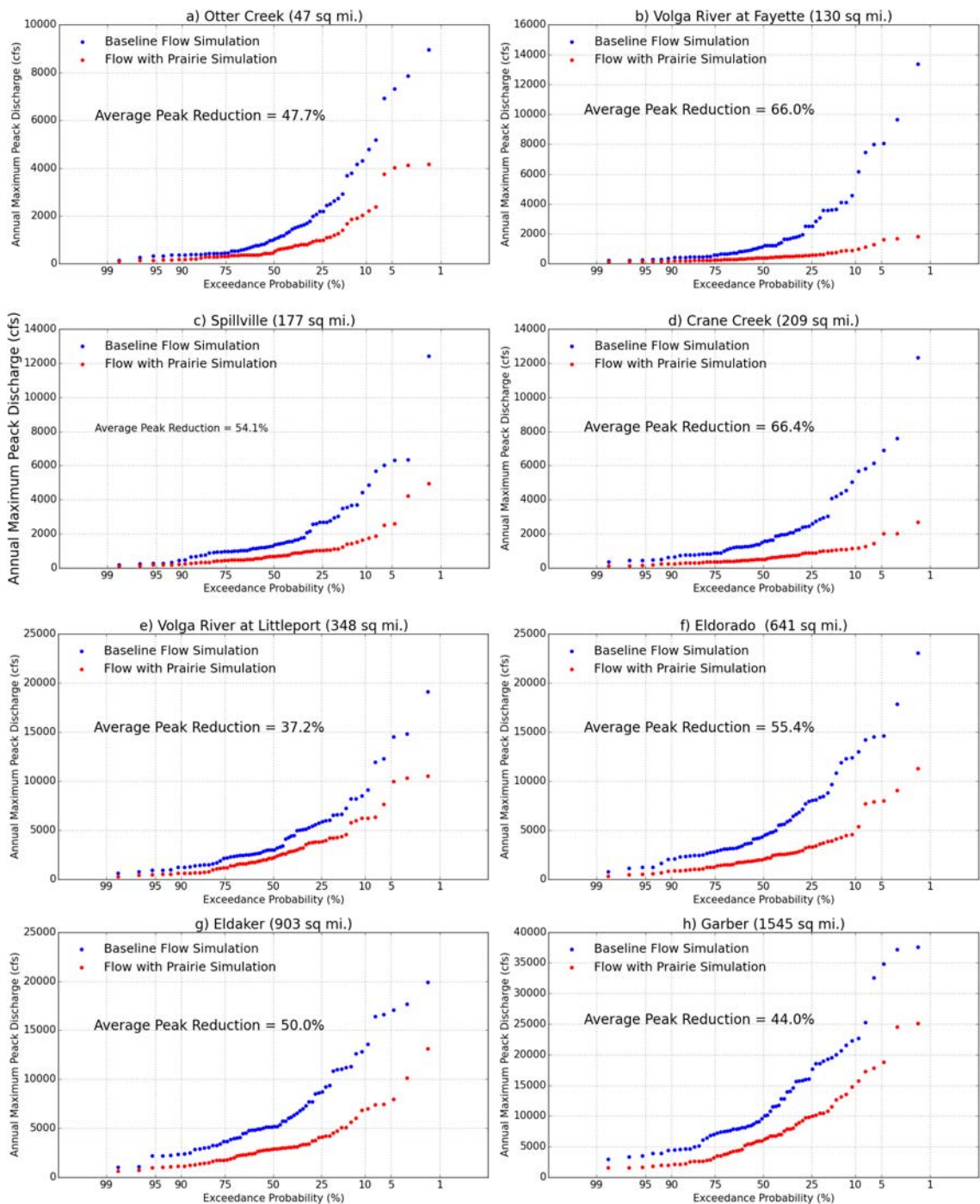
Figure 10.7: Sample probability distribution of annual maximum peak discharges for the baseline simulation and prairie scenario for 8 of 9 locations.
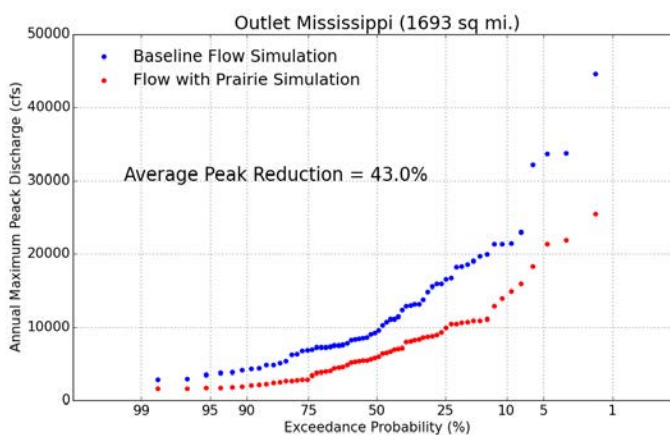
Figure 10.8: Sample probability distribution of annual maximum peak discharges for the baseline simulation and prairie scenario for the Mississippi Outlet.

Location	Drainage Area (mi^2)	Average (%)	Return Period (%)			
			2-year	10-year	25-year	50-year
Otter Creek	47	47.7	51.7	53.3	46.1	51.8
Spillville	177	54.1	49.0	63.5	48.9	55.6
Crane Creek	209	66.4	67.1	78.6	72.1	77.4
Eldorado	641	55.4	53.9	61.1	47.1	50.7
Elkader	903	50.0	44.3	47.7	49.0	36.4
Garber	1,545	44.0	37.6	32.4	41.1	33.4
Outlet at Mississippi	1,693	43.0	37.3	32.6	36.0	41.0
Volga at Fayette	130	66.0	67.3	82.7	81.2	85.6
Volga at Littleport	348	37.2	27.7	29.3	31.1	41.4

Table 10.1: Peak reduction effect for the prairie scenario (relative to the baseline simulation). The average reduction is shown (in %) for the 64 annual maximum events. Also shown are the reductions (in %) for the 2-, 10-, 25-, and 50-year return period events. The reductions are evaluated at the nine index locations.

hour design storm event for the prairie scenario for only the Otter Creek location. It saw a 24.4% reduction in peak flow with increasing the infiltration by 15% (the curve numbers were reduce by 15%). In total a half inch of rainfall was infiltrated into the ground across the entire watershed. HSPF's 50-year return period saw over double the reduction of the HEC-HMS results for Otter Creek at 51.8%. This large difference is in part because the comparison is between a 50-year flow based on a design storm approach, and a 50-year flow estimated from a long simulated flow record. Another factor is that HEC-HMS only represents the change in storm runoff for a prairie landscape (by changing only the curve number parameter). In contrast, HSPF represents the entire water cycle of the prairie landscape (by changing six parameters), including the changes in soil moisture conditions at the time of extreme rainstorms. Figure 10.9 shows the results for both models for the Otter Creek location.

10.5   Chapter Summary

In this chapter agricultural lands are converted back to the native tall-grass prairie within the Turkey River Watershed. This hypothetical scenario had a greater amount of reduction compared to the previous pond scenario. The tall-grass prairie greatly increased infiltration and storages compared to the cultivated lands that are there now. Within the simulation, annual maximum peak discharge was simulated and compared to the annual maximum peak discharge from baseline conditions. The index location saw anywhere from 37% to 66% in average peak reduction. The amount reduced for the larger storm events (10-, 25-, 50-year return periods) depended on
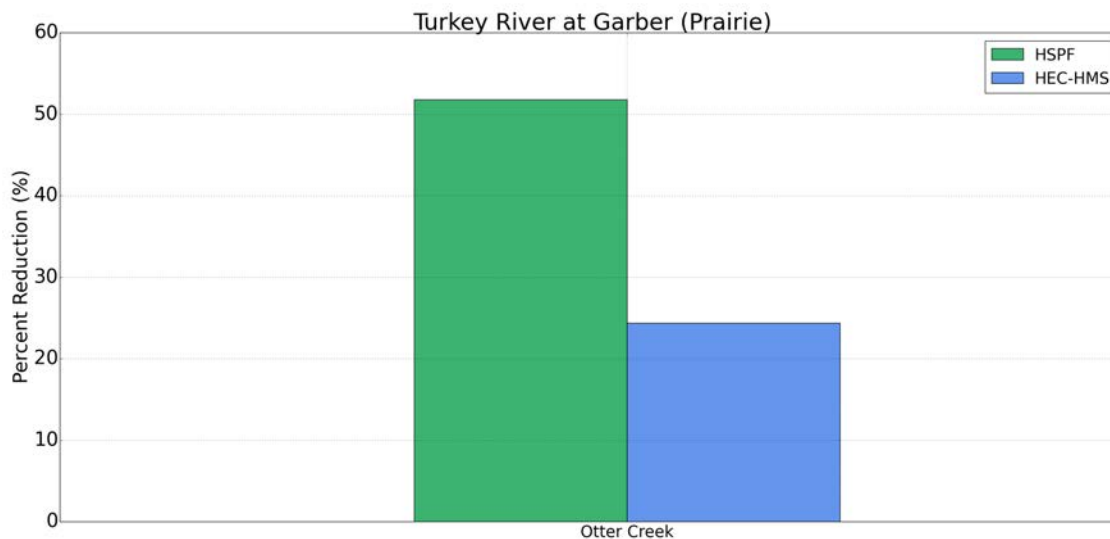
Figure 10.9: This figure compares the results from the HEC-HMS model and HSPF model for the prairie scenario. The HSPF model had far greater reduction to peak flows than the HEC-HMS model for Otter Creek.

the drainage area. For larger drainage areas, the percent reduction for larger return periods are less than the average peak reduction, but for smaller drainage areas, the large return periods are greater than the average peak reduction. This scenario showed that prairies are effective at reducing peak discharges and in turn delaying flow by storing water in the soil, eventually making its way to the stream through the groundwater. In addition to converting agricultural lands back to the native tall-grass prairie, converting urban developments back to their native prairie would also reduce flood frequency and magnitude. Granted, it is only roughly 5% of the total watershed, it would still have some effect on reducing runoff and streamflow because it produces some of the highest runoff due to the large percentage of impervious land. Based on the results shown, the adjusted parameters used for this scenario seemed
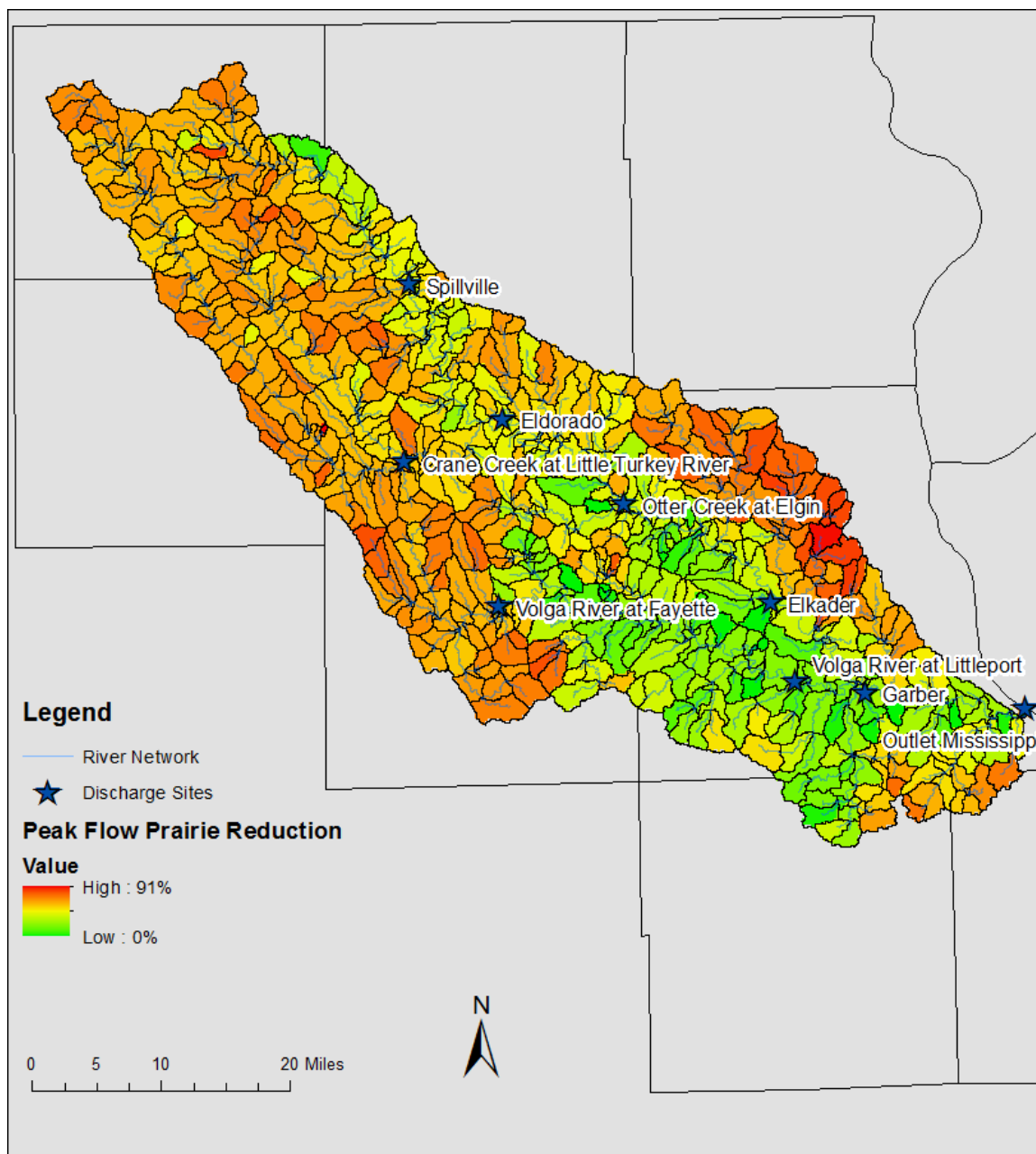
Figure 10.10: Average peak discharge reduction (in %) for locations in the Turkey River Watershed for the prairie scenario. The annual maximum peak discharge for the subbasin outlets from the 64-year simulations are compared for the prairie scenario and the baseline simulation. The average peak reduction effect was computed from the 64 ranked annual events.

justified based off previous results from *Gerla* (2007), *Schilling et al.* (2014), and *Bharati et al.* (2002) in Appendix E.

CHAPTER 11
CONCLUSION

This study examined the hydrologic response of land use and land cover changes. The focus was on the Turkey River Watershed in the northeastern Iowa. The objective of this study was to evaluate how well the continuous simulation model HSPF can predict the water cycle and flood hydrology using LULC as driving factors; assess trends in streamflow and determine whether land use or climate change play a role; and lastly, use HSPF to run two hypothetical flood mitigation strategies, comparing the continuous HSPF model results with an event based simulation model HEC-HMS used in the Hydrologic Assessment of the Turkey River Watershed report.

11.1   Turkey River's HSPF Model

Within this study, the Turkey River Watershed was examined from October 1, 1948 to September 30, 2012 using a computer simulation model called Hydrological Simulation Program — FORTRAN (HSPF), developed by the EPA. Within the 64 year period, the model made long-term continuous simulations using historical precipitation, and simulated flows were compared to observed streamflow records. The historical precipitation data came from the NOAA's National Climate Data Center (NCDC) and the stream gauge data came from the United States Geological Survey (USGS). Eleven meteorological stations were selected in or near the Turkey River Watershed. From those stations hourly precipitation and air temperature time series inputs were developed giving the watershed a spatially varying distribution. Other

weather time series were obtained from the Waterloo airport weather station. The watershed was then sub-divided into 710 subbasins, creating 710 river reaches. Within each subbasin it was further subdivided into land uses; cultivated lands (corn and soybean), grasslands, pastures, wetlands, and urban areas. Grasslands (barren rock) and urban development areas both had impervious portions of land. Hydrologic processes for different land uses were simulated using pervious and impervious model land segments (e.g. PWATER and IWATER).

11.2   Turkey River's Calibration and Validation

HSPF model parameters were estimated using a model calibration process called Shuffled Complex Evolution-University of Arizona (SCE-UA). SCE-UA adjusts an initial set of model parameters so that simulated discharge matches observed discharge at the stream gauge at Garber, Iowa (USGS 05412500). The Turkey River Watershed HSPF model was calibrated using observed daily discharges for a 20-year period, from water years 1993 to 2012. The last portion of the 64 year historical record was used for calibration, since it should be more representative of current land use conditions. The calibration process first involved both manual adjustments of parameters, and then a multi-objective automated approach (SCE-UA), which attempts to find parameters that perform well for the simulation of both high and low flows. After calibration of model parameters, model validation assessed the predictive capability of the model to simulate discharge for other periods (previous 44 years 1949-1992). The remaining 44-year simulation period, from water years 1949 to 1992, was

used for model validation. Comparisons of simulated and observed flows were made for the monthly water cycle, annual flows, and annual maximum peak discharges, using a fixed set of model parameters for the entire simulation. Overall, the model predicts the annual cycle of monthly average flows quite well (Figure 6.3); it slightly underestimates the total runoff volume for the calibration period (by 6.5%), but overestimates the volume for the entire simulation period by 7.78% (64 year period). For annual flows, the model tends to overestimate annual flows for dry and average years, but underestimate flows for the wettest years, which mostly occur in recent decades (during the calibration period) (Figure 6.6). For the largest peak flows the model shows a tendency to underestimate (Figure 6.7). As a result, the statistical characteristics of simulated and observed peak discharge matches the same general trend fairly well but under predicts (Figure 6.8). The under prediction could partially be due to the dramatic landscape conversion previously stated. The HSPF model can be used but with the understanding that there may be some biases.

11.3 Turkey River's Water Cycle

The water cycle of the Turkey River Watershed was examined using historical precipitation and streamflow records. The average annual precipitation for the Turkey River Watershed is 33.5 inches. Of this precipitation amount, 70.8% (23.68 inches) evaporates back into the atmosphere and the remaining 29.2% (9.7 inches) runs off the landscape into the streams and rivers. The majority of the runoff amount is baseflow (69.0% or 6.69 inches), and the rest is surface flow (31.0% or 3.09 inches). Average

monthly streamflow peaks in March, and decreases slowly through the summer's growing season. In some years, the largest discharge observed during the year occurs in March or April, associated with snow melt, rain on snow events, or heavy spring rains. However, in the majority of years, the largest discharge is observed between May and August, when the heaviest rainfall can occur (Figure 3.2). It is also during this season when the largest floods on record have occurred within the watershed (e.g. 2008).

11.4   Assessment of Hydrologic Trends

Since the mid 1800s, the Corn Belt of the Midwest experienced a dramatic landscape conversion from native perennials to annual cropping systems. Iowa has been converted from native, low runoff prairies to high runoff agricultural lands and the increase of these agricultural lands as well as climate have led to higher annual runoff and increased streamflow, changing the annual water cycle. Iowa has seen an increase in precipitation, changes in timing of precipitation, and changes in the frequency of intense rain events. Streamflow records in Iowa suggest that median flows, low flows, and perhaps high flows have all increased and become more variable. The relative contributions of land use and climate changes are difficult to sort out. However, the Turkey River Watershed's increasing streamflow was due in large part to the increase in cultivated lands (Chapter 7).

11.5 Iowan Surface and Paleozoic Plateau Differences

The Turkey River calibrated HSPF model was used to identify areas within the watershed with high runoff potential. High annual runoff depths mostly occur in the Iowan Surface portion of the watershed, right above the Iowan Surface and Paleozoic Plateau divide, with more medium to low runoff depths occurring in the Paleozoic Plateau region (Figure 7.2). For the Iowan Surface high runoff areas, agriculture land use dominates (as it does for the entire watershed in general), but there is less forest and grassland areas than in other locations. Implementing projects that can reduce runoff from the high runoff areas should be a priority.

The Turkey River Watershed HSPF model was also used to identify locations within the watershed where the flood magnitudes are relatively high. This analysis integrates the effect of runoff from upstream areas and the influence of the stream network as water moves downstream, to show downstream areas most impacted by high runoff, which is displayed in Figure 7.6. Many high flood areas tend to be located just downstream of the confluence of two tributaries of similar size. When two tributaries come together, the timing of flow arrival and the combination of flows often results in higher annual floods. High flood areas should be a focus in mitigation planning; they make good locations for assessing the overall impact of upstream mitigation projects.

Finally, the Turkey River Watershed HSPF model was used to examine the severity and extent of simulated flooding throughout the watershed over the 64-year simulation period. The top flood years were identified based on a flood severity

index (evaluated at all subbasin outlets). The top flood year is 2008 and is unique for its widespread extent of intense flooding; nearly all subbasins were simulated to have experienced sufficient flow to produce flooding. In all the other top flood years, some portion of the watershed had no flooding. Some years are notable for their high intensity but localized flood extent (1991); others were more widespread and less intense locally (1999 and 1993). One advantage of using a continuous simulation model, like HSPF, is that it can represent the nature of flooding that occurs in the watershed and can evaluate the performance of flood mitigation measures over a range of potential flood conditions.

11.6 Hypothetical Watershed Scenarios

The calibrated Turkey River HSPF model was next used to explore several hypothetical watershed scenarios. One scenario examined the use of flood storage to store excess runoff temporarily, which reduced the flood peak discharge for the event. The other scenario examined the flood hydrology of the tall-grass prairie landscape that existed in the watershed before today's current agricultural landscape. For both flood mitigation scenarios the HSPF model results were compared to the HEC-HMS model results of the HATRW report. Both models used the same flood mitigation scenarios (storage ponds and prairie conversion).

11.7 Flood Storage Scenario

In some ways, using ponds to temporarily store floodwaters is an attempt to replace the loss of water that was stored in soils in the pre-agricultural landscape.

In the hypothetical scenario involving pond storage, 19,537.2 acre-feet of storage was added to the Turkey River Watershed with 402 prototype ponds. For the upstream areas that have runoff that drains through the ponds, this is equivalent to an added storage depth of 0.47 inches of runoff. However, for the Turkey River Watershed as a whole (not just the areas with ponds), the added storage depth decreases to 0.22 inches. Peak discharges for the 25-year return period flood are reduced by as much as 21% just downstream of the ponds. However, further downstream the peak reduction effect is less. At Garber, the 25-year peak is about 9.6% less with ponds (Table 9.2). Still, compared to the other scenarios, the flood storage scenario is one that is more realistically achievable.

As a flood mitigation strategy, ponds are very effective in reducing flood peaks immediately downstream of their headwater sites. Further downstream, floodwaters originate from locations throughout the watershed, arriving at vastly different times; some areas have ponds, others do not. The result is that the storage effect from ponded areas is distributed throughout in time, instead of being concentrated at the time of highest flows. Hence, as one moves further downstream in the watershed, the flood peak reduction of storage ponds slowly diminishes.

11.8   Tall-Grass Prairie Scenario

The conversion of native tall-grass prairie to agriculture land use has resulted in a significant reduction in the infiltration capacity of the landscape and runoff. The model predicts that the average runoff would be 24% less with a tall-grass prairie

landscape than agricultural land. The effect on flood events is even larger. At the 25-year return period, which has a flood level that has a 4% chance of being exceeded in any given year, the model predicts that the peak discharge would be between 31% to 81% less than current conditions (Table 10.1). With prairies, potential floodwaters are stored within the landscape because prairies are effective at infiltrating large amount of water into the ground. Obviously, converting today's agricultural landscape back to tall-grass prairie is not a practical or economically desirable strategy. Still, from a hydrologic point of view, targeted projects that enhance infiltration by land-use change could be an effective part of watershed's flood mitigation efforts.

11.9   HEC-HMS and HSPF Results

The comparison of the two lumped parameter models did show similar results for areas of high runoff within the Turkey River Watershed (Figure 7.3 and Figure 7.4). However, there were notable differences in the quantitative results for the two flood scenarios. For instance, at Otter Creek the HEC-HMS model predicts a greater peak flow reduction for the pond scenario (34.1%) than the prairie scenario (24.4%), based on a 50 year - 24 hour design storm. The HSPF model predicts a greater flow reduction for the prairie scenario (51.8%) than the pond scenario (21.3%), based on the estimated 50-year return period peak discharge.

Comparing a single design event simulation of the ponds using HEC-HMS, with a 64 year continuous simulation of the ponds using HSPF, reveals results in a slightly different interpretation of the benefits of flood storage ponds. The ponds

are represented in the same way in both models. All the ponds were in the same 250 headwater subbasins, having the same 402 theoretical ponds, having half of the upstream subbasin's drainage area drained into the ponds, and having the same storage to discharge relationship for each pond. HEC-HMS predicts the greatest peak reduction effect at smaller drainage areas and a rapid decrease in peak reduction as the drainage area increases (Figure 9.6) for a single design event. HSPF predicts a more consistent downstream peak reduction at the index locations when considering all the events that occur over a 64 year period.

Comparing a single design event simulation of a prairie landscape using HEC-HMS, with a 64 year continuous simulation of a prairie landscape using HSPF, the predicted effects of the prairie on flood peaks are quite different. HSPF predicts a much greater peak reduction for the prairie landscape than HEC-HMS (Figure 10.9). The prairie landscape is represented differently in the two models. HEC-HMS model only changed infiltration, by "infiltration, increasing it by 15%", to represent prairie like condition. The HSPF model changed six parameters to represent prairie like conditions (Appendix E). This is where the models differ greatly, HEC-HMS models runoff processes and little to no groundwater processes compared to the HSPF model modeling both runoff and groundwater processes. They also have different simulation periods, HEC-HMS is an event based model (24 hour storm events), giving instantaneous results, in contrast to the continuous based HSPF model, giving averaged results over a 64 year period.

In the end, each model has its own strengths. The HEC-HMS model is ideal

for simulating a single storm event — either an event from the historical record, or a design storm for flood assessment. Since the model can neglect groundwater processes and evapotranspiration, it is easier to apply. The HSPF model looks not just at individual flood events but the entire water cycle over long continuous period. It is more difficult to apply because it requires more data — both in terms of historical weather data, used to drive the simulation model, but also terms of parameters, used to describe the surface, sub-surface, and the evaporation characteristics of the watershed. Still, the Turkey River Watershed analysis with HSPF shows an in depth look at the watershed over 64 years. HSPF can produce continuous simulated record of flows almost anywhere in the watershed. Also, HSPF looks at all the individual events, not just a single event like HEC-HMS, showing flood characteristics and all aspects of the water cycle throughout the period of record.

11.10   Final Summary

The purpose of the study was to understand the hydrologic behavior of the Turkey River Watershed, study areas of high runoff and areas of flooding concern, and then implement certain hypothetical scenarios to lessen the frequency and severity of flooding (introduce ponds and convert agricultural lands to prairies). The two flood mitigation strategies were performed and evaluated in the Turkey River Watershed using HSPF. The two either focused on storing flood waters, which delay the waters time of arrival reducing peak flows (storage ponds), or enhancing the water's infiltration into the ground also reducing peak flows (converting agricultural lands

to prairies). The alternatives chosen were hypothetical and somewhat unrealistic. Although, they offer an understanding of potential flood mitigation practices. Applying a small portion of either one or combination of the two alternatives, like prairie restoration or installing ponds, could offer profound flooding relief. Obviously part of the flood mitigation process includes factors such as the cost and benefits of alternatives and landowner willingness to participate, which should all be considered in addition to the hydrology. Hopefully this study can be used as guidelines for implementing such practices and be a helpful resource for future hydrologic assessments and flood mitigation projects.

APPENDIX A
CALIBRATION AND VALIDATION SITES
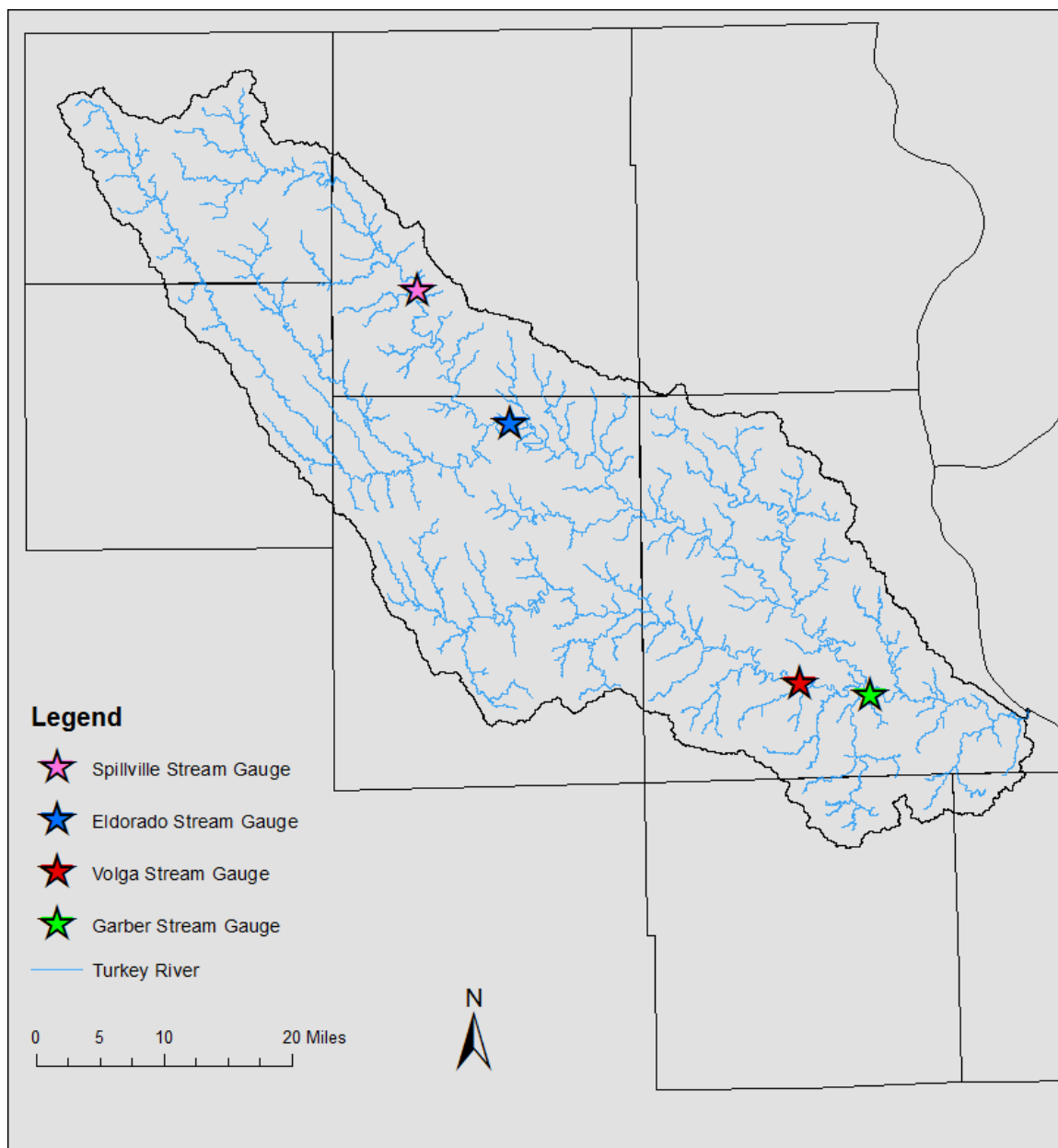
Figure A.1: Calibration and Validation gauge locations within the Turkey River Watershed.
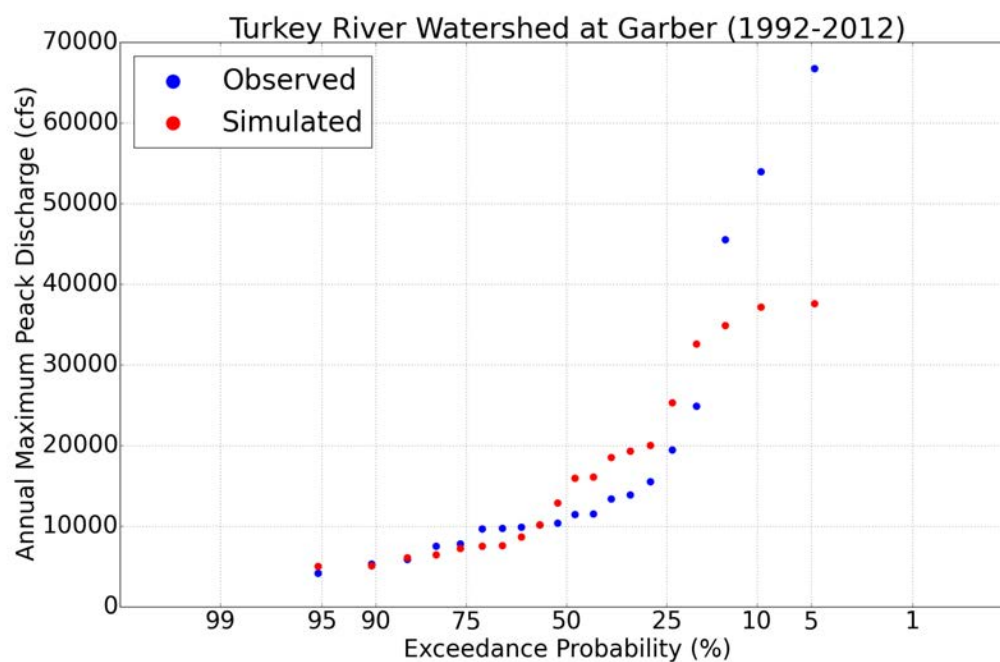
Figure A.2: Flood frequency analysis of annual maximum peak discharges for simulated and observed flows for the Turkey River Watershed at Garber (USGS 05412500). The annual maximums are for the entire period of record (1993 to 2012)
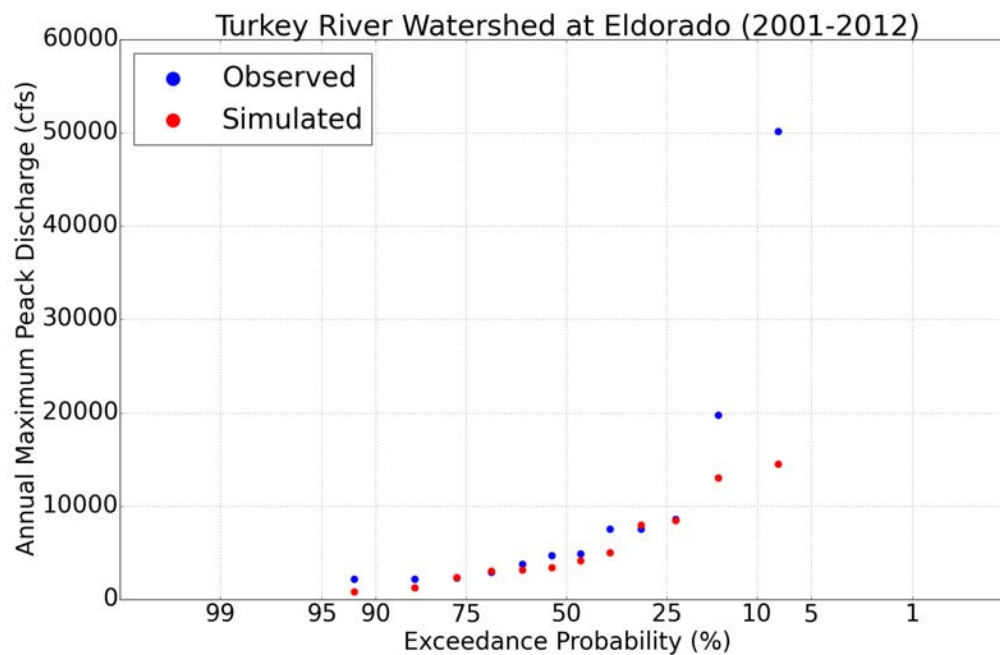
Figure A.3: Flood frequency analysis of annual maximum peak discharges for simulated and observed flows for the Turkey River Watershed at Eldorado (USGS 05411850). The annual maximums are for the entire period of record (2001 to 2012).
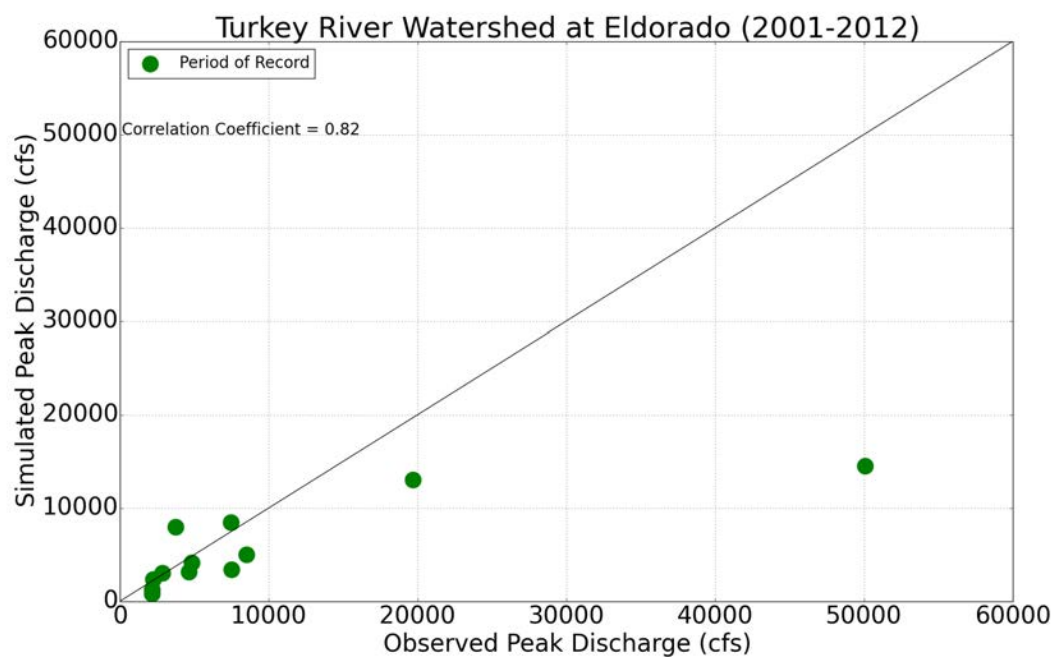
Figure A.4: Annual peak simulated and observed flows for the Turkey River Watershed at Eldorado (USGS 05411850). The annual maximums are for the entire water years from 2001 to 2012 (the entire simulation period).
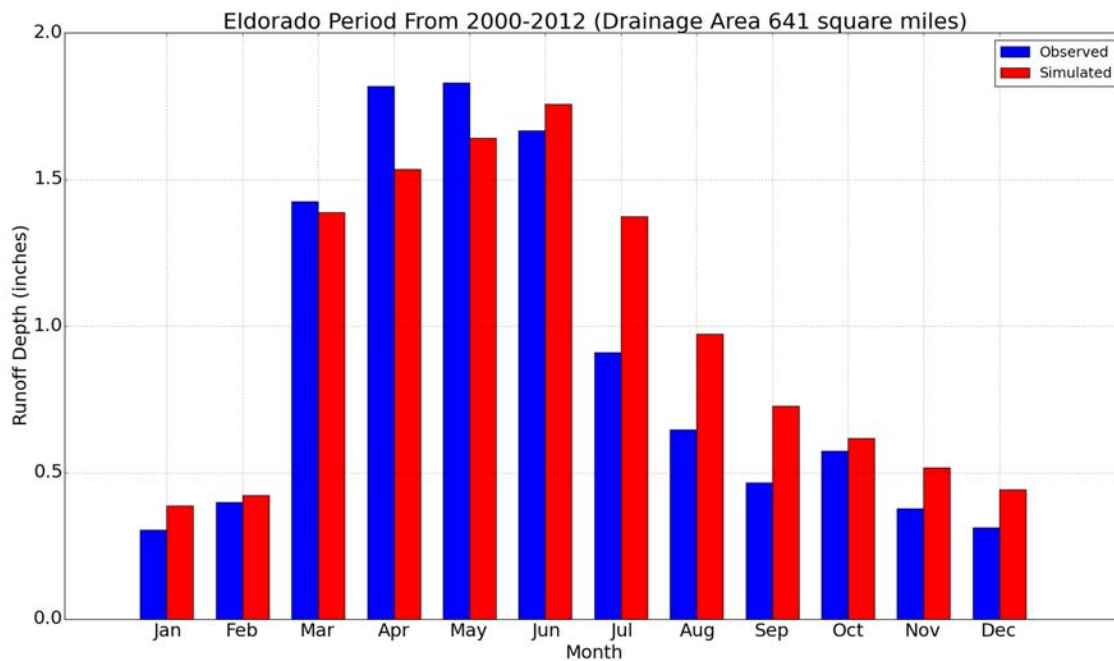
Figure A.5: Average monthly water balance for the period of record for Eldorado stream gauge.

Figure A.6: Flood frequency analysis of annual maximum peak discharges for simulated and observed flows for the Turkey River Watershed at Spillville (USGS 05411600). The annual maximums are for the entire period of record(1956 to 2012).
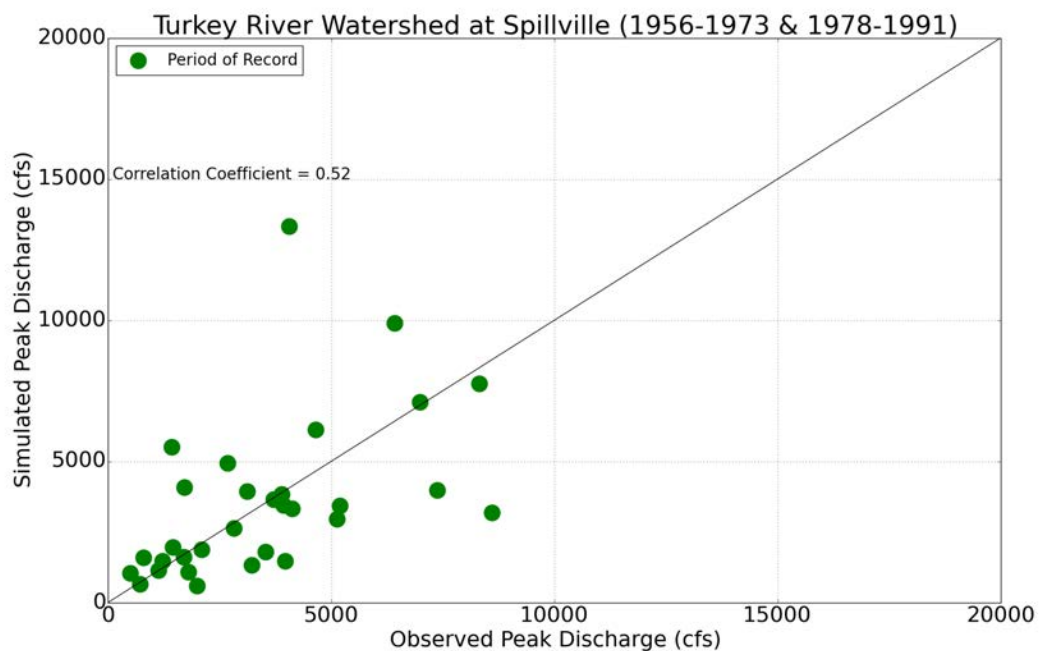
Figure A.7: Annual peak simulated and observed flows for the Turkey River Watershed at Spillville (USGS 05411600). The annual maximums are for the entire water years from 1956 to 2012 (the entire simulation period).
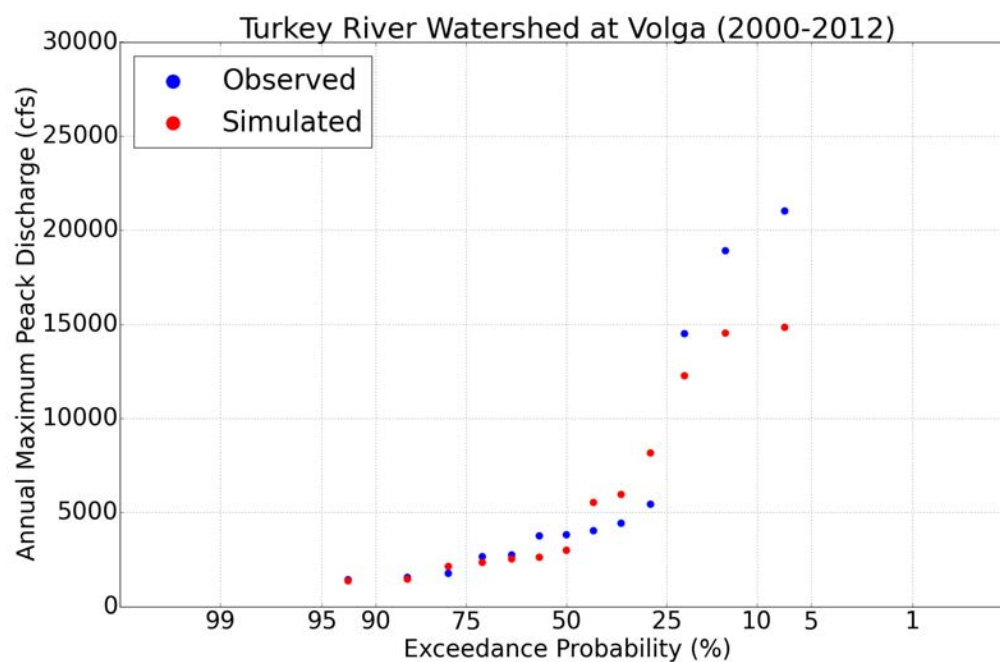
Figure A.8: Flood frequency analysis of annual maximum peak discharges for simulated and observed flows for the Turkey River Watershed for Volga River at Fayette (USGS 05412340). The annual maximums are for the entire period of record(2000 to 2012).
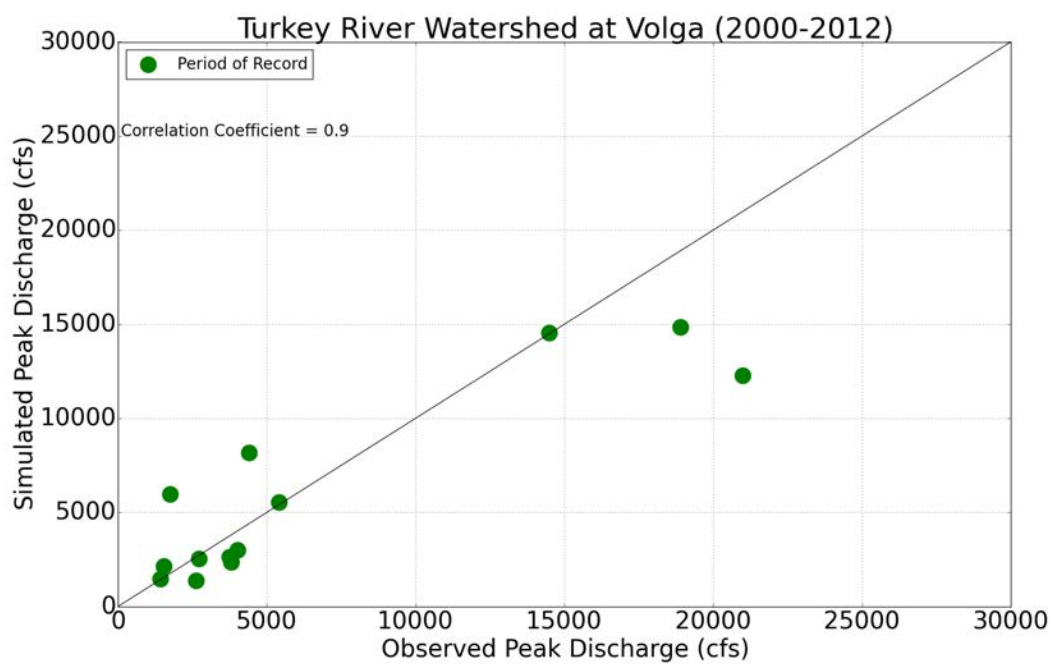
Figure A.9: Annual peak simulated and observed flows for the Turkey River Watershed at Volga River at Fayette (USGS 05412340). The annual maximums are for the entire water years from 2000 to 2012 (the entire simulation period)
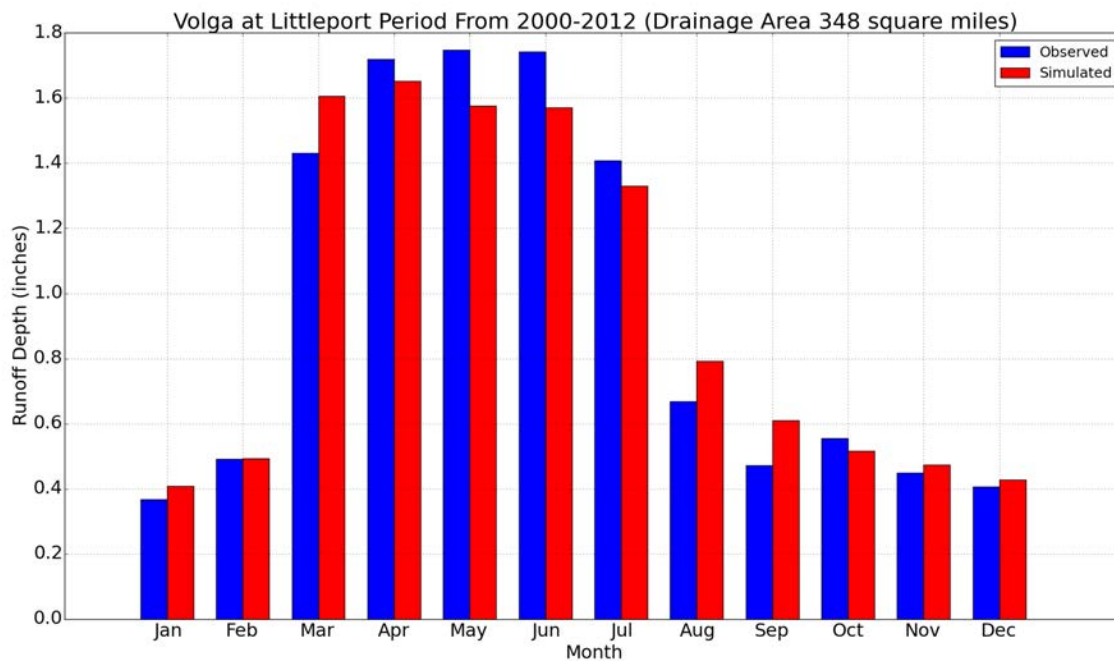
Figure A.10: Average monthly water balance for the period of record for Volga at Littleport stream gauge.

APPENDIX B
METEOROLOGICAL STATIONS IDW LOCATIONS

Saratoga Closest	Station	Station ID	Lat	Long	Distance (miles)	Date Start	End
	Saratoga	IA137410	43.367	-92.367	0.00	4/30/1949	2/29/1968
1	Elma	IA132638	43.241	-92.443	9.50	8/31/2003	5/19/2014
2	Cresco	IA131954	43.389	-92.094	13.80	3/31/1948	12/31/2012
3	New Hampton	IA135952	43.045	-92.312	22.39	3/29/1928	12/31/2012
4	Spring Valley	MN217941	43.693	-92.393	22.62	8/1/1948	12/31/2012
5	Osage	IA136305	43.279	-92.811	23.13	3/31/1948	12/31/2012
6	Spillville	IA137855	43.205	-91.954	23.59	8/1/1948	5/31/2007
7	Charles City	IA131402	43.078	-92.671	25.21	8/1/1948	10/31/1953
8	Waucoma	IA138742	43.095	-92.033	25.23	11/30/1954	12/31/2012
Waucoma Closest	**Station**	**Station ID**	**Lat**	**Long**	**Distance (miles)**	**Date Start**	**End**
	Waucoma	IA138742	43.095	-92.033	0.00	11/30/1954	12/31/2012
1	Spillville	IA137855	43.205	-91.954	8.63	8/1/1948	5/31/2007
2	New Hampton	IA135952	43.045	-92.312	14.52	11/30/1954	12/31/2012
3	Fayette	IA132864	42.850	-91.816	20.15	7/13/1947	12/31/2012
4	Cresco	IA131954	43.389	-92.094	20.60	3/31/1948	12/31/2012
5	Postville	IA136766	43.091	-91.558	23.97	12/31/1990	12/31/2012
6	Saratoga	IA137410	43.367	-92.367	25.23	4/30/1949	2/29/1968
Fayette Closest	**Station**	**Station ID**	**Lat**	**Long**	**Distance (miles)**	**Date Start**	**End**
	Fayette	IA132864	42.850	-91.816	0.00	7/13/1947	12/31/2012
1	Oelwein	IA136200	42.647	-91.913	14.92	3/31/1948	10/31/2005
2	Strawberry Point	IA138009	42.684	-91.535	18.29	8/1/1948	12/31/2012
3	Elkader	IA132603	42.775	-91.454	19.09	3/31/1948	12/29/2006
4	Waucoma	IA138742	43.095	-92.033	20.15	11/30/1954	12/31/2012
5	Postville	IA136766	43.091	-91.558	21.12	12/31/1990	12/31/2012
6	Tripoli	IA138339	42.813	-92.258	22.54	7/31/1948	12/31/2012
7	New Hampton	IA135952	43.045	-92.312	28.51	11/30/1954	12/31/2012

Table B.1: The eleven meteorological stations with the closest meteorological stations. This was used for IDW and completing missing data for the eleven meteorological stations used within this study for weather information.

Guttenberg Closest	Station	Station ID	Lat	Long	Distance (miles)	Date Start	End
	Guttenberg	IA133517	42.785	-91.096	0.00	3/31/1948	12/3/2006
1	McGregor	IA135315	43.017	-91.183	16.62	10/1/1951	12/31/2012
2	Elkader	IA132603	42.775	-91.454	18.18	3/31/1948	12/29/2006
3	Prairie Du Chien	WI476827	43.051	-91.135	18.50	5/31/1948	12/31/2012
4	Strawberry Point	IA138009	42.684	-91.535	23.40	8/1/1948	12/31/2012
5	Dubuque	IA132364	42.541	-90.656	28.04	3/31/1948	12/31/2012
6	Delaware/Manchester*	IA135086	42.452	-91.452	29.33	3/31/1976	12/31/2012
Cresco Closest	Station	Station ID	Lat	Long	Distance (miles)	Date Start	End
	Cresco	IA131954	43.389	-92.094	0.00	3/31/1948	12/31/2012
1	Harmony	MN213520	43.545	-92.012	11.52	8/31/1939	3/30/2014
2	Saratoga	IA137410	43.367	-92.367	13.80	4/30/1949	2/29/1968
3	Spillville	IA137855	43.205	-91.954	14.55	8/1/1948	5/31/2007
4	Decorah	IA132110	43.304	-91.795	16.13	3/31/1948	12/31/2012
5	Spring Valley	MN217941	43.693	-92.393	25.79	8/1/1948	12/31/2012
6	New Hampton	IA135952	43.045	-92.312	26.21	11/30/1954	12/31/2012
7	Osage	IA136305	43.279	-92.811	36.83	3/31/1948	12/31/2012
Spillville Closest	Station	Station ID	Lat	Long	Distance (miles)	Date Start	End
	Spillville	IA137855	43.205	-91.954	0.00	8/1/1948	5/31/2007
1	Waucoma	IA138742	43.095	-92.033	8.63	11/30/1954	12/31/2012
2	Decorah	IA132110	43.304	-91.795	10.50	3/31/1948	12/31/2012
3	Cresco	IA131954	43.389	-92.094	14.55	3/31/1948	12/31/2012
4	New Hampton	IA135952	43.045	-92.312	21.21	3/29/1928	12/31/2012
5	Postville	IA136766	43.091	-91.558	21.47	12/31/1990	12/31/2012
6	Saratoga	IA137410	43.367	-92.367	23.59	4/30/1949	2/29/1968
7	Waukon	IA138755	43.273	-91.476	24.48	3/31/1948	12/31/2012

Table B.2: The eleven meteorological stations with the closest meteorological stations. This was used for IDW and completing missing data for the eleven meteorological stations used within this study for weather information.

| New Hampton | | | | | | Date | |
Closest	Station	Station ID	Lat	Long	Distance (miles)	Start	End
	New Hampton	IA135952	43.045	-92.312	0.00	3/29/1928	12/31/2012
1	Waucoma	IA138742	43.095	-92.033	14.52	11/30/1954	12/31/2012
2	Tripoli	IA138339	42.813	-92.258	16.28	7/31/1948	12/31/2012
3	Charles City	IA131402	43.078	-92.671	18.28	8/1/1948	10/31/1953
4	Saratoga	IA137410	43.367	-92.367	22.39	4/30/1949	2/29/1968
5	Osage	IA136305	43.279	-92.811	29.89	3/31/1948	12/31/2012
6	Oelwein	IA136200	42.647	-91.913	34.18	3/31/1948	10/31/2005
Elkader						Date	
Closest	Station	Station ID	Lat	Long	Distance (miles)	Start	End
	Elkader	IA132603	42.775	-91.454	0.00	3/31/1948	12/29/2006
1	Strawberry Point	IA138009	42.684	-91.535	7.54	8/1/1948	12/31/2012
2	Guttenberg	IA133517	42.785	-91.096	18.18	3/31/1948	12/3/2006
3	Fayette	IA132864	42.850	-91.816	19.09	7/13/1947	12/31/2012
4	Delaware/Manchester*	IA135086	42.452	-91.452	22.36	3/31/1976	12/31/2012
5	Oelwein	IA136200	42.647	-91.913	24.97	3/31/1948	10/31/2005
6	Waucoma	IA138742	43.095	-92.033	36.71	11/30/1954	12/31/2012
Postville						Date	
Closest	Station	Station ID	Lat	Long	Distance (miles)	Start	End
	Postville	IA136766	43.091	-91.558	0.00	12/31/1990	12/31/2012
1	Waukon	IA138755	43.273	-91.476	13.23	3/31/1948	12/31/2012
2	Decorah	IA132110	43.304	-91.795	19.00	3/31/1948	12/31/2012
3	McGregor	IA135315	43.017	-91.183	19.62	10/1/1951	12/31/2012
4	Fayette	IA132864	42.850	-91.816	21.12	7/13/1947	12/31/2012
5	Spillville	IA137855	43.205	-91.954	21.47	8/1/1948	5/31/2007
6	Prairie Du Chien	WI476827	43.051	-91.135	21.54	5/31/1948	12/31/2012
7	Elkader	IA132603	42.775	-91.454	22.44	3/31/1948	12/29/2006
8	Waucoma	IA138742	43.095	-92.033	23.97	11/30/1954	12/31/2012
McGregor						Date	
Closest	Station	Station ID	Lat	Long	Distance (miles)	Start	End
	McGregor	IA135315	43.017	-91.183	0.00	10/1/1951	12/31/2012
1	Prairie Du Chien	WI476827	43.051	-91.135	3.40	5/31/1948	12/31/2012
2	Guttenberg	IA133517	42.785	-91.096	16.62	3/31/1948	12/3/2006
3	Elkader	IA132603	42.775	-91.454	21.62	3/31/1948	12/29/2006
4	Waukon	IA138755	43.273	-91.476	23.04	3/31/1948	12/31/2012
Strawberry Point						Date	
Closest	Station	Station ID	Lat	Long	Distance (miles)	Start	End
	Strawberry Point	IA138009	42.684	-91.535	0.00	8/1/1948	12/31/2012
1	Elkader	IA132603	42.775	-91.454	7.54	3/31/1948	12/29/2006
2	Delaware/Manchester*	IA135086	42.452	-91.452	16.63	3/31/1976	12/31/2012
3	Fayette	IA132864	42.850	-91.816	18.29	7/13/1947	12/31/2012
4	Oelwein	IA136200	42.647	-91.913	19.38	3/31/1948	10/31/2005

Table B.3: The eleven meteorological stations with the closest meteorological stations. This was used for IDW and completing missing data for the eleven meteorological stations used within this study for weather information.

APPENDIX C
FTABLE SUMMARY

Sites Used in Calibration			
Name	USGS site	Drainage Area (mi^2)	R^2 Value
Turkey River, Garber, IA	4512500	1,545	0.988
Turkey River above French Hollow, IA	5412020	903	0.991
Turkey River at Elkader, IA	5412000	891	0.991
Turkey River at Eldorado, IA	5412850	641	0.994
Turkey River at Spillville, IA	5411600	177	0.993
Sites Used in Validation			
Turkey River at Luana, IA	5412060	4.39	0.829
Roberts Creek, Saint Olaf IA	5412100	70.7	0.579
Volga River at Fayette, IA	5412340	130	0.941
Volga River at Littleport, IA	5412400	348	0.934

Table C.1: Power relation Calibration and Validation Site Summary. R^2 value is the relationship between Drainage Area and Discharge.

Assumptions	
H:V	2.5
$S_{floodplain}$	0.1
n	0.035

Table C.2: Watershed Assumptions in Power Relation.

DEPTH	AREA	VOLUME	DISCH	FLO-THRU
(FT)	(ACRES)	(AC-FT)	(CFS)	(MIN)
0.000	0.849	0.000	0.000	0.0
0.161	0.908	0.141	1.101	93.1
0.321	0.967	0.292	3.506	60.4
0.482	1.025	0.452	6.929	47.3
0.642	1.084	0.621	11.27	40.0
0.803	1.143	0.800	16.48	35.2
1.071	1.240	1.119	27.04	30.0
1.338	1.338	1.464	39.92	26.6
1.606	1.436	1.835	55.14	24.2
2.141	16.477	6.630	144.42	33.3
2.677	31.519	19.477	441.84	32.0
3.212	46.560	40.376	1068.6	27.4
3.747	61.601	69.327	2124.8	23.7
4.283	76.642	106.330	3699.5	20.9
4.818	91.684	151.385	5874.6	18.7
6.424	136.807	334.863	16747.6	14.5

Figure C.1: Example of a FTable for reach with a drainage area of 8.35 square miles and length of 1.16 miles

APPENDIX D
2006 NATIONAL LAND COVER DATA (NLCD) SET CLASSES

NLCD Land Cover Classification Legend

- 11 Open Water
- 12 Perennial Ice/ Snow
- 21 Developed, Open Space
- 22 Developed, Low Intensity
- 23 Developed, Medium Intensity
- 24 Developed, High Intensity
- 31 Barren Land (Rock/Sand/Clay)
- 41 Deciduous Forest
- 42 Evergreen Forest
- 43 Mixed Forest
- 51 Dwarf Scrub*
- 52 Shrub/Scrub
- 71 Grassland/Herbaceous
- 72 Sedge/Herbaceous*
- 73 Lichens*
- 74 Moss*
- 81 Pasture/Hay
- 82 Cultivated Crops
- 90 Woody Wetlands
- 95 Emergent Herbaceous Wetlands

* Alaska only
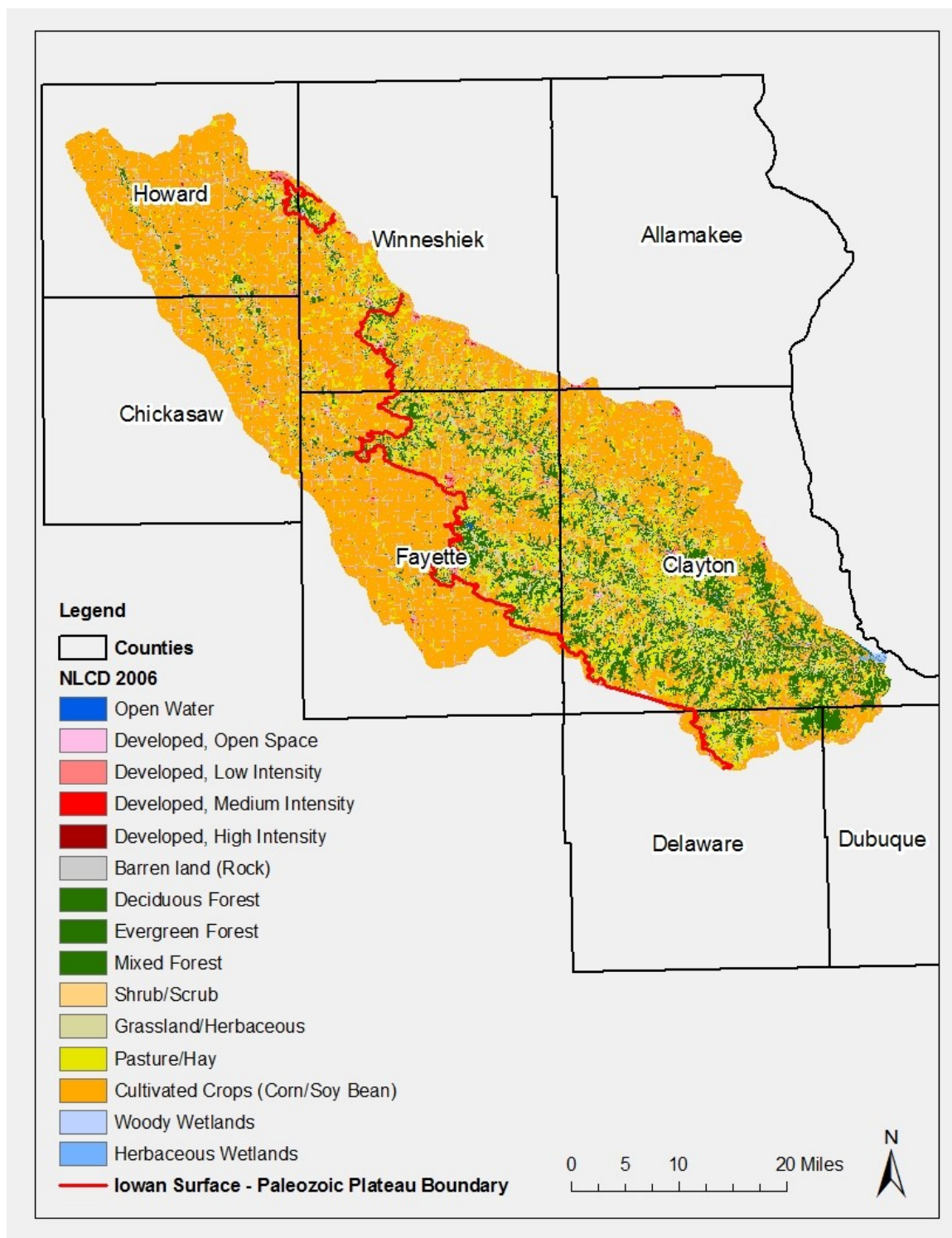
Figure D.1: 2006 National Land Cover
Data (NLCD) set classes.

Figure D.2: 2006 National Land Cover Data (NLCD) map of Turkey River Watershed (*IFC*, 2014).

Class\ Value	Classification Description
Water	
11	**Open Water** - areas of open water, generally with less than 25% cover of vegetation or soil.
12	**Perennial Ice/Snow** - areas characterized by a perennial cover of ice and/or snow, generally greater than 25% of total cover.
Developed	
21	**Developed, Open Space** - areas with a mixture of some constructed materials, but mostly vegetation in the form of lawn grasses. Impervious surfaces account for less than 20% of total cover. These areas most commonly include large-lot single-family housing units, parks, golf courses, and vegetation planted in developed settings for recreation, erosion control, or aesthetic purposes.
22	**Developed, Low Intensity** - areas with a mixture of constructed materials and vegetation. Impervious surfaces account for 20% to 49% percent of total cover. These areas most commonly include single-family housing units.
23	**Developed, Medium Intensity** – areas with a mixture of constructed materials and vegetation. Impervious surfaces account for 50% to 79% of the total cover. These areas most commonly include single-family housing units.
24	**Developed High Intensity** -highly developed areas where people reside or work in high numbers. Examples include apartment complexes, row houses and commercial/industrial. Impervious surfaces account for 80% to 100% of the total cover.
Barren	
31	**Barren Land (Rock/Sand/Clay)** - areas of bedrock, desert pavement, scarps, talus, slides, volcanic material, glacial debris, sand dunes, strip mines, gravel pits and other accumulations of earthen material. Generally, vegetation accounts for less than 15% of total cover.
Forest	
41	**Deciduous Forest** - areas dominated by trees generally greater than 5 meters tall, and greater than 20% of total vegetation cover. More than 75% of the tree species shed foliage simultaneously in response to seasonal change.
42	**Evergreen Forest** - areas dominated by trees generally greater than 5 meters tall, and greater than 20% of total vegetation cover. More than 75% of the tree species maintain their leaves all year. Canopy is never without green foliage.
43	**Mixed Forest** - areas dominated by trees generally greater than 5 meters tall, and greater than 20% of total vegetation cover. Neither deciduous nor evergreen species are greater than 75% of total tree cover.
Shrubland	
51	**Dwarf Scrub** - Alaska only areas dominated by shrubs less than 20 centimeters tall with shrub canopy typically greater than 20% of total vegetation. This type is often co-associated with grasses, sedges, herbs, and non-vascular vegetation.
52	**Shrub/Scrub** - areas dominated by shrubs; less than 5 meters tall with shrub canopy typically greater than 20% of total vegetation. This class includes true shrubs, young trees in an early successional stage or trees stunted from environmental conditions.
Herbaceous	
71	**Grassland/Herbaceous** - areas dominated by gramanoid or herbaceous vegetation, generally greater than 80% of total vegetation. These areas are not subject to intensive management such as tilling, but can be utilized for grazing.
72	**Sedge/Herbaceous** - Alaska only areas dominated by sedges and forbs, generally greater than 80% of total vegetation. This type can occur with significant other grasses or other grass like plants, and includes sedge tundra, and sedge tussock tundra.
73	**Lichens** - Alaska only areas dominated by fruticose or foliose lichens generally greater than 80% of total vegetation.
74	**Moss** - Alaska only areas dominated by mosses, generally greater than 80% of total vegetation.
Planted/Cultivated	
81	**Pasture/Hay** – areas of grasses, legumes, or grass-legume mixtures planted for livestock grazing or the production of seed or hay crops, typically on a perennial cycle. Pasture/hay vegetation accounts for greater than 20% of total vegetation.
82	**Cultivated Crops** – areas used for the production of annual crops, such as corn, soybeans, vegetables, tobacco, and cotton, and also perennial woody crops such as orchards and vineyards. Crop vegetation accounts for greater than 20% of total vegetation. This class also includes all land being actively tilled.
Wetlands	
90	**Woody Wetlands** - areas where forest or shrubland vegetation accounts for greater than 20% of vegetative cover and the soil or substrate is periodically saturated with or covered with water.
95	**Emergent Herbaceous Wetlands** - Areas where perennial herbaceous vegetation accounts for greater than 80% of vegetative cover and the soil or substrate is periodically saturated with or covered with water.

Figure D.3: National Land Cover Database classification descriptions. Only two land types had pervious area within the model, Urban Development (Open Space (10%), Low (20%), Medium (50%), and High (80%)) and Barren Rock (85%).

APPENDIX E
PRAIRIE SCENARIO

Table E.1 summarizes the adjustments made to the Turkey River HSPF model parameters to represent a tall-grass prairie landscape. What follows is a discussion of the parameter adjustments.

Parameter	Adjustment
CPSC	Same maximum as corn with adjusted annual cycle for growing and dormant season
LZSN	2 x Calibrated value for corn and soybeans
UZSN	2.5 x Calibrated value and adjusted annual cycle
INFILT	4.65 x Calibrated value for corn and soybean
NSUR	Increase to a constant 0.30 for continuous prairie vegetation
LZETP	Increased maximum to 0.90 and adjusted annual cycle

Table E.1: Adjustments in HSPF model parameters from those calibrated for croplands to reflect a tall-grass prairie landscape.

CEPSC is interception storage capacity (depth). It represents the storage of water on vegetation and depressions at the surface. Corn crops have extensive interception storage at maturity; after harvesting the interception storage is quite low. For the prairie land segments, we assumed the maximum interception storage was the same as mature corn. However, we adjusted its annual cycle to reflect the higher interception storage of a prairies continuous vegetation cover during the growing and dormant seasons (*Schilling and Drobney*, 2014). Outside the growing season for corn and soybean (November through April) a permanent 0.09 CEPSC was used. It is a third higher than what was previously used. Figure-E.1 shows the monthly intercep-

tion storage for before (baseline-gold) and after the scenario for prairie (green).
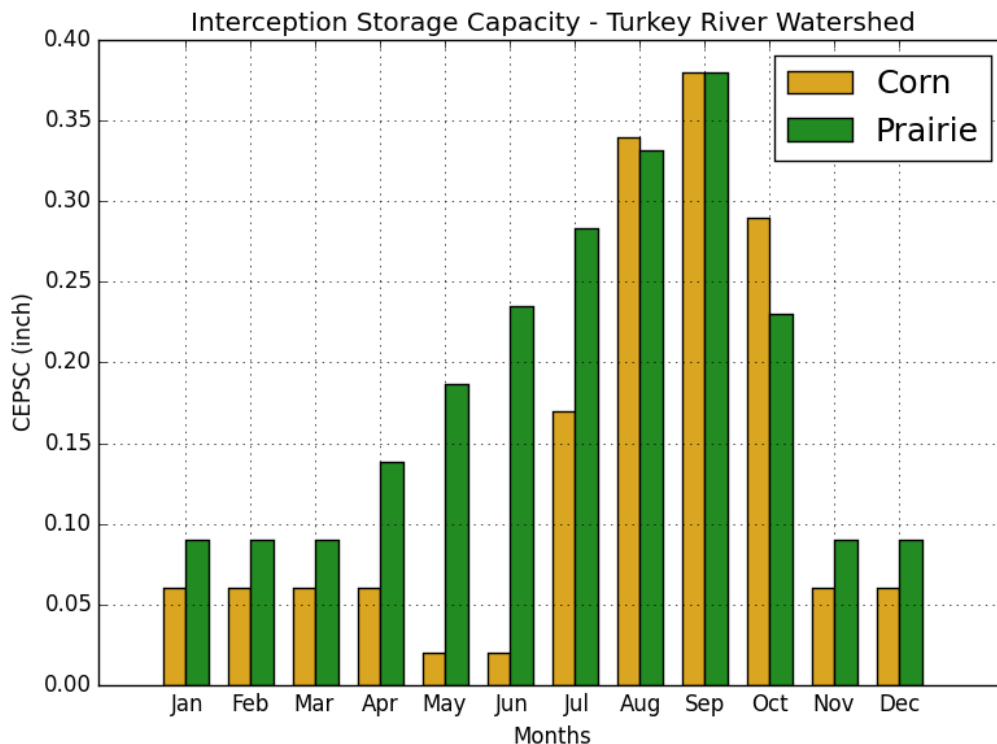
Figure E.1: Interception storage capacity for before (baseline) and after the scenario for prairie.

LZSN (lower zone nominal storage) is related to the available water capacity (depth) of the root zone. Since the root zone depth of tall-grass prairie vegetation is typically about twice that of mature corn, we increased the calibrated LZSN by a factor of 2. Going from 2.358 to 4.715 inches. The root zone for corn roughly 4 feet as were root zone for prairie is roughly 8 feet (*E. Weaver*, 1926). Also stated by *Schilling et al.* (2014), deep roots of perennial vegetation reduces volumetric water

content and increases soil moisture storage because the deep roots are able to access water deeper in the soil profile (*Schilling and Drobney*, 2014; *Hodnett et al.*, 1995; *Huxman et al.*, 2005). Adding to the fact that deeper roots of native prairies create more storage.

UZSN (upper zone nominal storage) is related to the depression and pore storage in the near-surface soils. *Donigian and J. Kittle* (1983) illustrate using the Natural Resource Conservation Service (NRCS) runoff curve number (CN) for initial estimates of UZSN. This approach was used to determine the ratio of the initial estimate of UZSN for a prairie to that for row crops (using a mixture of conventional tillage, no tillage, terraces, and contours). As a result, we increased the calibrated UZSN by a factor of 2.5 for the prairie land segment. For the months between April and August a linear increase was used rather than following how corn fluctuates. Native prairie would assume to have a increasing storage during the growing months sense it is untouched as where corn is tilled every year and have to regrow annually. Figure E.2 displays the monthly upper zone nominal storage for before (baseline) and after the scenario for prairie.

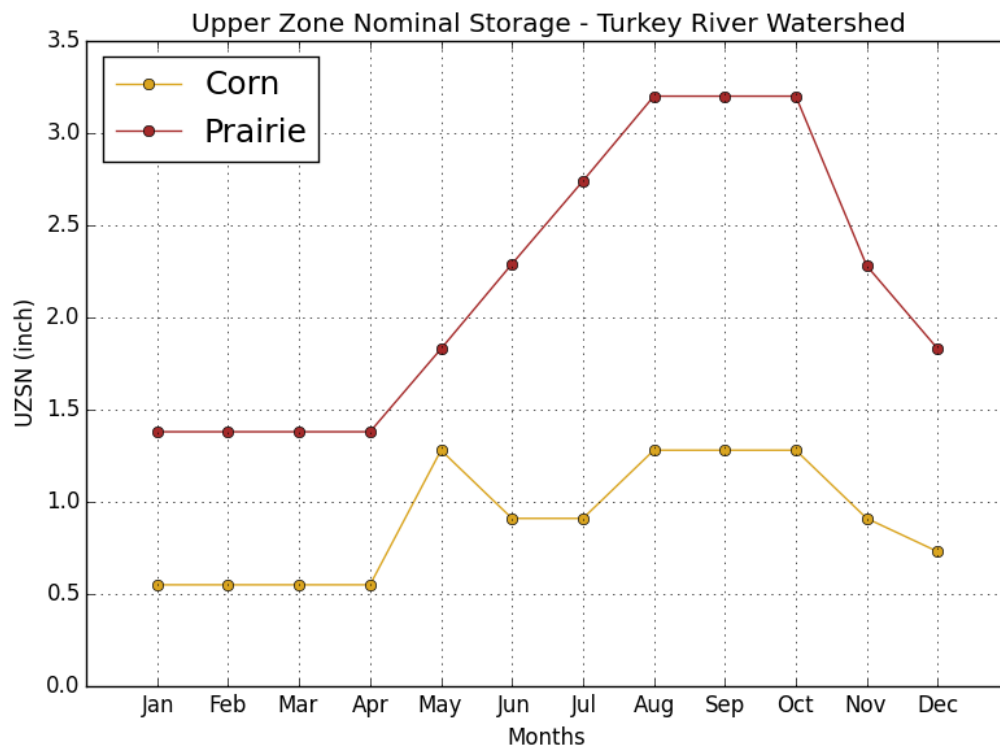Figure E.2: Upper zone nominal storage for before (baseline-gold) and after the scenario for prairie (red).

INFILT is an index to the infiltration capacity of the soil. *Donigian and J. Kittle* (1983) illustrated using Holtans infiltration equation for initial estimates of INFILT. We used this approach to determine the ratio of the initial estimate of INFILT for a prairie to that for a row crop mixture. As a result, we increased the calibrated INFILT by a factor of 4.65 for the prairie land segment. This assumption is not to fair off from actual results showed by Bharati. After converting from cropland to switchgrass, a native tall grass prairie species, after 6 years, the infiltration capacity went from 2 inches per hour to more than 7.5 inches per hour (*Schilling and Drobney*,

2014). That's a factor of 3.75 or more increase over a 6 year period converting from farmland to switchgrass. Not too far off from our assumed 4.65 increase for mixed native tall grass prairie for a 64 year simulation period.

NSUR is a measure of the roughness of the surface for water flowing (known as Mannings n). *Donigian and J. Kittle* (1983) provide recommended NSUR values for different land uses. Using these values as guidance, we increased the maximum NSUR value from 0.25 to 0.30. The roughness for row crops varies throughout the growing season; we assumed the roughness for prairie remains constant throughout the year. Figure E.3 shows the manning's n for each month.
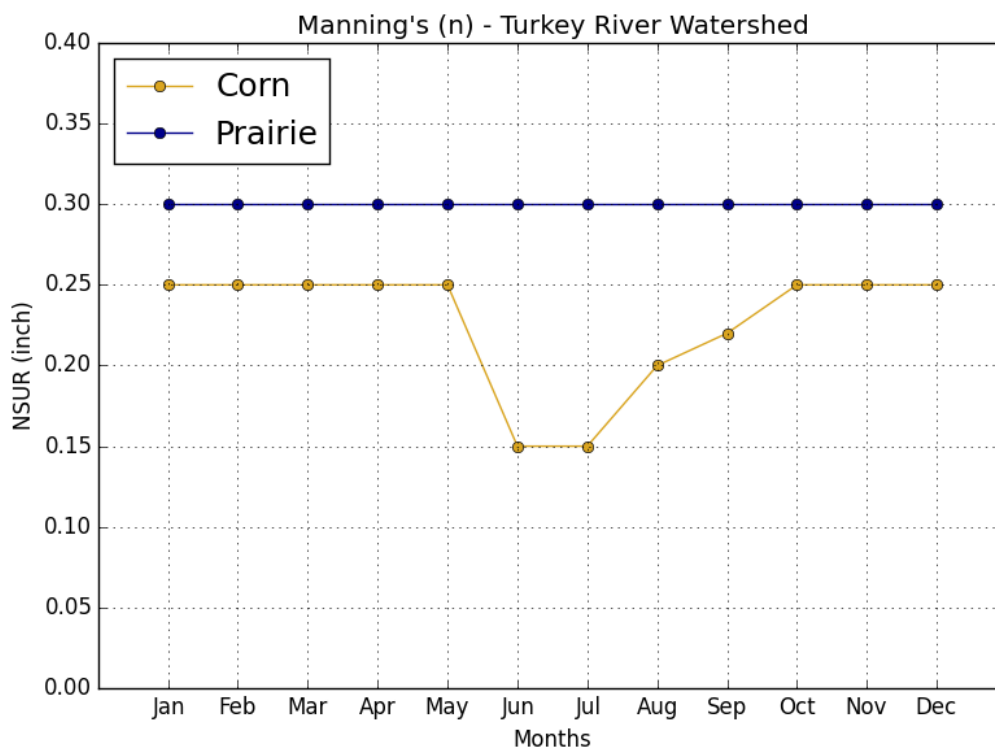

Figure E.3: Mannings n for before (baseline-gold) and after the scenario for prairie (blue).

LZETP (lower zone evapotranspiration parameter) is an index to the density of deep rooted vegetation. The parameter determines the amount (depth) of evapotranspiration from the lower zone, given the lower zone soil moisture condition. Given its empirical nature, we assumed that the maximum LZETP increases from 0.80 (calibrated for corn and soybeans) to 0.90. This is because much of the prairie's precipitation is diverted into interception and infiltration allowing more time for evapotranspiration to occur (*Schilling and Drobney*, 2014). We also adjusted the annual cycle to reflect the higher evaporation potential of a prairies continuous vegetation cover during the growing and dormant seasons. Figure E.4 shows the lower zone evapotranspiration for before (baseline) and after the scenario for prairie.
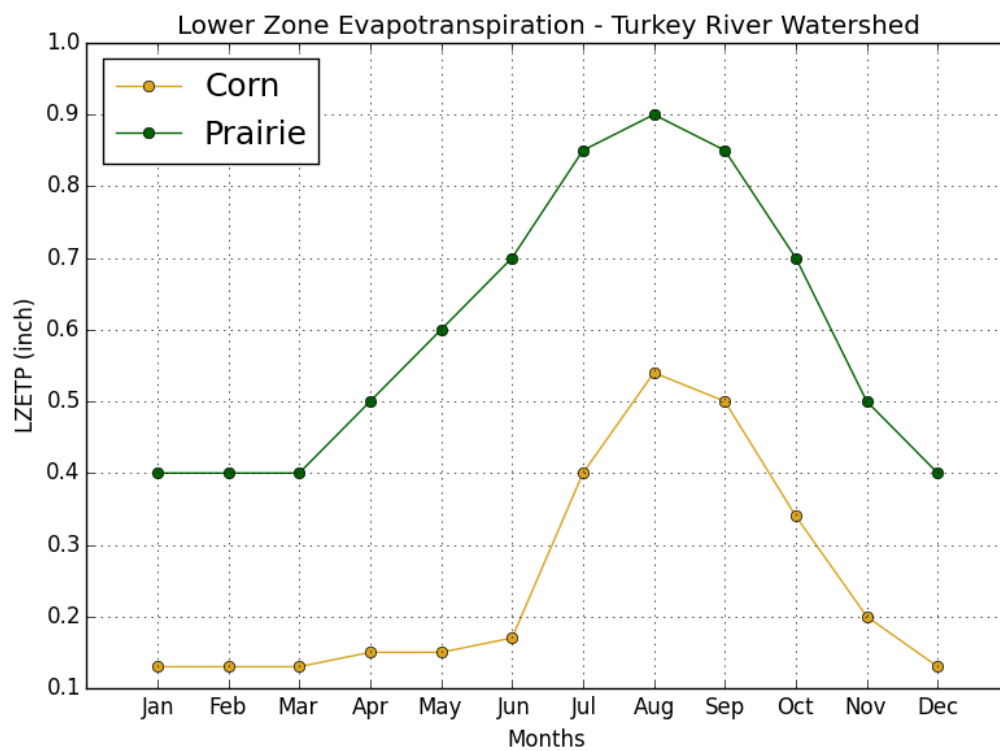
Figure E.4: Lower zone evapotranspiration parameter for before (baseline-gold) and after the scenario for prairie (green).

APPENDIX F
SIMULATED BASELINE FLOWS

	Return Period (cfs)			
Name	2-year	10-year	25-year	50-year
Otter Creek	1,010.10	4,543.08	7,529.26	7,498.54
Spillville	1,317.73	4,635.35	6,320.91	5,577.43
Crane Creek	1,520.24	5,340.56	7,173.23	9,671.18
Eldorado	4,395.06	12,694.63	15,901.46	18,855.30
Elkader	5,130.96	13,188.21	17,297.39	17,558.45
Garber	9,786.08	22,478.21	35,746.78	34,337.91
Outlet Missip.	9,352.19	21,394.22	33,722.27	37,327.20
Volga at Fayette	1,157.90	5,349.60	8,694.69	10,427.46
Volga at Littleport	2,985.93	8,788.80	14,632.62	15,568.88

Table F.1: Simulated baseline flows from the Turkey River cali-brated HSPF model. These flows were found empirically from the 64-year simulation annual maximum flows.

REFERENCES

AquaTerra (2011), About HSPF.

Arnold, J. G., R. Srinivasan, R. S. Muttiah, and J. R. Williams (1998), Large Area Hydrologic Modeling and Assessment Part I: Model Development.

Bharati, L., K.-H. Lee, T. Isenhart, and R. Schultz (2002), Soil-Water Infiltration Under Crops, Pasture, and Established Riparian Buffer in Midwestern USA, *Agroforestry systems*, *56*(3), 249–257.

Bicknell, B. R., J. C. Imhoff, J. L. Kittle Jr, A. S. Donigian Jr, and R. C. Johanson (1997), *Hydrological Simulation Program–Fortran: User's Manual for Version 12*, 114-118 pp., US Environmental Protection Agency, National Exposure Research Laboratory Athens, GA.

Donigian, J. D. B. D. H., A., and M. Walter (1984), *HSPF Parameter Adjustments to Evaluate the Effects of Agricultural Best Management Practices*, Environmental Research Laboratory, Athens, Georgia.

Donigian, J. J. I. B. B., A., and J. J. Kittle (1983), *Application Guide for the Hydrological Simulation Program - Fortran*, U.S. Environmental Protection Agency, Environmental Research Laboratory, Athens, Georgia.

Duan, Q. Y., S. Sorooshian, and V. Gupta (1992), Effective and Efficient Global Optimization for Conceptual Rainfall-Runoff Models, *Water Resources Research*, *28*(4), 1015–1031, doi:Doi 10.1029/91wr02985.

E. Weaver, J. (1926), Root Development of Field Crops.

EPA (2000), *BASINS Technical Note 6 - Estimating Hydrology and Hydraulic Parameters for HSPF*, US Environmental Protection Agency.

EPA (2007), *BASINS Technical Note 2 - Two Automated Methods for Creating Hydraulic Function Tables (FTABLES)*, US Environmental Protection Agency.

Extension, I. S. U., and Outreach (2015), Iowa Corn and Soybean County Yields.

FGDC, F. G. D. C. (2002), Federal Standards for Delineation of Hydrologic Unit Boundaries, *Proposal, Version*, *1*.

Gerla, P. J. (2007), Estimating the Effect of Cropland to Prairie Conversion on Peak Storm Run-Off, *Restoration Ecology*, *15*(4), 720–730.

Hernandez-Santana, V., X. Zhou, M. J. Helmers, H. Asbjornsen, R. Kolka, and M. Tomer (2013), Native Prairie Filter Strips Reduce Runoff from Hillslopes Under Annual Row-Crop Systems in Iowa, USA, *Journal of Hydrology*, *477*, 94–103, doi:10.1016/j.jhydrol.2012.11.013.

Hodnett, M., L. P. Da Silva, H. Da Rocha, and R. C. Senna (1995), Seasonal Soil Water Storage Changes Beneath Central Amazonian Rainforest and Pasture, *Journal of hydrology, 170*(1), 233–254.

Hummel, P., J. Kittle Jr, and M. Gray (2001), WDMUtil Version 2.0, A tool for Managing Watershed Modeling Time-Series Data: Users Manual, *Contract*, (68-C), 98–010.

Huxman, T. E., B. P. Wilcox, D. D. Breshears, R. L. Scott, K. A. Snyder, E. E. Small, K. Hultine, W. T. Pockman, and R. B. Jackson (2005), Ecohydrological Implications of Woody Plant Encroachment, *Ecology, 86*(2), 308–319.

IFC, I. F. C. (2014), Iowa watersheds project.

Khakbaz, B., B. Imam, K. Hsu, and S. Sorooshian (2012), From Lumped to Distributed Via Semi-Distributed: Calibration Strategies for Semi-Distributed Hydrologic models, *Journal of Hydrology, 418*, 61–77.

Linhart, S. M., and D. A. Eash (2010), *Floods of May 30 to June 15, 2008, in the Iowa River and Cedar River Basins, Eastern Iowa*, US Geological Survey.

Love, O. (2015), Organization Launches 32 Million Plan for Turkey River Flooding, *TheGazette Site Wide Activity RSS*.

Menne, M. J., I. Durre, R. S. Vose, B. E. Gleason, and T. G. Houston (2012), An Overview of the Global Historical Climatology Network-Daily Database, *Journal of Atmospheric and Oceanic Technology, 29*(7), 897–910.

NOAA (1995), National climatic data center, *National Oceanic and Atmospheric Administration, ISSN*, pp. 0039–1972.

NRCS, U. (2004), National Engineering Handbook: Part 630Hydrology, Chapter 7, *USDA Soil Conservation Service: Washington, DC, USA*.

Penman, H. L. (1948), Natural Evaporation from Open Water, Bare Soil and Grass, *Proceedings of the Royal Society of London Series a-Mathematical and Physical Sciences, 193*(1032), 120–&, doi:DOI 10.1098/rspa.1948.0037.

Phillips, J. V., and S. Tadayon (2006), *Selection of Manning's Roughness Coefficient for Natural and Constructed Vegetated and Non-Vegetated Channels, and Vegetation Maintenance Plan Guidelines for Vegetated Channels in Central Arizona*, Citeseer.

Ponce, V. M., and R. H. Hawkins (1996), Runoff Curve Number: Has it Reached Maturity?, *Journal of hydrologic engineering, 1*(1), 11–19.

Schilling, K. E., and P. Drobney (2014), Restoration of Prairie Hydrology at the Watershed Scale: Two Decades of Progress at Neal Smith National Wildlife Refuge, Iowa, *Land, 3*(1), 206–238.

Schilling, K. E., M. K. Jha, Y.-K. Zhang, P. W. Gassman, and C. F. Wolter (2008), Impact of Land Use and Land Cover Change on the Water Balance of a Large Agricultural Watershed: Historical effects and Future Directions, *Water Resources Research*, *44*(7).

Schilling, K. E., K.-S. Chan, H. Liu, and Y.-K. Zhang (2010), Quantifying the Effect of Land Use Land Cover Change on Increasing Discharge in the Upper Mississippi River, *Journal of Hydrology*, *387*(3), 343–345.

Schilling, K. E., P. W. Gassman, C. L. Kling, T. Campbell, M. K. Jha, C. F. Wolter, and J. G. Arnold (2014), The Potential for Agricultural Land Use Change to Reduce Flood Risk in a Large Watershed, *Hydrological Processes*, *28*(8), 3314–3325.

Shuttleworth, D. M. e., W. (1993a), *Handbook of Hydrology*, 4.1–4.53 pp., McGraw-Hill, New York.

Shuttleworth, D. M. e., W. (1993b), *Handbook of Hydrology*, 10.7–10.8 pp., McGraw-Hill, New York.

Techniques, E. S. (2012), ET GeoWizards 10.1, *ET Spatial Techniques. Faerie Glen, South Africa*.

USDA (2014), World Agricultural Supply and Demand Estimates.

Vrugt, J. A., H. V. Gupta, W. Bouten, and S. Sorooshian (2003), A Shuffled Complex Evolution Metropolis Algorithm for Optimization and Uncertainty Assessment of Hydrologic Model Parameters, *Water Resources Research*, *39*(8), doi:Artn 1201 Doi 10.1029/2002wr001642.

Wehmeyer, L. L., and F. H. Weirich (2010), Effect of Historic Land Cover Change on Runoff Curve Number Estimation in Iowa, *Journal of Hydrologic Engineering*, *15*(9), 692–695, doi:Doi 10.1061/(Asce)He.1943-5584.0000234.

Wu, J., and X. Zhu (2006), Using the Shuffled Complex Evolution Global Optimization Method to Solve Groundwater Management Models, in *Frontiers of WWW Research and Development-APWeb 2006*, pp. 986–995, Springer.

Xu, X., B. R. Scanlon, K. Schilling, and A. Sun (2013), Relative Importance of Climate and Land Surface Changes on Hydrologic Changes in the US Midwest since the 1930s: Implications for Biofuel Production, *Journal of Hydrology*, *497*, 110–120.